Cell Reports

Resource

An *in vivo* resource of age-regulated *C. elegans* intestinal secretory-pathway proteins highlights secreted enzymes associated with lifespan regulation

Graphical abstract

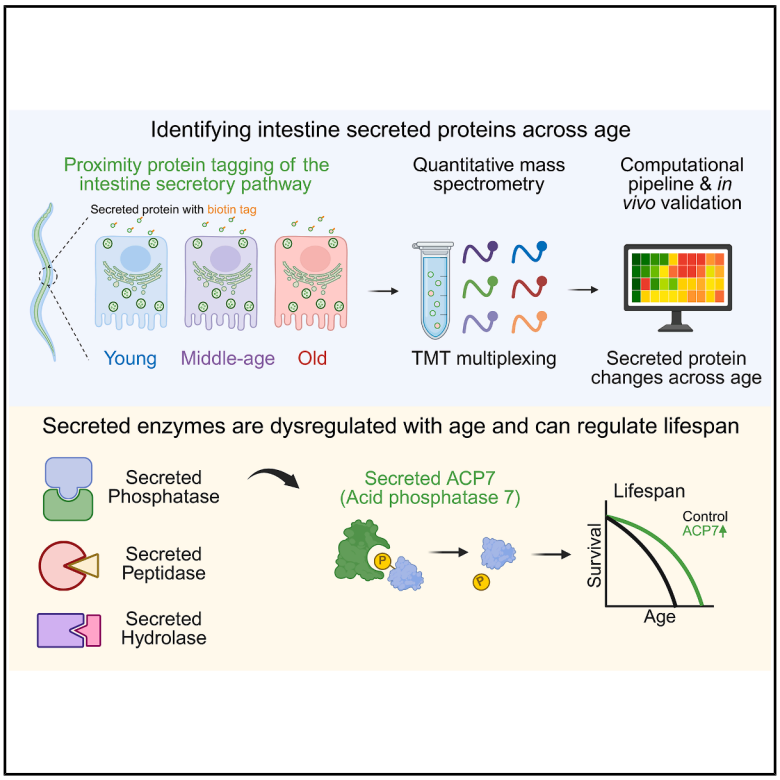

Authors

Jason W. Miklas, Katharina Papsdorf, Eric D. Sun, ..., Joshua E. Elias, Monther Abu-Remaileh, Anne Brunet

Correspondence

abrunet1@stanford.edu

In brief

Miklas et al. characterize age-related *C. elegans* intestinal secretory-pathway proteins using proximity labeling tools and *in vivo* proteomics. They identify a conserved secreted phosphatase, ACP7, that extends lifespan in a secretion- and phosphatase-dependent manner. This resource highlights the role of extracellular enzymes in regulating lifespan.

Highlights

- *In vivo* resource for age-related *C. elegans* intestinal secretory-pathway proteins
- Identification of several conserved intestine-secreted proteins that change with age
- ACP7 is a conserved secreted phosphatase that can extend *C. elegans* lifespan
- Our dataset also identifies a vesicle-bound protein that modulates lifespan

Miklas et al., 2026, Cell Reports *45*, 117902
September 22, 2026 © 2026 The Authors. Published by Elsevier Inc.
https://doi.org/10.1016/j.celrep.2026.117902

CellPress

Cell Reports

CellPress
OPEN ACCESS

Resource

An *in vivo* resource of age-regulated *C. elegans* intestinal secretory-pathway proteins highlights secreted enzymes associated with lifespan regulation

Jason W. Miklas,[1] Katharina Papsdorf,[1,12] Eric D. Sun,[1,2] Aleksandra Tsenter,[1] Nicole R. Haseley,[1] Brandon Ameglio,[1,3,4] Uche N. Medoh,[1,5,6,13] Daniel Richard,[1] Frank McCarthy,[7] Karen L. Artiles,[8] Andy Hims,[1,5,6] Aleksandra Levina,[1,5,6] Olivia Y. Zhou,[1,3,9] Joshua E. Elias,[7] Monther Abu-Remaileh,[1,5,6] and Anne Brunet[1,10,11,14,*]

[1]Department of Genetics, Stanford University, Stanford, CA, USA
[2]Biomedical Informatics Graduate Program, Stanford University, Stanford, CA, USA
[3]Stanford Biophysics Graduate Program, Stanford University, Stanford, CA, USA
[4]Arc Institute, Palo Alto, CA 94304, USA
[5]Department of Chemical Engineering, Stanford University, Stanford, CA, USA
[6]The Institute for Chemistry, Engineering & Medicine for Human Health, Stanford University, Stanford, CA, USA
[7]Biohub, San Francisco, CA, USA
[8]Department of Pathology, Stanford University School of Medicine, Stanford, CA, USA
[9]Stanford Medical Scientist Training Program, Stanford University, Stanford, CA, USA
[10]Glenn Center for the Biology of Aging, Stanford University, Stanford, CA, USA
[11]Wu Tsai Institute of Neurosciences, Stanford University, Stanford, CA, USA
[12]Present address: Institute of Molecular Biology (IMB), Mainz, Germany
[13]Present address: Arc Institute, Palo Alto, CA 94304, USA
[14]Lead contact
*Correspondence: abrunet1@stanford.edu
https://doi.org/10.1016/j.celrep.2026.117902

SUMMARY

Secreted proteins are essential to modulate homeostasis in the extracellular space and facilitate communication to distal cells or tissues. Yet, the identity and functional importance of extracellular proteins in aging have been understudied. Here we use proximity labeling followed by quantitative proteomics to systematically characterize proteins along the intestinal secretory pathway in *C. elegans*, focusing on secreted proteins. We identify intestine-secreted proteins that are modulated with age, and validate the secretion of these proteins *in vivo*. One of these secreted proteins, ACP7, is well conserved in humans, and its overexpression extends lifespan in a secretion-dependent manner. Interestingly, we find that ACP7 acts as a secreted phosphatase in the extracellular space. Finally, we identify additional proteins along the secretory pathway that regulate lifespan. Our systematic characterization of tissue-specific secreted proteins during aging uncovers conserved proteins that impact lifespan and highlights extracellular enzymes associated with lifespan regulation.

INTRODUCTION

Aging is a multifaceted process that results in organismal decline and death. While intracellular pathways that drive aging are well characterized,[1] much less is known about how the extracellular milieu functionally impacts this process. Secreted factors are critical for the modulation of homeostasis in the extracellular space and communication between cells, tissues, and organs.[2–12] Secreted hormones or peptides are produced by specific tissues in species ranging from *C. elegans* to humans,[3,4,7,13–16] and they represent powerful therapeutic targets likely because of their important systemic effects.[14,17–25] In addition, there has been high interest in analyzing proteins present in accessible extracellular fluids (e.g., blood or cerebrospinal fluid) in mammals,[18,19,26–31] and such proteins have been found to serve as excellent biomarkers of age and disease.[18,27–29,31–34] But how the "secretome"—the ensemble of secreted proteins—changes with age and functionally regulates lifespan is still largely unknown.

Quantitatively assessing secreted proteins that originate from specific tissues is technically challenging, especially for low-abundance proteins. Quantitative proteomics has been performed in several species during aging, either on whole animals[35–38] or whole organs.[39–43] These studies have identified key processes that change with age, such as redox regulation,[43] protein ubiquitination,[38] and protein aggregation.[36,37,39–41] Moreover, organelle-specific proteomics has also been conducted in young animals, uncovering lysosome proteins implicated in metabolic regulation and aging.[42,44,45] While these datasets have provided important information on intracellular pathways and how they change with age, they did not quantify secreted proteins. Thus, we still lack a systematic and

This is an open access article under the CC BY-NC-ND license (http://creativecommons.org/licenses/by-nc-nd/4.0/).

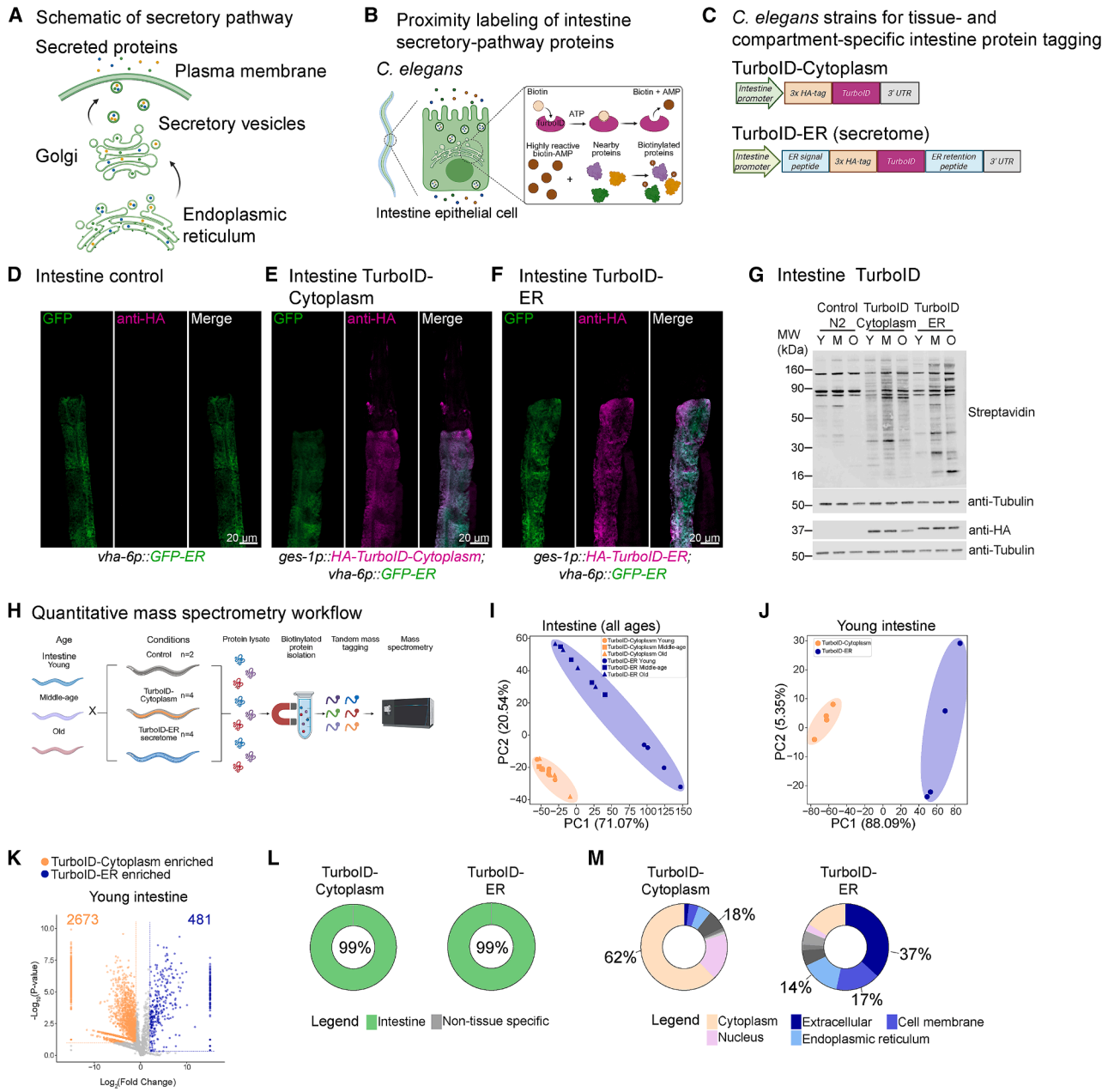

Figure 1. Capturing the intestinal secretome with tissue- and compartment-specific protein proximity labeling followed by quantitative mass spectrometry

(A) Schematic of the "secretome" (the ensemble of extracellular/secreted proteins) and other proteins that transit through the secretory pathway.

(B) Schematic outlining the proximity labeling protein TurboID localized to the endoplasmic reticulum (ER) of intestinal epithelial cells (TurboID-ER). TurboID-ER adds biotin to proteins that transit through the ER, thereby labeling proteins that are secreted outside the cell into the extracellular space (as well as other proteins along the secretory pathway, including ER-resident, Golgi, organelle, membrane, and vesicle-bound proteins).

(C) Schematic of *C. elegans* strains expressing TurboID in the cytoplasm (TurboID-Cytoplasm) or in the endoplasmic reticulum (TurboID-ER) in the intestine driven by the *ges-1* intestinal promoter (*ges-1p*, green). To facilitate detection, TurboID is tagged with several HA tags (3x HA-tag). To target and retain TurboID in the ER, a signal peptide (SP) is added to the N-terminal of TurboID and an ER-retention signal (KDEL) is added to the C-terminal of TurboID.

(D–F) Confocal microscopy images of *C. elegans* strains showing intestine localization of TurboID-Cytoplasm and TurboID-ER. Both TurboID-Cytoplasm and TurboID-ER (magenta) are expressed in the intestine (which is marked in green). A strain that expresses GFP localized to the ER (GFP-ER) driven by the *vha-6* intestine promoter (*vha-6p*) is used to visualize the intestine and the ER. An antibody against the HA-tag is used to visualize TurboID. Scale bars, 20 µm. For higher magnification images, see Figure S1A.

(G) Western blot of whole worm lysates at young (Y, 3 days post hatch), middle-age (M, 8 days post hatch) and old (O, 13 days post hatch) ages of control (N2), intestine TurboID-Cytoplasm, and intestine TurboID-ER strains. Streptavidin signal shows that more biotinylated proteins are found in the lysates from intestine

(legend continued on next page)

quantitative understanding of how a tissue secretome changes with age and how these changes influence lifespan.

Excitingly, the advent of proximity labeling technology has made the capture of tissue-specific secreted proteins feasible in several species.[2,26,27,46–53] Proximity labeling allows the tagging of specific proteins from a particular tissue and subcellular compartment, and these proteins can then be identified via proteomics. Proximity labeling in the endoplasmic reticulum (ER)—a compartment where proteins along the secretory pathway are generated[54]—has enabled the capture of secreted proteins from human cells *in vitro*[48] and from several tissues (e.g., liver, muscle, fat) *in vivo* in both Drosophila[2,52] and mice.[26,27,50,53] This approach can be more selective and sensitive than global proteomics.[55] Proximity labeling has so far only been used in young individuals, and applying this technology quantitatively on animals of different ages would provide new insight into tissue-specific secreted proteins during aging.

Here we characterize age-regulated *C. elegans* intestinal secretory-pathway proteins *in vivo* by leveraging engineered proximity labeling proteins to label proteins in a tissue- and compartment (ER)-specific manner, followed by quantitative proteomics. This resource uncovers a previously uncharacterized secreted phosphatase (ACP7) and a secretory vesicle protein (Vesicle-Associated Membrane Protein-Associated Protein A (VAPA)) involved in the regulation of lifespan. Our study systematically maps changes to intestine secretory pathway proteins during aging, including secreted proteins, and highlights secreted enzymes associated with lifespan regulation.

RESULTS

A toolkit for capturing age-regulated intestinal secretory-pathway proteins *in vivo*

We sought to systematically and specifically capture secreted proteins from the *C. elegans* intestine. The majority of proteins that are destined for secretion into the extracellular space transit through the ER (Figure 1A). We therefore used a proximity labeling protein (TurboID, codon-optimized for *C. elegans*[48]) targeted to the ER of intestinal cells to label proteins along the intestine secretory pathway, including secreted proteins—the "secretome"[2,26,27,50,51] (Figure 1B). To target TurboID to the ER, we added both an ER signal peptide and an ER retention peptide (KDEL) (TurboID-ER) (Figure 1C). As a comparison control for subcellular localization, we used TurboID without any ER localization or retention signals to allow cytoplasmic localization (TurboID-Cytoplasm)[48] (Figure 1C). Both TurboID-ER and TurboID-Cytoplasm proteins were tagged with HA tags (Figure 1C). We generated stable *C. elegans* strains to express TurboID-Cytoplasm and TurboID-ER in intestinal cells with the pan-intestine *ges-1* promoter (*ges-1p*) (Figure 1C).

We first validated the tissue expression and subcellular localization of the intestine TurboID-expressing strains. To this end, we crossed the intestine TurboID-expressing strains to a strain with the *vha-6* promoter (*vha-6p*) driving the expression of GFP fused to an ER-localized protein (SP12) (GFP-ER) in the intestine (along with the germline and hypodermis).[56] Immunofluorescence staining using antibodies against the HA tag showed that at the cellular level, intestine TurboID-Cytoplasm and TurboID-ER were indeed expressed in intestine cells of *C. elegans*, similar to the intestine GFP-ER reporter (Figures 1D–1F). At the subcellular level, intestine TurboID-Cytoplasm showed a relatively smooth cytoplasmic-like pattern (Figures 1E and S1A) whereas intestine TurboID-ER showed a web-like pattern similar to the GFP-ER reporter, which is characteristic of the ER (Figures 1F and S1A). As an independent validation, we generated strains expressing the fluorescent protein WormScarlet in the intestine with the same ER signal peptide and retention peptide and found that ER-localized WormScarlet showed a similar web-like pattern characteristic of the ER (Figure S1B). These results indicate that TurboID-Cytoplasm and TurboID-ER are expressed in the *C. elegans* intestine and are localized to their respective

TurboID strains than in the N2 control. Intestine TurboID-Cytoplasm and TurboID-ER are expressed at all ages, as shown by western blot with anti-HA antibody. An antibody against Tubulin is used as a loading control.

(H) Schematic of the quantitative mass spectrometry workflow. For each strain (N2 control, intestine TurboID-Cytoplasm, and intestine TurboID-ER), samples are collected at three ages: young (adult day 1, 3 days post hatch), middle-age (adult day 5, 8 days post hatch), and old (adult day 10, 13 days post hatch). Several independent biological replicates (n = 2 for N2 control, n = 4 for intestine TurboID-Cytoplasm strain, and n = 4 for intestine TurboID-ER strain), each comprising ~200,000 worms, are generated, each in separate cohorts. Whole-worm lysates are extracted, biotinylated proteins are pulled down using streptavidin beads, and the samples are trypsin-digested. Peptides are tagged with tandem mass tags (TMTs) to enable comparison between different conditions (young, middle-age, old), and mass spectrometry is performed for quantitative proteomics.

(I) Principal component analysis (PCA) of the intestine TurboID-Cytoplasm samples and TurboID-ER samples shows separation by compartment (Cytoplasm vs. ER) across all ages (young, middle-age, old). For differences with age, see Figures 3A and S3A.

(J) Principal component analysis (PCA) of the young intestine TurboID-Cytoplasm samples and TurboID-ER samples shows separation by compartment (cytoplasm vs. ER) at a young age.

(K) Compartment analysis for TurboID-ER and TurboID-Cytoplasm in young intestine. Volcano plot shows the fold change and significance of the TurboID-ER compartment proteins compared to the TurboID-Cytoplasm compartment proteins. Proteins with a positive fold change ($Log_2(FC) > 0$) signify proteins that are more abundant in the TurboID-ER compartment as compared to the TurboID-Cytoplasm compartment, and vice versa for negative fold change ($Log_2(FC) < 0$), indicating proteins that are more abundant in the TurboID-Cytoplasm compartment as compared to the TurboID-ER compartment. The blue and orange lines signify the fold change and p value cutoffs used to generate high-confidence TurboID-Cytoplasm enriched (orange) or high-confidence TurboID-ER enriched (blue) protein lists (see STAR Methods for details). Gray dots within these lines indicate a protein that fits these criteria but is categorized as not expressed in the appropriate tissue. Unique proteins (proteins found in only one compartment) are on the extreme left or right of the plot. The number of high-confidence proteins in each compartment is indicated at the top.

(L) Pie charts denote the tissue expression of the intestine (green)—the percentage of identified proteins that have their transcripts expressed in their respective tissues.

(M) Pie charts show each compartment's subcellular protein localization. Figure legend at the bottom denotes what each color represents.

subcellular compartments (cytoplasm or ER) (see also Figures 1I–1M and S1F–S1J for direct compartment specificity analysis).

TurboID is a promiscuous biotin ligase that adds biotin molecules to neighboring proteins.[57] To determine if intestine TurboID-Cytoplasm and TurboID-ER biotinylate proteins *in vivo* in adult animals, we performed a western blot on protein samples from worms of different ages expressing these proteins, and we used streptavidin to detect biotinylated proteins. Samples from *C. elegans* strains expressing TurboID-Cytoplasm and TurboID-ER in the intestine exhibited more biotinylated proteins compared to samples from wild-type (N2) control animals (there was some background biotinylation in control animal samples, likely from natively biotinylated proteins) (Figure 1G). Intestine TurboID-Cytoplasm and TurboID-ER could biotinylate proteins in young, middle-aged, and old animals (Figure 1G). Interestingly, intestine TurboID-Cytoplasm and TurboID-ER samples displayed several different biotinylated proteins, suggestive of compartment specificity (Figure 1G, see also Figures 1I–1M and S1F–S1J for direct compartment specificity analysis).

Together, these results indicate that proximity labeling tools targeted to different subcellular compartments in the intestine can successfully label proteins *in vivo.* In addition, this labeling works in animals of different ages, enabling analysis of the aging intestinal secretome.

Systematic and quantitative assessment of the intestinal secretome

To systematically and quantitatively characterize age-dependent intestinal secretory-pathway proteins, we used tandem mass tag (TMT) mass spectrometry. We generated protein samples from the intestine TurboID-Cytoplasm and TurboID-ER strains (as well as wild-type worms as a negative control) at three different ages—young (3 days post hatch), middle-age (8 days post hatch), and old (13 days post hatch) (Figure 1H). For each condition, we generated 4 independent biological samples (over 4 independent cohorts), each containing ~200,000 individual worms for TurboID strains (and 2 independent biological samples for control wild-type worms) (Figure 1H). To identify TurboID-tagged proteins, we isolated whole-animal protein lysates and performed a pull-down of biotinylated proteins using streptavidin beads (wild-type animals were used to control for native biotinylated background proteins). With this approach, proximity-labeled proteins were isolated from the entire worm lysates rather than fluids, thereby also including proteins along the secretory pathway. While on beads, proteins were trypsin-digested, and TMTs were used to multiplex the resulting peptide samples (Figure 1H, see Table S1A and STAR Methods for the multiplex design). We then performed quantitative mass spectrometry to generate proteomics datasets (Tables S1B and S1E).

We first assessed the quality of these proteomics datasets by examining the correlation between replicates. There was high correlation between replicates for all conditions (r = 0.90–0.99) (Figures S1C–S1E). Principal component analysis (PCA) also showed good separation by subcellular compartments (TurboID-Cytoplasm vs. TurboID-ER) for the intestine (Figures 1I, 1J, and S1F; Table S1F, see STAR Methods for details) dataset. There was also good separation by age in the intestine dataset (see Figures 3A and S3A). Together, these correlations and PCA analyses indicate the high-quality of the proteomics datasets and highlight the separation by subcellular compartment.

We identified proteins that were enriched in the TurboID-Cytoplasm versus TurboID-ER datasets at each age (Figures 1K–1M and S1G–S1J; Table S2A). We verified the tissue expression of the identified proteins using a combination of published transcriptomic datasets[58,59] and WormBase for the corresponding transcripts. We found that nearly 100% of the TurboID-Cytoplasm-enriched and TurboID-ER enriched proteins for intestine were indeed expressed in the intestine, confirming the tissue specificity of our toolkit (Figures 1L and S1H; Table S2A).

Importantly, we verified that the TurboID-Cytoplasm and TurboID-ER enriched proteins exhibited compartment specificity. To that end, we first curated a list of 20 proteins from the intestine cytoplasm (and nucleus)[60–64] and 20 proteins from the intestine secretory pathway (ER, Golgi, and bona fide secreted proteins)[65–69] from the *C. elegans* literature and WormBook.[70] We visualized these proteins in the volcano plot of intestine TurboID-Cytoplasm enriched and TurboID-ER enriched in young animals (Figure S1K; Table S2A). We found that these proteins, notably bona fide secreted proteins such as vitellogenins,[71] were represented in the correct compartments in our dataset (Figure S1K).

To further benchmark our approach, we used the deep-learning tool DeepLoc2.1[72] to annotate the subcellular localization of the identified proteins (Tables S2A and S2B). Consistent with expectations, we found more cytoplasmic proteins in the TurboID-Cytoplasm-enriched dataset and, conversely, more proteins along the secretory pathway (including extracellular/secreted proteins) in the TurboID-ER-enriched dataset (Table S2A). For example, in young intestine, there were 3740 TurboID-Cytoplasm enriched proteins (Log_2(Fold Change) < 0, intestine-expressed), and 60% were predicted to be cytoplasmic; there were 1038 TurboID-ER enriched proteins (Log_2(Fold Change) > 0, intestine-expressed), and 49% were predicted to be in the secretory pathway (24% extracellular, 13% cell membrane and 12% ER) (Table S2C). These data confirm the compartment-specificity of our toolkit.

We next generated high-confidence TurboID-Cytoplasm-enriched and high-confidence TurboID-ER enriched protein lists. For this, we performed a statistical analysis analogous to receiver operating characteristic (ROC) for each compartment—a standard for TurboID analyses[57] (Figures 1K–1M and S1G–S1I) (see STAR Methods for details; optimized Fold Change and p values are in Table S2). These high-confidence TurboID-Cytoplasm-enriched and high-confidence TurboID-ER-enriched proteins are in Tables S2C–S2E and color-coded in the volcano plot (Figures 1K and S1G). For example, in the young intestine, we identified 2673 high-confidence TurboID-Cytoplasm-enriched proteins (orange), of which 62% were predicted to be cytoplasmic. Importantly, in the young intestine, we identified 481 high-confidence TurboID-ER-enriched proteins (blue), of which 68% were predicted to be in the secretory pathway, and 37% were predicted to be bona fide secreted proteins (Figure 1K-right; Table S2C).

CellPress
OPEN ACCESS

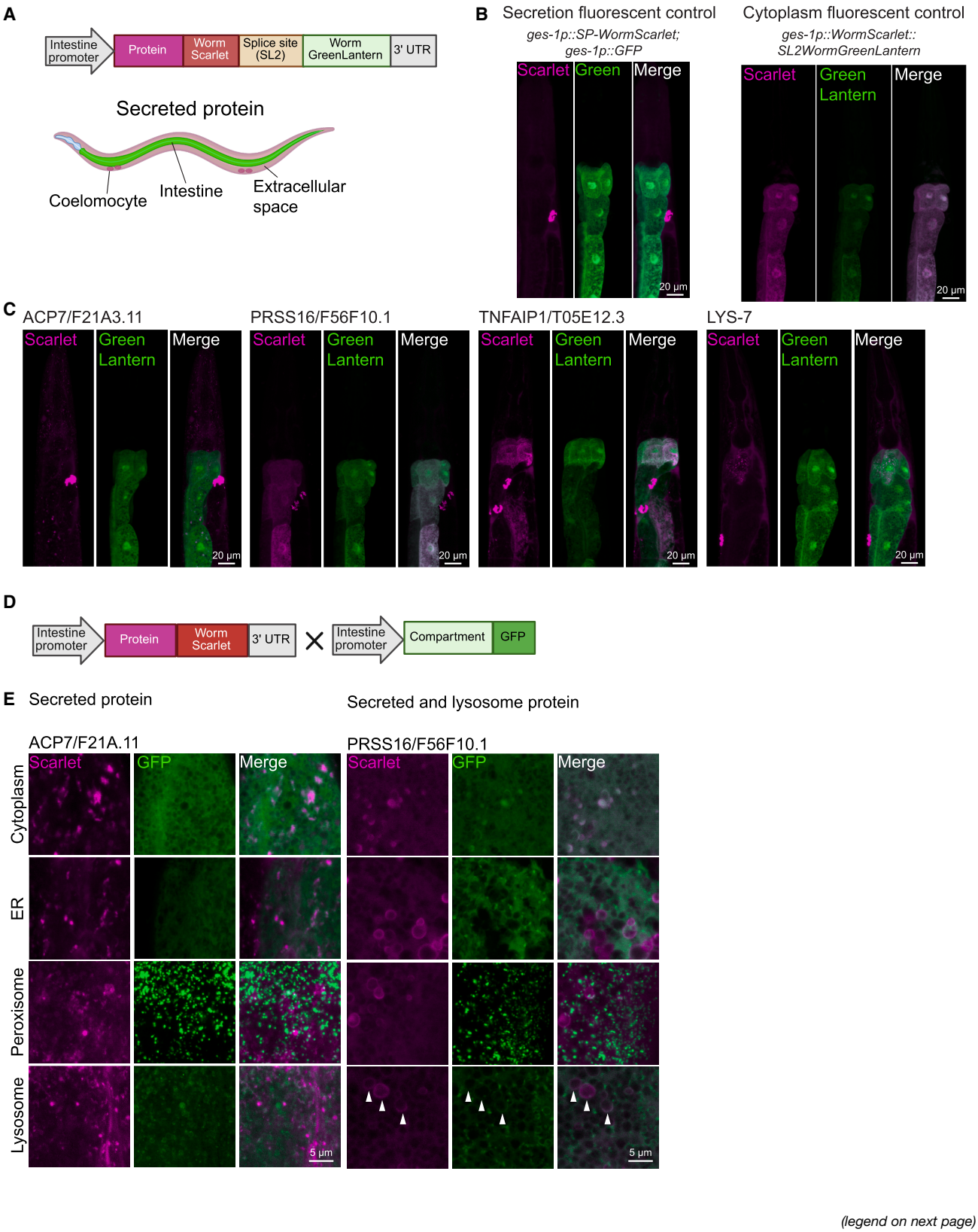

(legend on next page)

We particularly focused on the "secretome"—the extracellular/secreted proteins in the high-confidence TurboID-ER enriched datasets. In the intestine across all ages, we identified a total of 238 extracellular/secreted proteins (Table S2F) (for independent validation of secreted proteins, see Figure 2 later in discussion).

This proteomic dataset represents a high-quality resource for tissue-specific proteins in the secretory pathway, and it enables the identification of secreted proteins that could represent key regulators of the extracellular space during aging.

Validating protein localization *in vivo*

To independently validate the localization of some of the secreted proteins identified by proximity labeling and proteomics, we leveraged the transparent nature of *C. elegans* to perform cell biology experiments *in vivo*. This is important because our TurboID-ER approach uses entire worm lysates (not fluids) and a deep-learning tool to identify secreted proteins. We generated dual reporter transgenic strains with the *ges-1* intestine promoter (*ges-1p*) driving expression of the candidate proteins tagged with the red fluorescent protein WormScarlet followed by an SL2 splice site[10] and a cytoplasmic worm codon-optimized green fluorescent protein (WormGreenLantern)[73] (Figure 2A). In these strains, secretion of a protein from the intestine should result in red fluorescence both in the extracellular space outside the green intestine and within coelomocytes, which are phagocytic cells analogous to macrophages that can engulf extracellular proteins[20,74] (Figure 2A). As a positive control, we verified that secreted WormScarlet (WormScarlet with an ER secretion signal peptide) indeed showed this extracellular and coelomocyte pattern (Figure 2B), whereas WormScarlet without a signal peptide remained inside the intestine (Figure 2B).

We tested two identified secretome proteins (i.e., found in the high-confidence TurboID-ER list and annotated as secreted by DeepLoc2.1) (see Tables S2B, S2F): ACP7/F21A3.11 and LYS7. We also tested PRSS16/F56F10.1 (which was annotated as Lysosome/Vacuole and also extracellular/secreted by DeepLoc2.1) (Table S2B). In addition, we also tested a protein that was identified in both compartments and predicted by DeepLoc2.1 to be both cytoplasmic and ER and also extracellular/secreted (TNFAIP1/T05E12.3). We found that all four proteins tagged with WormScarlet (red fluorescence, colored as magenta) were secreted outside the intestine (green fluorescence) and present in the extracellular space (Figure 2C). They were also found in coelomocytes, which are phagocytic cells functionally akin to macrophages that can engulf secreted proteins (Figure 2C). Interestingly, these proteins also exhibited different localization patterns in the extracellular space, either in the head of the animal (likely extracellular space in the head) (ACP7/F21A3.11, LYS7) or in the body cavity (extracellular space in the body) (ACP7/F21A3.11, LYS7, and TNFAIP1/T05E12.3) (Figure 2C). These *in vivo* experiments independently validated that proximity labeling of the ER compartment, followed by mass spectrometry, indeed identifies proteins from the intestine that are truly secreted into the extracellular space. These proteins were not previously annotated as secreted in WormBase, also highlighting that our secretome dataset could identify key extracellular proteins.

Deeploc2.1[72] predicted some proteins to be both secreted in the extracellular space and localized in organelles (e.g., PRSS16/F56F10.1 in the lysosome) or in the ER and cytoplasm (e.g., TNFAIP1/T05E12.3). To test the localization of secreted proteins to other compartments, we crossed *C. elegans* strains expressing WormScarlet-tagged secretome proteins in the intestine with strains expressing compartment-specific marker proteins (e.g., lysosome protein [GLO1], peroxisome protein [PTS1], and so forth) tagged with GFP in the intestine (Figure 2D). For localization in the intestinal cytoplasm, we used the dual reporter strains (secretome protein tagged with WormScarlet and WormGreenLantern expressed in the intestinal cytoplasm). We found that PRSS16/F56F10.1 was not only secreted but also colocalized with lysosomes (Figure 2E). TNFAIP1/T05E12.3 was both secreted from the intestine and present in the intestine cytoplasm (and to some extent in the ER) (Figure S2A). In contrast, ACP7/F21A3.11 and LYS-7 were exclusively secreted and not found in other intracellular compartments tested (Figures 2E and S2A), suggesting that these proteins could act entirely in the extracellular space.

Figure 2. Validating secretion and compartment localization *in vivo* of secretome proteins identified by proximity labeling and mass spectrometry

(A) Scheme of *C. elegans* strains used to identify secreted proteins *in vivo*. An intestine-specific *ges*-1 promoter (*ges-1p*) is used to drive the expression of a candidate protein tagged with WormScarlet for visualization of the candidate protein. This is followed by a splice site (SL2) and WormGreenLantern, which allows the visualization of the intestine cytoplasm, facilitating the observation of whether a protein is secreted (i.e., observed outside the green intestine).

(B) Control dual reporters of a secreted WormScarlet and non-secreted WormScarlet with either GFP or WormGreenLantern expressed in the intestine. Scale bars, 20 μm. For the secreted WormScarlet, Wormscarlet was fused to a well-annotated signal peptide (signal peptide from F21A3.11/ACP7, see STAR Methods). This secreted WormScarlet (SP-WormScarlet) can be seen outside the green intestine concentrated in coelomocytes. In contrast, the expression of WormScarlet without a signal peptide stays within the intestinal cytoplasm.

(C) Representative fluorescence images validating secretome proteins identified by proximity labeling and mass spectrometry: ACP7/F21A3.11, PRSS16/F56F10.1, and LYS-7. ACP7/F21A3.11 and LYS-7 were predicted to be extracellular/secreted by DeepLoc2.1 PRSS16/F56F10.1 was predicted to be lysosome and extracellular by Deeploc2.1. TNFAIP1/T05E12.3 (predicted to be both extracellular/secreted and in the cytoplasm) was also validated. Secretome proteins are tagged with WormScarlet and shown in magenta. Note that TNFAIP1/T05E12.3 is also expressed in the intestine cytoplasm/ER (see Figure S2A). *C. elegans* intestine is visualized in green via WormGreenLantern. Scale bars, 20 μm.

(D) Scheme of *C. elegans* strains used to identify compartment localization of candidate proteins *in vivo*. An intestine-specific *ges*-1 promoter is used to drive the expression of a candidate protein tagged with WormScarlet for visualization. This strain is then crossed into different organelle reporter strains that express a compartment-localized protein (cytoplasm, ER, peroxisome, lysosome) tagged with GFP in the *C. elegans* intestine (driven by the *ges-1* or *vha-6* promoters).

(E) Representative fluorescence images identifying potential subcellular compartments for secretome proteins. ACP7/F21A3.11 is secreted and not found in any organelles tested. PRSS16/F53F10.1 is secreted and found in lysosomes (white arrowheads). The cytoplasm or secretome proteins are in magenta, and the compartments (cytosol, endoplasmic reticulum, peroxisome, and lysosome) are in green. Scale bars, 5 μm.

CellPress
OPEN ACCESS

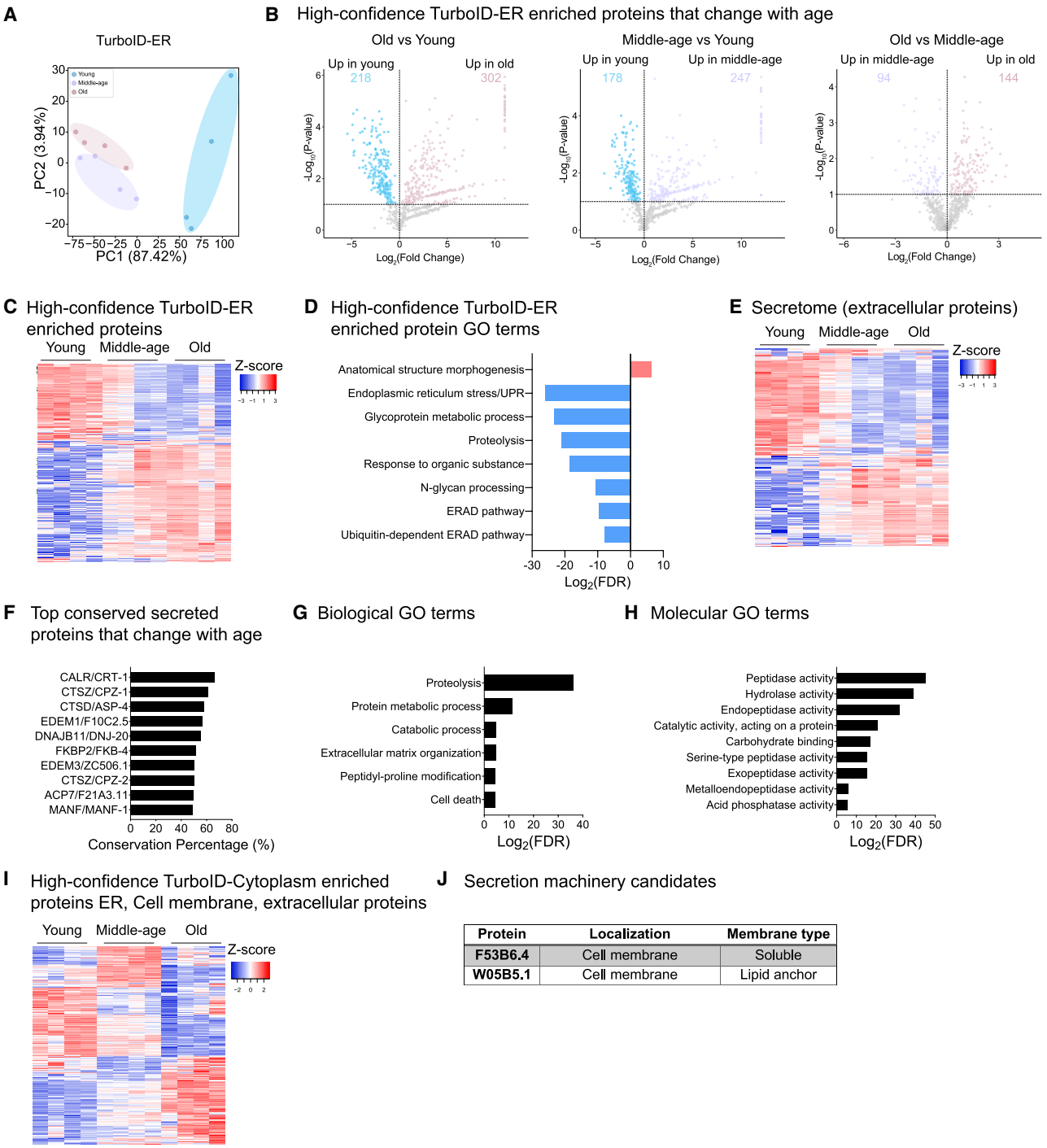

Protein	Localization	Membrane type
F53B6.4	Cell membrane	Soluble
W05B5.1	Cell membrane	Lipid anchor

Figure 3. Identifying intestine secretome proteins that change with age

(A) PCA of the intestine TurboID-ER proteome samples across different ages. Blue – young, purple – middle-age, and red – old.

(B) Volcano plots for the pairwise comparison of the intestine TurboID-ER-enriched compartment of proteins that change with age. Blue dots: proteins that significantly changed in young, purple dots: proteins that significantly changed in middle-age, and Red dots: proteins that significantly changed in old. Values at the top of each volcano plot denote the number of significantly changed proteins increasing in abundance for a denoted age. A protein is considered significantly changed if it has a p value less than 0.1. p values calculated by a two-sided Welch's t test.

(C) Heatmap of the intestine high-confidence TurboID-ER enriched proteins that significantly change with age (p value <0.1) across all three ages.

(D) Biological GO term analysis of intestine high-confidence TurboID-ER enriched proteins that significantly increase in abundance (red) or decrease in abundance (blue) with age (p value <0.1, pairwise for old vs. young).

(legend continued on next page)

Together, these results show that the localization of 4 out of 4 new proteins identified to be secreted by quantitative proteomics (and annotation) could be independently validated as indeed secreted outside the intestine by *in vivo* cell biology. These results indicate that while we still need to rely on DeepLoc2.1 annotation of the TurboID-ER dataset for localization of proteins (because it is technically challenging to isolate fluids in *C. elegans*), this approach can identify bona fide secreted proteins.

Identifying conserved intestine secreted proteins that change with age

The intestine is a highly conserved tissue that secretes a number of proteins[75–78] and is important for organismal health and lifespan.[10,20,79–83] However, the secreted proteins that change with age in the intestine remain largely unknown. Using our datasets, we systematically examined how the intestinal secretome (and other proteins along the secretory pathway) are remodeled during aging. We verified that there was good separation between ages, particularly young vs. middle-age and young vs. old, in the TurboID-ER total dataset using PCA (Figure 3A; Table S3A).

To characterize the proteins that significantly change with age, we compared protein levels between young, middle-age, and old animals in the high-confidence TurboID-ER enriched dataset, defining proteins with $p < 0.1$ in any pairwise comparison as significantly changing with age (Figures 1J, 3B, and S1F; Table S3B). We verified that the proteins that change with age still exhibited a similar percentage of proteins along the secretory pathway, including secreted/extracellular proteins (Figure S1J; Table S3B). A heatmap of all the high-confidence TurboID-ER-enriched proteins that significantly change with age showed many proteins along the secretory pathway both increasing and decreasing in abundance with age (Figure 3C). GO term analysis (Old vs. Young) indicated that high-confidence TurboID-ER enriched proteins that increased in abundance with age were involved in general terms such as "anatomical structure morphogenesis" and "muscle structure" (Figure 3D, red; Table S3C). High-confidence TurboID-ER enriched proteins that decreased in abundance with age were enriched for pathways such as unfolded protein response and proteolysis (Figure 3D, blue; Table S3C).

We were particularly interested in how the intestine secretome changes with age, with the goal of identifying conserved secreted proteins that could extend lifespan. A heatmap of the high-confidence age-dependent TurboID-ER enriched proteins that were predicted to be secreted (191 proteins total) showed 90 proteins that were more abundant with age and 101 proteins that were less abundant with age (young vs. old) (Figure 3E). An example of a secreted protein that increases in abundance with age is vitellogenin (VIT-3), which is part of a well-known family of secreted proteins that is known to increase in abundance with age[36,84,85] (see also Figure S1K). The list of secreted proteins that change with age also encompassed interesting proteins: LYS-7 (C02A12.4) (extracellular, defense response lysozyme) and PRSS16/F56F10.1 (extracellular and lysosome, a peptidase involved in innate immunity[35]). Out of the age-changed secreted proteins, 89 (47%) were conserved in humans (Figure 3F; Table S3D). The top 10 highest sequence-conserved proteins encompass 2 proteins that were increased in abundance with age (CTSD/ASP-4 and ACP7/F21A3.11) and 8 proteins that were decreased in abundance with age (e.g., CALR/CRT-1, CTSZ/CPZ-1, MANF/MANF-1). Some of these proteins (ACP7/F21A3.11 and MANF/MANF-1) were not just enriched but, in fact, unique to the TurboID-ER dataset, suggesting very high compartment specificity (Figure 3F; Table S3D). Interestingly, ACP7/F21A3.11 is a predicted protein phosphatase[86–88] and MANF/MANF-1 is a neurotrophic factor involved in metabolic diseases such as diabetes[89] (Figure 3F). These results reveal interesting, secreted proteins that change with age, including potential secreted enzymes (for functional validation of ACP7, see Figure 4 later in discussion).

GO term analysis of the conserved secretome with age were associated with proteolysis, metabolic process, extracellular matrix organization, and cell death (Figure 3G; Table S3E). Interestingly, almost all of the identified terms were associated with enzymatic functions such as peptidase, hydrolase, metalloendopeptidase, and acid phosphatase activity (Figure 3H; Table S3E). This observation raises the intriguing possibility that enzymatic regulation of the extracellular space is altered with age.

Finally, we characterized proteins that change with age in the intestine high-confidence TurboID-Cytoplasm enriched dataset. These proteins also show separation with age via PCA (Figures S3A–S3D; Tables S3F–S3H). We verified that the high-confidence TurboID-Cytoplasm-enriched proteins that change with age still exhibited a similar percentage of cytoplasmic and nuclear proteins (61.23% cytoplasmic and 18.77% nuclear), as expected. GO term analysis indicated that high-confidence TurboID-Cytoplasm proteins that change with age were involved in cellular pathways such as ribosome biogenesis (Figures S3C and S3D). Given our interest in proteins along the secretory pathway, we focused on the small number of annotated "Cell Membrane" proteins that were unique to the TurboID-Cytoplasm compartment and changed with age (25 proteins)

(E) Heatmap of only the extracellular/secreted intestine high-confidence TurboID-ER enriched proteins that significantly change with age (p value <0.1) across all three ages.
(F) Ranking of the top 10 extracellular/secreted candidates by sequence conservation to human. ACP7 and MANF were uniquely found in the intestine high-confidence TurboID-ER-enriched protein dataset (these proteins were not found in the TurboID-Cytoplasm dataset).
(G) Biological GO term analysis of only the extracellular/secreted intestine high-confidence TurboID-ER enriched proteins that significantly change with age.
(H) Molecular GO term analysis of only the extracellular/secreted intestine high-confidence TurboID-ER enriched proteins that significantly change with age.
(I) Heatmap of only the ER, cell membrane, and extracellular/secreted proteins from the intestine high-confidence TurboID-Cytoplasm enriched dataset that significantly change with age (p value <0.1) across all three ages.
(J) List of intestine high-confidence TurboID-Cytoplasm-enriched proteins that are predicted to be cell membrane proteins and either classified as soluble or lipid anchor. Two proteins were identified: F53B6.4, which has similarities with human Vesicle-Associated Membrane Protein-Associated Protein A (VAPA), and W05B5.1, which has no similarities to any human protein.

CellPress
OPEN ACCESS

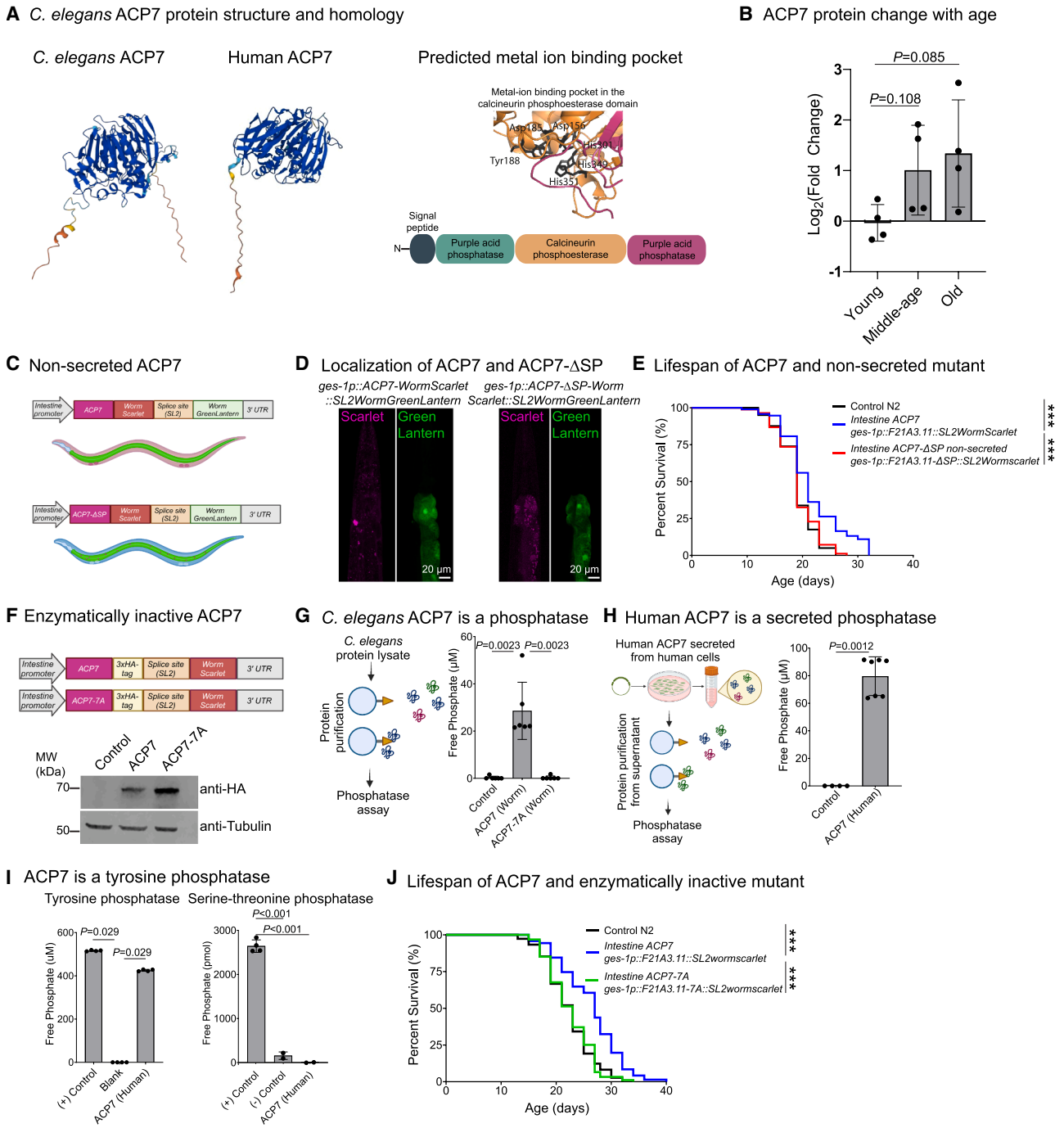

Figure 4. ACP7 is a phosphatase whose overexpression extends lifespan in a secretion- and enzymatic-activity-dependent manner

(A) Left: 3D protein structure of *C. elegans* and human ACP7 predicted from AlphaFold. Right, top panel: PyMOL model 3D protein structure of C. elegans ACP7 metal-ion binding pocket within the calcineurin phosphoesterase domain, which encompasses 7 residues that are conserved and predicted to be important for metal-ion binding, potentially required for ACP7 enzymatic activity. Right, bottom panel: *C. elegans* ACP7 domains, including a signal peptide (dark blue), two purple acid phosphatase domains (green and pink), and a calcineurin phosphoesterase domain (orange).

(B) ACP7 protein levels increase with age. Quantitative mass spectrometry results of Log_2(fold change) of ACP7 in young, middle-aged, and old ages. Bar plot representing mean ± standard deviation. Each dot represents a sample obtained in an independent biological experiment (n = 4 samples/experiments, each composed of ~200,000 worms). p values calculated by one-way ANOVA.

(C) Schematic for the generation of *C. elegans* strains driving overexpression of wild-type secreted ACP7 and a mutant of ACP7 that is not secreted (ACP7-ΔSP) from the intestine *ges-1* promoter (*ges-1p*). ACP7 is tagged with WormScarlet for visualization of ACP7 localization. This is followed by a splice site (SL2) and WormGreenLantern, which allows visualization of the intestinal cytoplasm to determine whether ACP7 is secreted (i.e., observed outside the green intestine).

(legend continued on next page)

as some of these could also be part of the secretory pathway (but labeled from the cytoplasmic side by TurboID-Cytoplasm) (Figure 3I; Tables S3G and S3I). While most of these 25 proteins were classified as transmembrane proteins, two proteins were also considered soluble or lipid anchors: F53B6.4 and W05B5.1 (Figure 3J). While W05B5.1 had no similarities to human proteins, F53B6.4 had some sequence and structural similarity to human VAPA (22% sequence similarity to the MSP domain, 18% overall structural similarity). Human VAPA is generated in the cytoplasm but is known to associate with the ER and secretory vesicles,[90] raising the possibility that *C. elegans* F53B6.4 could be labeled by TurboID-Cytoplasm (for localization and functional validation of F53B6.4, see Figures S6 and S7 later in discussion).

Together, these results provide a high-confidence resource of proteins that change with age in a compartment-specific manner. This resource highlights both secreted proteins and proteins along the secretion pathway that are remodeled during aging.

ACP7 is a conserved secreted protein whose overexpression extends lifespan in a secretion-dependent manner

Acid phosphatase 7 (ACP7/F21A3.11) is a secreted candidate regulator of aging identified in the aging intestine secretome dataset and validated *in vivo*. ACP7 belongs to a family of phosphatases with a metal-ion binding pocket that is highly conserved across species, including in humans.[86,88,91] Indeed, human ACP7 shares both sequence and structural homology with *C. elegans* F21A3.11 (Figure 4A), including a signal peptide at the N terminus, two phosphatase domains, and a calcineurin phosphoesterase domain containing a metal-ion binding pocket (Figures 4A and S4A). Moreover, human ACP7 is present in human fluids (blood, cerebrospinal fluid) in existing datasets.[28,34]

Our quantitative mass spectrometry data in *C. elegans* showed that ACP7 protein increased in overall abundance between young and middle-age worms, and that this is further increased in old age (Figure 4B). Consistently, *ACP7*/F21A3.11 transcripts also increased in overall abundance with age, as shown by reverse transcription followed by quantitative polymerase chain reaction (RT-qPCR) (Figure S4B), although these methods do not specifically assess how the secreted form of ACP7 changes with age.

We next used the power of *C. elegans* to test the functional importance of ACP7 in organismal lifespan. To this end, we generated a transgenic strain overexpressing the secreted wild-type ACP7 protein driven by the *ges-1* intestine promoter (Figure 4C). Overexpression of secreted ACP7 resulted in significant lifespan extension (10% lifespan extension at 50% survival and 22% lifespan extension at 10% survival) (Figure 4E). RNAi-based knockdown of ACP7 did not shorten lifespan (Figures S4C and S4D), perhaps because of the presence of other ACP family members. The lifespan extension of ACP7-overexpressing worms, coupled with the increase in overall ACP7 transcript and protein with age, suggests that this increase could be a compensatory mechanism during aging.

An important question is whether the secretion of ACP7 is critical for lifespan extension by ACP7 overexpression. We generated a strain overexpressing a non-secreted form of ACP7 by deleting the signal peptide (first 21 amino acids) of ACP7 (ACP7-ΔSP) (Figure 4C). We verified that this signal peptide deletion resulted in a form of ACP7 (tagged with WormScarlet) that remained inside the intestine and was not secreted (Figure 4D). In contrast to overexpression of secreted ACP7, overexpression of the non-secreted mutant of ACP7 no longer extended lifespan (Figure 4E). These results indicate that lifespan extension by ACP7 overexpression requires the secretion of ACP7 in the extracellular space. Thus, ACP7 is a

(D) Representative fluorescence images showing ACP7 tagged with WormScarlet (magenta) is secreted from the intestine (green), while the non-secreted mutant of ACP7 (ACP7-ΔSP) is not secreted from the intestine (i.e., magenta-ACP7 stays within the green intestine). Scale bars, 20 μm.

(E) Overexpression of secreted ACP7 extends lifespan, while overexpression of non-secreted ACP7 (ACP7-ΔSP) does not extend lifespan. $n \geq 100$ worms for each condition. p values calculated with Log rank (Mantel-Cox) test. *** denotes $p < 0.001$. Representative of 3 independent experiments (see source data for additional experiments).

(F) Top panels: Schematic for the generation of *C. elegans* strains driving expression of wild-type secreted ACP7 and a mutant of ACP7 that has 7 amino acids changed to alanines (7A) in the metal-binding pocket (ACP7-7A) expressed in the intestine using the *ges-1* promoter (*ges-1p*). Both proteins are tagged with a 3xHA-tag. Bottom panels: western blot shows whole-worm lysate of control (N2), ACP7, and ACP7-7A strains (young adults). ACP7 protein visualized using anti-HA antibodies. An antibody against Tubulin is used as a loading control.

(G) Left panel: Schematic of phosphatase assay from *C. elegans* lysates. Lysates from *C. elegans* strains expressing ACP7 or ACP7-7A were obtained, and a bead pull-down of native ACP7 or ACP7-7A from *C. elegans* was performed using anti-HA antibodies. Control is lysate from N2 *C. elegans* subjected to the same bead pull-down. Right panel: Phosphatase assay shows that *C. elegans* ACP7 has phosphatase activity, while the mutant ACP7-7A does not have phosphatase activity. Dot plot represents mean ± standard deviation. Each dot represents a phosphatase reaction assay for a sample of ∼1000 worms. $n = 6$ samples, combined over 2 independent experiments. p values calculated by Mann-Whitney.

(H) Left panel: Schematic of phosphatase assay from human cell supernatant. Supernatant from human Expi293F cells expressing human ACP7 was obtained, and a pull-down of human ACP7 was performed using HisPur Ni-NTA resin from the supernatant. Right panel: Phosphatase assay shows that human ACP7 has phosphatase activity. Control is reaction buffer. Dot plot represents mean ± standard deviation. Each dot represents a phosphatase reaction assay for a sample, $n = 4$ (control) and $n = 7$ (human ACP7) samples, combined over 2 independent experiments. p values calculated by Mann-Whitney.

(I) Left panel: Phosphatase assay shows that human ACP7 has tyrosine phosphatase activity. Positive (+) Control is alkaline phosphatase. Right panel: Phosphatase assay shows that human ACP7 does not have serine-threonine phosphatase activity. Positive (+) Control is alkaline phosphatase and negative (−) control is ACP7 with no substrate. Dot plot represents mean ± standard deviation. Each dot represents a phosphatase reaction assay for a sample. Tyrosine phosphatase assay: $n = 4$ for all samples. Serine-threonine phosphatase assay: $n = 4$ (control), $n = 2$ negative control, and $n = 2$ human ACP7. p values calculated by Mann-Whitney.

(J) Overexpression of ACP7 extends lifespan, whereas the secreted but enzymatically inactive mutant of ACP7 (ACP7-7A) is not able to extend lifespan. $n \geq 80$ worms per condition. p values calculated with Log rank (Mantel-Cox) test, *** denotes $p < 0.001$. Three independent experiments (see Source Data).

conserved extracellular protein that can extend lifespan when overexpressed and secreted from the intestine.

ACP7 functions as a phosphatase, and lifespan extension by ACP7 overexpression requires an enzymatically active phosphatase

ACP7 has two phosphatase domains and a calcineurin domain that contains a predicted metal-ion binding pocket (see Figure 4A). To test if *C. elegans* ACP7 acts as a phosphatase, we generated a transgenic *C. elegans* strain expressing HA-tagged ACP7 protein driven by the *ges-1* promoter (Figure 4F). Using this strain, we pulled down the HA-tagged ACP7 protein from whole-worm lysate and measured phosphatase activity using the 6,8-difluoro-4-methylumbelliferyl phosphate (DiFMUP) substrate. We observed phosphate release when ACP7 was incubated with this substrate (Figure 4G), indicating that *C. elegans* ACP7 can act as a phosphatase.

As *C. elegans* and human ACP7 share close sequence homology, we asked whether the human ACP7 protein can also act as a phosphatase. We expressed human ACP7 in human Expi293F cells.[92] We purified His-tagged human ACP7 protein from the supernatant of Expi293F cells using Ni^{2+} affinity chromatography (Figures 4H and S4E, see STAR Methods) and tested its phosphatase activity using the same phosphatase assay. Similar to *C. elegans* ACP7, human ACP7 was both secreted (i.e., present in the cell supernatant) and exhibited phosphatase activity (Figure 4H). Interestingly, human ACP7 exhibited phosphatase activity toward tyrosine residues but not serine/threonine residues (Figure 4I), indicating that ACP7 is a tyrosine phosphatase.

We computationally predicted tyrosine-phosphorylated proteins in the extracellular space that could be potential substrates of ACP7. Using NetPhos3.1, we found that 28 conserved proteins secreted from the intestine have a high probability of being phosphorylated on several tyrosine residues (e.g., AMY2A, EDEM3, and the collagen protein COL6A3) (see STAR Methods for details) (Table S4A). Some of these conserved proteins could represent extracellular ACP7 substrates both in *C. elegans* and humans.

Is the phosphatase activity of ACP7 important for its ability, when overexpressed, to extend lifespan in *C. elegans*? Other phosphatases with metal-ion binding pockets (e.g., red kidney bean purple acid phosphatase) require the binding of iron or zinc for their phosphatase function.[93] We therefore disrupted the metal-ion binding pocket of *C. elegans* ACP7 by mutating the 7 amino acids that are predicted to act as metal-ion-stabilizing residues into alanines (ACP7-7A) (Figure 4A). We generated a transgenic *C. elegans* to express HA-tagged ACP7-7A driven by the *ges-1* intestine promoter (Figure 4F). Purification of the ACP7-7A mutant protein followed by a phosphatase activity assay revealed that ACP7-7A no longer had any phosphatase activity and was catalytically inactive (Figure 4G). Importantly, ACP7-7A (tagged with WormScarlet) was still secreted because it was observed outside the intestine, in the head region, and in coelomocytes just like wild-type ACP7 (Figure S4F). These experiments identify an ACP7 mutant that is secreted but lacks phosphatase activity, thereby uncoupling secretion from enzymatic function. We used this mutant to test whether ACP7 phosphatase activity is required for lifespan regulation in the context of overexpression. Overexpressing the secreted but phosphatase-inactive variant of ACP7 (ACP7-7A) from the intestine no longer extended lifespan (Figure 4J). These results suggest that lifespan extension by ACP7 overexpression requires an enzymatically active phosphatase, although other catalytic functions of ACP7 could also be involved.

Thus, proximity labeling followed by quantitative proteomics uncovered ACP7, a previously uncharacterized conserved secreted phosphatase that changes with age and acts in the extracellular space to extend lifespan. As ACP7 was below the threshold of detection in other *C. elegans* mass spectrometry datasets,[35,36,42] these results also underscore the power of compartment-specific proximity labeling to discover new secreted proteins impacting longevity. These findings also illustrate the importance of enzymatic activity in the extracellular space for the regulation of lifespan.

ACP7 overexpression impacts several uncharacterized pathways

To identify the downstream pathways regulated by ACP7, we first assessed if ACP7 could induce well-known longevity pathways, such as the insulin/IGF-1-FOXO pathway,[94,95] the autophagy-TFEB/HLH-30 pathway,[96] the p38 MAPK/PMK-1 innate immunity pathway,[97] and the unfolded protein response in the ER[98] and mitochondria[99] (Figure S5A). We crossed the ACP7 overexpressing strain into translational reporter strains for FOXO/DAF-16 (*daf-16p::daf-16a/b::GFP*)[100] and TFEB/HLH-30 (*hlh-30p::hlh-30::GFP*)[96] and transcriptional reporter strains for the p38 MAPK/PMK-1 innate immunity pathway (*T24B8.5p::GFP*[101]), UPR-ER (*hsp-4p::GFP*[102]), and UPR-mitochondria (*hsp-6p::GFP*[4,103]). We found that ACP7 overexpression did not result in the nuclear localization of FOXO/DAF-16 or TFEB/HLH-30, nor did it induce the innate immunity pathway (Figure S5B). Moreover, ACP7 overexpression only slightly regulated the UPR-ER reporter (down) and UPR-mitochondria reporter (up) (Figure S5B). These observations suggest that ACP7 has little effect on these well-established longevity pathways and that it may regulate other downstream pathways.

We unbiasedly identified gene expression pathways that are modulated downstream of ACP7 to gain insight into global phenotypic changes induced by this secreted phosphatase. To this end, we performed RNA-sequencing (RNA-seq) on worm lysates from three different *C. elegans* strains—control, ACP7 overexpression, and ACP7-7A (secreted but catalytically inactive ACP7)—in young adult (3 days post-hatch) in quintuplets (Figure 5A; Tables S5A–S5C). PCA analysis of this RNA-seq dataset showed good separation between the ACP7 overexpression transcriptome and either the control or the ACP7-7A transcriptomes (Figures 5B and S5C; Table S5D).

We next characterized the differentially expressed genes and pathways in ACP7 overexpression vs. control strains. This analysis identified 306 upregulated genes (red) and 26 downregulated genes (blue) in ACP7 vs. control (Log_2(fold change) > or <1, $P_{adj} < 0.05$) (Figures 5C and 5D; Table S5A). Interestingly, GO term analysis revealed that genes upregulated in the ACP7 overexpression strain showed enrichment for several gene expression pathways: protein dephosphorylation, dephosphorylation, and

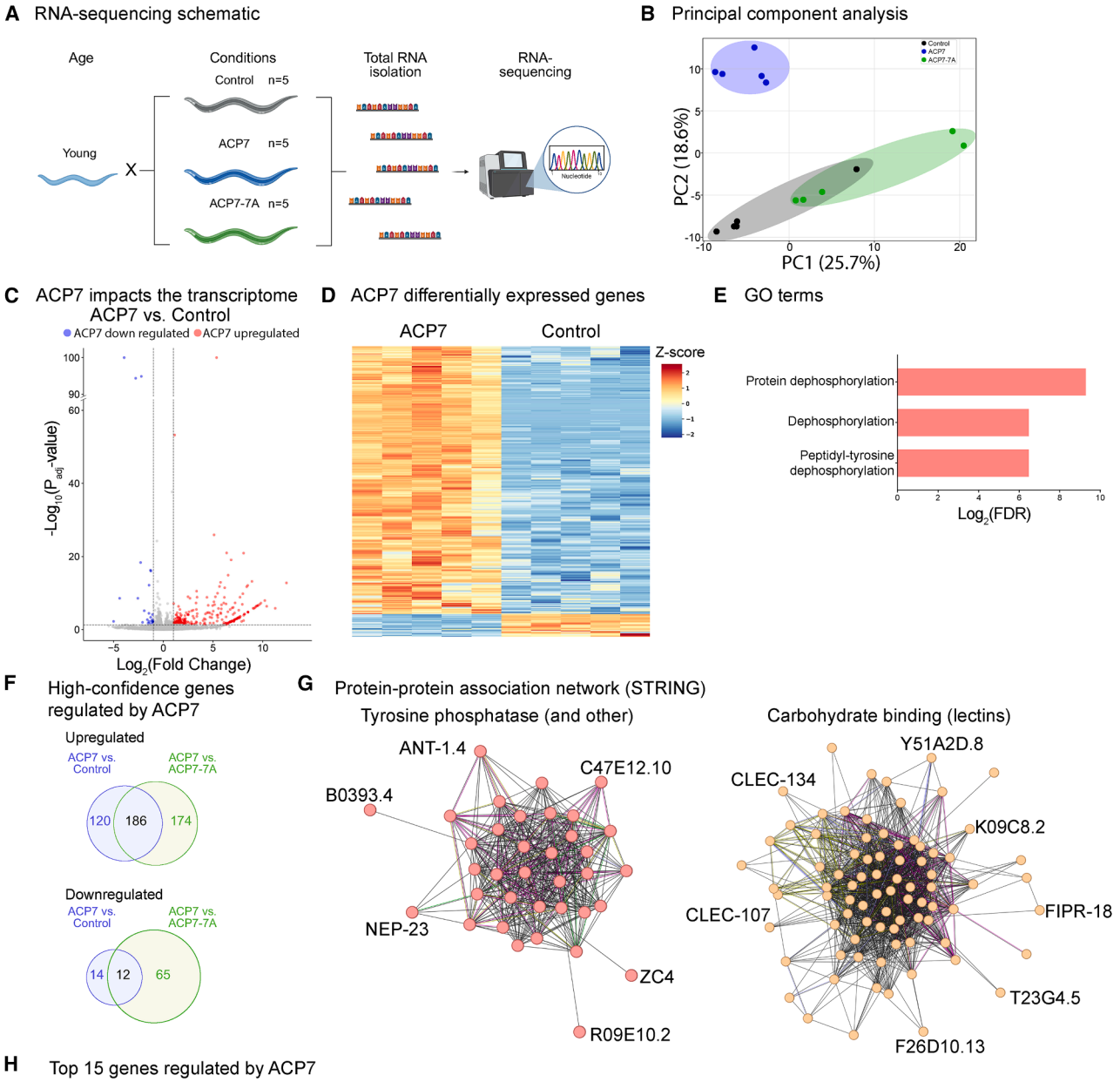

H Top 15 genes regulated by ACP7

Transcript name	Log_2(FC)	$-Log_{10}(P_{adj})$	Tissue	Localization	Protein domain
C38D9.2	-3.94	100.00	Intestine	Cytoplasm|Nucleus	
F15D4.5	-2.21	94.88	Intestine/muscle	Cytoplasm	
F56A4.3	-2.78	94.37	Intestine/neuron	Nucleus	Glutathione S-transferase
C07G3.9	1.13	53.21	Intestine/muscle /germline	Endoplasmic reticulum	Glycogen phosphorylase
ZK39.8	5.10	25.94	Germline	Extracellular	C-type lectin
F09C6.10	6.37	21.00	Neuron	Extracellular	
T10D4.4	8.07	20.95	Coelomocyte	Extracellular	Insulin related peptide beta
C50F4.3	6.81	19.04	Germline	Extracellular	Cysteine protease
Y19D10A.9	-1.29	16.20	Intestine/neuron	Extracellular	C-type lectin
F56A4.2	-1.26	16.00	Intestine	Extracellular	
F26D2.16	6.52	14.85	-	Extracellular	Membrane lipoprotein lipid
F36F12.6	8.91	13.15	Neuron/germline	Extracellular	C-type lectin
M151.10	5.75	12.89	-	Extracellular	
F15D4.6	-1.44	12.12	Neuron/germline	Cytoplasm|Extracellular	
K12H6.9	8.48	12.05	Germline	Extracellular	

(legend on next page)

peptidyl-tyrosine dephosphorylation, while there were no enriched GO terms for the downregulated genes (Figure 5E; Table S5E). Thus, overexpression of ACP7—an extracellular phosphatase—impacts several phosphate-related gene expression pathways in worms, consistent with the findings that other ACP family members in plants[104] and mammals[105] regulate overall phosphate levels.

To identify specific high-confidence genes regulated by ACP7, we examined the overlap between genes upregulated by ACP7 vs. control and ACP7 vs. ACP7-7A (Figures 5F and S5D–S5F). There were 186 upregulated genes that overlapped between ACP7 vs. control and ACP7 vs. ACP7-7A. There were 12 downregulated genes that overlapped between ACP7 vs. control and ACP7 vs. ACP7-7A (Table S5F). Notably, 66% of these high-confidence genes, including many of the top regulated genes, were predicted to encode extracellular proteins (Figures 5G and 5H; Table S5G). STRING analysis indicated that the proteins encoded by these genes were involved in phosphorylation and carbohydrate-binding (lectin) pathways (Figures 5G and 5H; Table S5G). These observations raise the possibility that ACP7 could influence several pathways involved in extracellular phosphate and carbohydrate homeostasis.

Together, the combination of reporter and transcriptomics data indicates that ACP7 is unlikely to act via several well-known longevity pathways (although we have not exhaustively tested all pathways), but that it may affect phosphate and carbohydrate binding metabolism.

Systematic evaluation of secretome and secretory pathway proteins regulating lifespan

Are other secretome or secretory pathway proteins that change with age affecting lifespan? We performed a targeted RNAi knockdown screen for lifespan on 17 additional proteins from our proteomics datasets (Figure 6A). We selected these 17 candidates based on significant changes with age: 6 of them (TNFAIP1/T05E12.3, BMPER/VIT-5, TTR/TTR-51, ULE-1, LRO-1, and LYS-7) significantly increased with age ($p < 0.05$) and 9 of them (VAPA/F53B6.4, PRSS16/F56F10.1, RCN2/CALU-2, F21H7.5, REN/ASP-1, PGC/ASP-2, ECE-1/NEP-22, CTSB/CPR-5, and F10G2.1) significantly decreased with age ($p < 0.05$) (Table S6A). Two of them (FCGBP/VIT-3 and VIT4) significantly changed with age but were not found in the TurboID-ER-enriched dataset, as they were identified in both TurboID-ER and TurboID-Cytoplasm (Figure S1K) and were known to regulate lifespan[95,106] (Table S6A). Among these 17 candidates, 10 were predicted to be secreted (VIT-3/FCGBP, VIT-4, VIT-5/BMPER, TTR-51/TTR, ULE-4, ASP-1/REN, CPR-5/CTSB, F10G2.1, LYS-7 and ASP-2/PGC), 2 were predicted to be ER-resident and secreted (T05E12.3/TNFAIP1 and CALU-2/RCN2), 1 was predicted to be in the lysosome and secreted (F56F10.2/PRSS16) and 4 (F53B6.4/VAPA, F21H7.5, NEP-22/ECE-1, LRO-1) were associated with cell membrane or secretory machinery (Table S6A). The secretion of 3 of these proteins (T05E12.3/TNFAIP1, F56F10.1/PRSS16, and LYS-7) was orthogonally validated in Figure 2. Interestingly, 11 of the 17 candidates showed similarities with human proteins, and 4 were predicted or validated to be extracellular enzymes (PRSS16/F56F10.1, REN/ASP-1, CTSB/CPR-5, and PGC/ASP-2) (Table S6A).

By performing a targeted RNAi screen, we found that 6 out of these 17 candidates, when knocked down, extended lifespan (Figures 6A and 6B). These included secreted proteins such as the vitellogenin BMPER/VIT-5 (a known secreted lipid transporter, which has been previously shown to extend lifespan when knocked down[95]), PRSS16/F56F10.1 (a secreted serine protease,[35] validated to be secreted in Figure 2), VIT-4 (another known secreted lipid transporter), TTR/TTR-51 (a known secreted *trans*-thyretin like protein[7]), TNFAIP1/T05E12.3 (a protein involved in protein homo-oligomerization[35] that we validated to be secreted in Figure 2). We also identified VAPA/F53B6.4 (a protein with homology to the vesicle-protein VAPA in humans[107]), as a protein whose knockdown extended lifespan.

VAPA/F53B6.4 knockdown produced the largest extension of lifespan in this targeted screen (Figures 6A and 6B). VAPA/F53B6.4 is a potential secretory vesicle protein found in the cytoplasm, with some structural homology to the vesicle-associated protein VAPA in humans[107] (see Figure 7 later in discussion). We validated that knockdown of *VAPA*/F53B6.4 via RNAi in the whole animal extended lifespan (8% lifespan extension at 50% survival and 18.5% lifespan extension at 10% survival) (Figures 6C and S6C). Knocking down *VAPA*/F53B6.4 via RNAi

Figure 5. ACP7 overexpression remodels the transcriptome

(A) Schematic of the RNA-sequencing workflow. For each strain (control (N2), ACP7 overexpression, and ACP7-7A overexpression), samples are collected at a young age (adult day 1, 3 days post hatch). Five independent biological replicates were generated per condition ($n = 5$ for control (N2), $n = 5$ for ACP7 overexpression strain, and $n = 5$ for ACP7-7A overexpression strain), each comprising ~1000 worms. Total RNA was extracted and sent for RNA-sequencing.

(B) Principal component analysis (PCA) of the transcriptomes of control, ACP7 overexpression, and ACP7-7A overexpression strains. ACP7 overexpression transcriptome shows separation from both control and ACP7-7A overexpression transcriptomes.

(C) Volcano plot of ACP7 vs. control shows changes in gene expression, with genes significantly upregulated by ACP7 overexpression in red (Log_2(fold change) > 1 and $P_{adj} < 0.05$) and genes significantly downregulated by ACP7 overexpression in blue (Log_2(fold change) < −1 and $P_{adj} < 0.05$). Gray dots denote non-significantly changed genes. *p* values calculated by Wald test, with Benjamini-Hochberg correction for P_{adj} values.

(D) Heatmap of ACP7 vs. control significantly changed genes.

(E) GO biological terms of significantly upregulated (red) genes for ACP7 vs. control.

(F) Venn diagrams showing high-confidence genes either upregulated (upper Venn diagram) or downregulated (lower Venn diagram) by ACP7 overexpression. High confidence genes are the intersection (or genes in common) between the pairwise comparisons of ACP7 vs. control and ACP7 vs. ACP7-7A.

(G) STRING protein interaction analysis of the up- and down-regulated high-confidence genes. Markov Cluster Algorithm (MCL) clustering with an inflation parameter of 3 was used to identify 9 clusters. The top two clusters consist of 36 proteins (red) and 82 proteins (orange). Molecular GO terms for the red cluster were determined to be enriched for tyrosine-specific protein phosphatases via STRING analysis. The orange cluster was carbohydrate binding, with many proteins having C-type lectin domains.

(H) A list of the top 15 high-confidence genes differentially regulated by ACP7 overexpression.

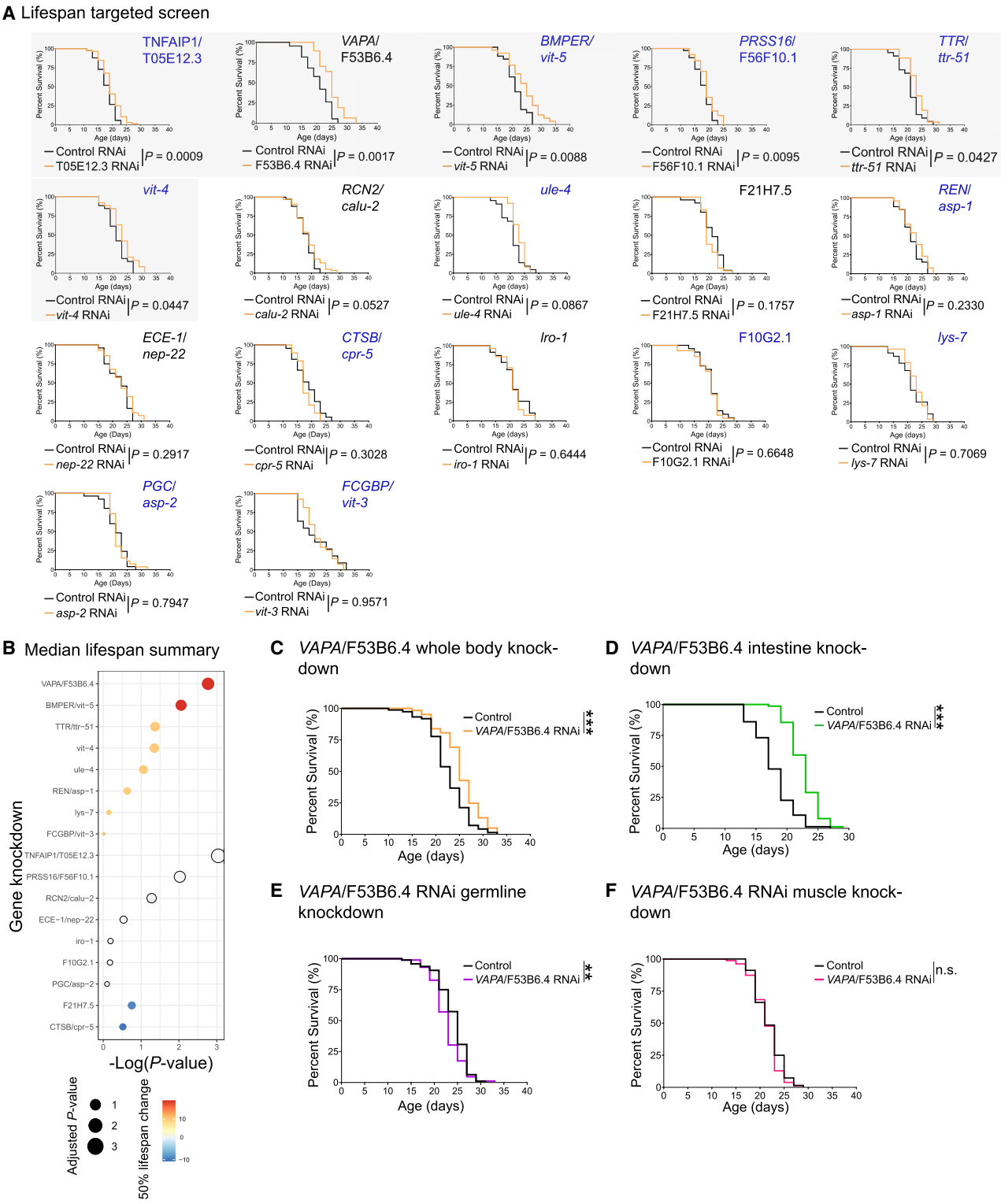

Figure 6. Targeted RNAi screen reveals additional secreted and secretory pathway proteins that regulate lifespan

(A) Knockdown of 17 genes encoding secreted and secretory pathway proteins that change with age via RNAi resulted in 6 genes that significantly extend lifespan when knocked down (*TNFAIP1*/T05E12.3, *VAPA*/F53B6.4, *BMPER*/*vit-5*, *PRSS16*/F56F10.1, *TTR*/*ttr-51*, *vit-4*). For the gene selection list, see Table S6A $n = 30–100$ worms per condition (except $n = 15$ worms for the control condition of the *vit-3* lifespan). p values calculated with Log rank (Mantel-Cox) test (see Source

(legend continued on next page)

in the intestine alone (using the VP303 strain[108]) also resulted in a significant lifespan extension (35% lifespan extension at 50% survival and 10% lifespan extension at 10% survival) (Figure 6D). By contrast, knocking down *VAPA*/F53B6.4 in the germline alone (using the DCL569 strain[109]) resulted in a significant decrease in lifespan by 8% (Figure 6E), and knocking down *VAPA*/F53B6.4 in the muscle (using the NR350 strain[110]) did not affect lifespan (Figure 6F). Together, these results indicate that *VAPA* regulates lifespan by acting mostly in the intestine (though we have not tested all tissues).

We also generated a *VAPA*/F53B6.4 knockout to determine if complete loss of *VAPA*/F53B6.4 impacts lifespan. Using CRISPR/Cas9, we generated a *VAPA*/F53B6.4 mutant with a 31-base-pair deletion in exon 2 that resulted in a frameshift and an early stop codon, predicted to result in a full knockout of *VAPA*/F53B6.4 (Figure S6B). We performed RT-qPCR to determine the extent of *VAPA*/F53B6.4 gene expression reduction in the knockout strain and found that both the predicted *VAPA*/F53B6.4 knockout (and knockdown of *VAPA*/F53B6.4) reduced transcript levels compared to control animals (Figure S6C). The knockout of *VAPA*/F53B6.4 did not significantly extend overall lifespan (unlike *VAPA*/F53B6.4 knockdown), although it resulted in a 9% lifespan extension at 50% survival compared to control animals (Figure S6D). The difference between *VAPA*/F53B6.4 knockdown and knockout for lifespan extension might be linked to its distinct effects on lifespan in different tissues.

Collectively, these findings indicate that several secreted proteins can regulate lifespan, which highlights the role of extracellular proteins in the aging process. These results also reveal that reducing *VAPA*/F53B6.4 levels, a potential secretory vesicle protein in the intestine, extends lifespan.

VAPA is a vesicle-associated protein

VAPA/F53B6.4 shares structural homology with Vesicle-Associated Membrane Protein A in humans (Figures 7A and 7B), which functions in vesicle trafficking.[107] Our subcellular localization observations indicate that VAPA/F53B6.4 is localized in small vesicle-like structures in the intestine (Figures S6E–S6H). Our quantitative proteomics dataset shows that the VAPA protein decreases in abundance with age (Figure 7C, left panel). Consistently, using RT-qPCR, we found that *VAPA*/F53B6.4 transcripts also decreased with age (Figure S6I). We also generated a *C. elegans* knockin strain to tag the endogenous VAPA/F53B6.4 protein with a 3xHA-tag. Using this strain, we confirmed that endogenous VAPA/F53B6.4 protein abundance declines with age (Figure 7C, right panel). The decrease in VAPA/F53B6.4 protein and transcript with age, coupled with the observation that *VAPA*/F53B6.4 knockdown in the intestine extends lifespan (see Figure 6), suggests that VAPA may be part of a compensatory mechanism during aging.

Is VAPA associated with intestinal secretory vesicles in *C. elegans*? If so, we reasoned that disrupting secretory vesicle trafficking should result in changes in VAPA protein localization. To test this possibility, we examined VAPA/F53B6.4 protein localization under control conditions or in response to knockdown of a gene involved in vesicle tethering (*uso-1*)[111] or in vesicle docking (*trpp-3*)[112] (Figure 7D). Under control conditions, VAPA/F53B6.4 was present in small vesicle-like structures in the intestine (Figure 7E). In response to *uso-1* or *trpp-3* knockdown, VAPA/F53B6.4-containing vesicle-like structures significantly increased in abundance (Figures 7E and 7F). VAPA/F53B6.4-containing vesicle-like structures also decreased in size in response to *trpp-3* knockdown (Figure 7G). These data suggest that VAPA is associated with small vesicle-like structures that are influenced by perturbation of genes involved in vesicle trafficking, consistent with the notion that VAPA may be associated with intestinal secretory vesicles.

VAPA knockdown induces the innate immune pathway and improves intestinal barrier function

As *VAPA*/F53B6.4 knockdown resulted in lifespan extension (Figure 6), we wanted to determine if reduction of *VAPA*/F53B6.4 levels could induce well-known longevity pathways (Figure S7A). We found that knockdown of *VAPA*/F53B6.4 via RNAi led to the upregulation of a transcriptional reporter of the p38 MAPK/PMK-1 innate immune pathway (*T24B8.5p::GFP*[101]), though *VAPA*/F53B6.4 knockout had no effect on this reporter (Figures 7H and S7B). These observations suggest that VAPA knockdown could induce the innate immune pathway. By contrast, *VAPA*/F53B6.4 knockdown did not lead to the nuclear localization of FOXO/DAF-16 (*daf-16p::daf-16a/b::GFP*),[100] TFEB/HLH-30 (*hlh-30p::hlh-30::GFP*),[96] or NFR-2/SKN-1 (*skn-1b/c::GFP*),[113] suggesting that *VAPA*/F53B6.4 does not act upstream of these longevity pathways (Figures S7C–S7E). Additionally, *VAPA*/F53B6.4 knockdown did not greatly impact transcriptional reporter strains for the unfolded protein response in the ER (UPR-ER, *hsp-4p::GFP*[102]), mitochondria (UPR-mitochondria, *hsp-6p::GFP*[4,103]), and cytoplasm (UPR-cytoplasm, *hsp-16.2p::GFP*[114]) (Figure S7F). Hence, while *VAPA*/F53B6.4 knockdown does not overtly affect many well-characterized longevity pathways, it leads to the upregulation of the p38 MAPK/PMK-1 innate immune pathway, which could be important for intestinal and organismal health.

Data). Independent validation for *VAPA*/F53B6.4 is in (C). Genes highlighted in blue encode secreted proteins identified in this study, including three secreted proteins that were independently validated by our *in vivo* cell biology approach (LYS7, TNFAPI1/T05E12.3, PRSS16/F56F10.1).
(B) Dot plot indicating the significance and percent change in median lifespan from the screen in (A).
(C) Knockdown of *VAPA*/F53B6.4 via RNAi in the whole animal extends lifespan. $n = 100$ worms for each condition. p values calculated by Log rank (Mantel-Cox) test. *** denotes $p < 0.001$. Representative of 3 independent experiments (see source data for other independent experiments).
(D) Knockdown of *VAPA*/F53B6.4 via RNAi only in the intestine (VP303 strain) extends lifespan. $n = 100$ worms for each condition. p values calculated by Log rank (Mantel-Cox) test. *** denotes $p < 0.001$. Representative of 2 independent experiments (see source data for another independent experiment).
(E) Knockdown of *VAPA*/F53B6.4 via RNAi in the germline only (DCL569 strain) decreases lifespan. $n = 100$ worms for each condition. p values calculated by Log rank (Mantel-Cox) test. ** denotes $p < 0.01$. One experiment (see Source Data).
(F) Knockdown of *VAPA*/F53B6.4 via RNAi in the muscle only (NR350 strain) does not change lifespan. $n = 100$ worms for each condition. p values calculated by Log rank (Mantel-Cox) test. ** denotes $p < 0.01$. One experiment (see Source Data).

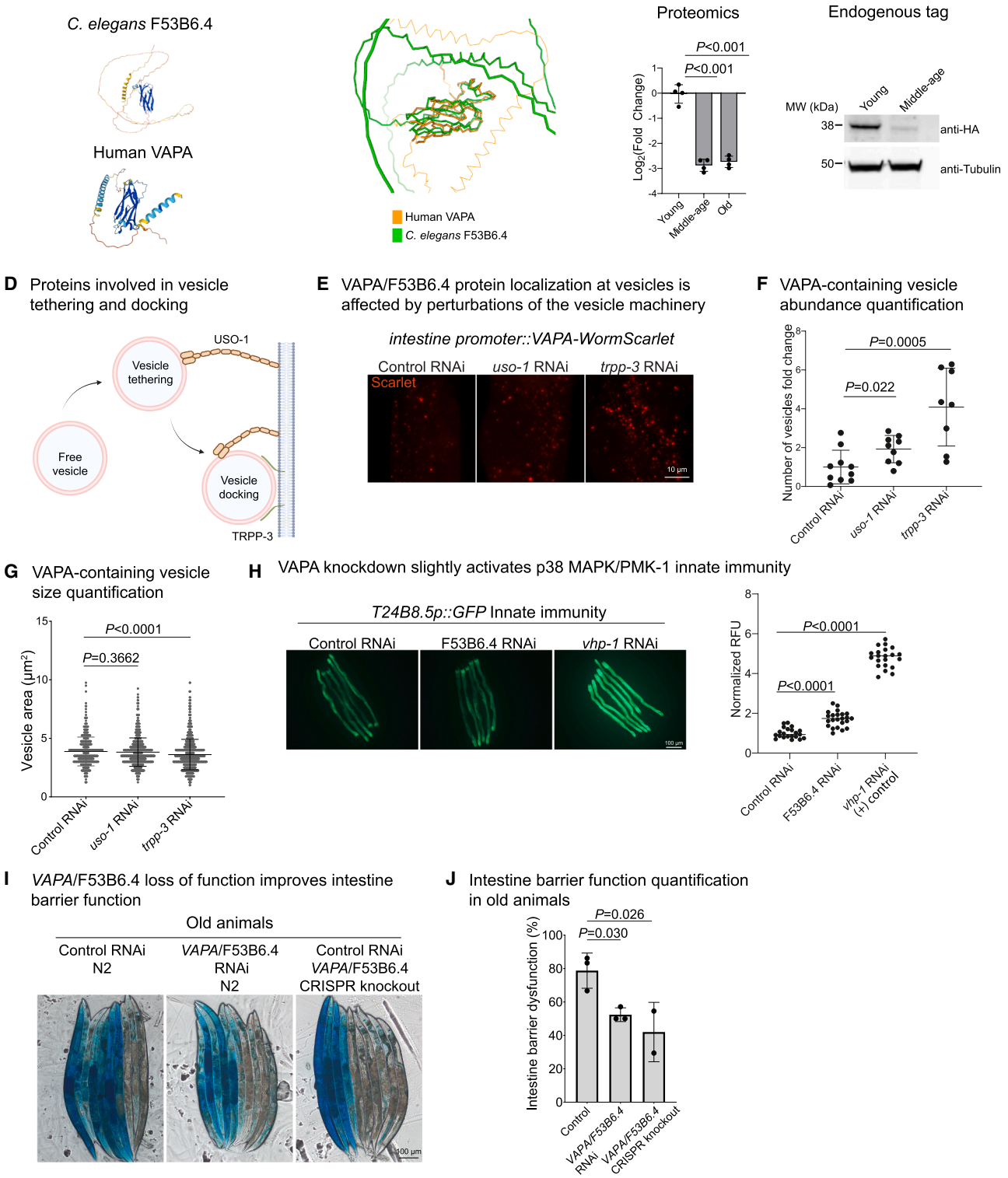

Figure 7. VAPA/F53B6.4 is a vesicle-associated protein that impacts intestinal barrier function

(A) 3D protein structure of *C. elegans* F53B6.4 and human VAPA (from AlphaFold).

(B) *C. elegans* F53B6.4 and human VAPA protein structure overlap shows a high degree of structural similarity (Dali).

(legend continued on next page)

The intestine has a barrier function, which is critical for organismal health and lifespan.[80,115] We asked whether *VAPA*/F53B6.4 knockdown could impact intestinal barrier function in old animals (13 days post-hatch) by quantifying the frequency of old animals that displayed intestinal leaking using a "Smurf" assay.[115] In this assay, animals are fed a blue dye that stays localized in the intestinal lumen if barrier function is effective or leaks into the animal's body cavity if the intestinal barrier function is compromised. Animals with RNAi knockdown of *VAPA*/F53B6.4 exhibited a significant reduction in the frequency of intestinal leakage at old age compared to age-matched control animals (Figures 7I and 7J). *VAPA*/F53B6.4 knockout animals also showed a reduction in intestinal leakage at old age compared to age-matched wild-type animals (Figures 7I and 7J). These results suggest that consistent with the ability of *VAPA*/F53B6.4 to extend lifespan when knocked down in the intestine (see Figure 6), *VAPA*/F53B6.4 knockdown preserves intestinal barrier function—a key aspect of intestinal health that prevents pathogen infection.[116] Prolonged intestinal barrier integrity during aging is critical for longevity,[80,115] and it might contribute to the ability of VAPA/F53B6.4 knockdown to extend lifespan.

Collectively, these results suggest that VAPA/F53B6.4 is a previously unidentified component of the secretory vesicle pathway and that reducing VAPA/F53B6.4 levels promotes an innate immune pathway and protects intestinal barrier function, which are crucial for health and lifespan.

DISCUSSION

Our study uses proximity labeling and quantitative proteomics to systematically characterize how the intestine secretome changes with age, highlighting the importance of secreted enzymes for longevity. The aging intestine datasets in our study represent robust resources that can be used to identify secreted proteins and proteins along the secretory pathway. The *C. elegans* intestine is an important tissue that secretes many proteins and shares physiological roles with human intestine, fat tissue, and liver.[117] Some intestine secreted proteins in *C. elegans* have previously been shown to influence lifespan, such as lipid binding protein 3 (LBP-3),[10] and to protect against infection, such as F56B6.6 (uncharacterized protein with cysteine-rich sequences)[20] and LYS-3 (lysozyme-like protein).[20] In mammals, several proteins secreted by specific tissues[2,26,118] at basal levels or in response to stimuli such as exercise[27,50] have been identified, though their role in lifespan is unknown. Our study identifies many previously uncharacterized proteins that are secreted by the intestine and change with age in *C. elegans*, uncovering different types of extracellular proteins and functions—notably key conserved extracellular enzymes.

Our pipeline for the systematic identification of secreted proteins from specific tissues is versatile, and it could be applied to other tissues and cells (muscle, hypodermis, and so forth). While previous proteomics studies in *C. elegans* have been effective at identifying key intracellular proteins and pathways that change with age,[35–38] comprehensively characterizing secreted proteins has been challenging, as secreted proteins are often of low abundance. In mammals, several studies have profiled proteins in extracellular fluids (e.g., blood),[119] including during aging,[120] identified senescent-associated secretory proteins,[33,121,122] and used proximity labeling proteins to analyze tissue-specific secretomes.[18,19,26–31,50,53] However, it is often unclear whether some of the identified proteins are truly *secreted* from cells or tissues or whether they are released as a consequence of cell death.

(C) Left panel: VAPA/F53B6.4 protein levels decrease with age. Quantitative mass spectrometry results of Log_2(Fold Change) of VAPA/F53B6.4 in young, middle-age, and old time points. Bar plot represents mean ± standard deviation. Each dot represents a sample obtained in an independent biological experiment (n = 4 samples/experiments, each composed of ~200,000 worms). p values calculated by one-way ANOVA. Right panel: western blot depicting the decrease in endogenous VAPA/F53B6.4 protein (knockin strain) between young (adult day 1, 3 days post hatch) and middle-age (adult day 5, 8-day post hatch). An antibody against Tubulin is used as a loading control.

(D) Schematic of proteins involved in vesicle tethering and docking. USO-1 is involved in vesicle tethering to an acceptor membrane (e.g., cell membrane). TRPP-3 is involved in vesicle docking to an acceptor membrane.

(E) Representative fluorescence images of VAPA/F53B6.4 protein localization upon knockdown of vesicle-tethering (*uso-1*) and vesicle-docking (*trpp-3*) genes via RNAi. Strain used for VAPA/F53B6.4 localization is ABR317 [*pha-1*(cc1299 [e2123ts]); staEx20[*ges-1p::F53B6.4-2xLinker-WormScarlet::unc-54 3′UTR* + *pha-1*(+)]. Scale bars, 10 μm.

(F) Quantification of VAPA-containing vesicle-like structure number in the first third of the intestine relative to the control condition. n = 8–10 worms per condition. Dot plot represents mean ± standard deviation. Each dot represents the average number of VAPA/F53B6.4 (tagged with WormScarlet) vesicle-like structures in the top 6 intestine cells of a single worm. p values calculated by the Mann-Whitney test. Representative of 2 independent experiments (see source data for another independent experiment).

(G) Quantification of VAPA-containing vesicle-like structure area in the first third of the intestine. n = 8–10 worms per condition. Dot plot represents mean ± standard deviation. Each dot represents the area of one VAPA/F53B6.4-scarlet vesicle in the top 6 intestine cells of 8–10 worms. p values calculated by Mann-Whitney test. Representative of 2 independent experiments (see source data for another independent experiment).

(H) *VAPA*/F53B6.4 knockdown upregulates the p38 MAPK/PMK-1 innate immune pathway ($p < 0.001$). Representative fluorescent images and quantification of the innate immune transcriptional reporter in three conditions – control RNAi, *VAPA*/F53B6.4 RNAi, and *vhp-1* RNAi (positive control). p values calculated by Mann-Whitney test. Dot plot represents the median, and each dot represents one animal. Representative of 3 independent experiments (see source data for two other independent experiments). Scale bars, 100 μm.

(I) *VAPA*/F53B6.4 reduction or loss of function, via RNAi or CRISPR knockout, improves intestinal barrier function in old animals. Representative images of old animals (13 days post-hatch) after the "Smurf" assay. Animals that have blue outside of their intestine are animals that have intestinal barrier defects. Scale bars, 100 μm.

(J) Quantification of images in (I). Bar plot represents mean ± standard deviation. Each dot represents an independent biological experiment, each with 6–39 assessed individual worms for the Smurf phenotype (see source data). Control: N2 worms with control RNAi bacteria. p values calculated by one-way ANOVA. Representative of 3 independent experiments for *VAPA*/F53B6.4 RNAi and 2 experiments for *VAPA*/F53B6.4 knockout (see source data for other independent experiments).

Leveraging *C. elegans* as a model organism, we captured the intestine secretome during aging *in vivo* and validated the secretion of four intestine proteins *in situ*. Secreted proteins identified by our approach are released through the conventional secretory pathway (ER, Golgi apparatus, and exocytosis), resulting in their direct secretion into the extracellular space rather than within extracellular vesicles. Identifying bona fide secreted proteins is important because it helps to distinguish extracellular proteins that have a regulatory role from those that are released because of cell death or non-specifically by extracellular vesicles. Notably, ACP7 is found in human fluids (e.g., blood) and is associated with several age-related diseases (e.g., type 2 diabetes, Alzheimer disease).[120,123,124] It will be interesting to investigate whether other conserved secreted proteins we identified in *C. elegans* are also present in human blood datasets (e.g., UK Biobank) and are associated with aging or age-related diseases. Overall, our study provides a proof-of-concept that this proximity labeling approach followed by quantitative mass spectrometry allows for the characterization of the secretome with cell and tissue resolution *in vivo*.

Our work highlights the utility of our dataset to uncover conserved secreted proteins that regulate organismal lifespan, with the identification of ACP7/F21A3.11, an extracellular phosphatase that can extend lifespan when overexpressed in *C. elegans*. ACP7/F21A3.11 is a well-conserved protein in humans and is found in human blood,[28] and it could represent a key target in the context of human aging. The phosphatase activity of ACP7 is critical for its ability to extend lifespan, which raises the possibility that this phosphatase has extracellular substrates. Another phosphatase of the same family involved in mammalian bone remodeling (ACP5)[87,125] has been shown to dephosphorylate bone matrix proteins.[126] Although identifying phosphatase substrates is notoriously challenging,[127,128] we determined the tyrosine selectivity of the ACP7 phosphatase and highlight several potential extracellular substrates. Future studies will be required to directly test the phosphatase activity of ACP7 *in vivo* via phosphoproteomics. Interestingly, ACP7 remodels gene expression pathways involved in phosphatase activity (as well as other pathways and genes), suggesting that ACP7 could act in part by regulating phosphate homeostasis. More generally, our observations indicate that enzymatic activity in the extracellular space is important for longevity. This is interesting in light of other circulating enzymes (e.g., phospholipases) that are produced in response to exercise.[129] Understanding the role of secreted enzymes in longevity—and in response to different interventions—will be helpful in identifying new therapeutic targets and designing new strategies to increase health.

We also leverage the short lifespan of *C. elegans* to perform a targeted RNAi lifespan screen for genes encoding age-changed secretome and secretory pathway proteins. From this targeted screen, we identified several genes that extend lifespan when knocked down, including *VAPA*/F53B6.4—a protein associated with small vesicles, potentially secretory vesicles. We find that knocking down *VAPA*/F53B6.4 extends lifespan, upregulates the p38 MAPK innate immune pathway, and improves intestinal health. Our findings suggest that not only are secreted proteins important for regulating lifespan, but that intestine-specific secretory vesicles could also impact organismal longevity—maybe by affecting the release of specific proteins and peptides. Together, ACP7/F21A3.11 and VAPA/F53B6.4 are two examples that highlight how labeling the secretory pathway, including secreted proteins, can identify new modulators of the aging process. It will be interesting to further identify the mechanisms by which ACP7 and VAPA regulate aging and to determine how these findings translate to other species, including humans.

Importantly, secreted proteins and peptides from different cells and organs are important for homeostasis and stress responses in species ranging from *C. elegans*[4–8,20,95,130] to mammals.[14,16,26,27] In mammals, several proteins and peptides were identified in the blood and released from specific organs, particularly in response to exercise,[27] nutrient changes,[21,22] or stress stimuli.[23] Interestingly, secreted peptides from the intestine in humans (e.g., GLP1) have been leveraged for drug design (GLP1 agonists) and found to be highly effective in treating systemic conditions such as obesity,[17] diabetes,[24] and maybe even neurodegenerative diseases.[14,25] Moreover, secreted proteins can also serve as excellent predictive biomarkers of longevity[31–33] and organ health.[28] Thus, the systematic identification of tissue-specific secreted proteins during aging, notably secreted enzymes, represents a key step in identifying new biomarkers and drug targets for aging and longevity that could have important applications for age-related diseases.

Limitations of the study

We are aware that the TurboID-ER method may have missed some secreted proteins, either because they transit through the ER too rapidly, because the protein is too small to be efficiently biotinylated, or because some proteins are only secreted in response to specific stimuli. In addition, we believe that the changes in protein levels with age in proximity labeling are to be interpreted with caution. While we have supporting evidence for changes with age from RNA transcripts (*ACP7* and *VAPA*) and protein (VAPA), some of the proteins that increase with age in the TurboID-ER dataset may be retained in the ER longer with age and may be better labeled by TurboID-ER. Some of the secretome changes with age could also result from changes in TurboID levels, enzymatic activity, or labeling efficiency with age (though TurboID levels are likely saturating).

Coupling the TurboID-ER discovery tool with whole worm lysates (rather than fluids) does not allow us to directly separate secreted proteins from other proteins along the secretory pathways (ER, Golgi, membrane, and vesicle-bound proteins). It also does not distinguish between the fraction of a secreted protein of interest (e.g., ACP7) that is still going through the secretory pathway and the fraction that is actually secreted and released in the extracellular milieu. In worms, the body cavity fluid is very small and challenging to isolate, which is not readily compatible with the material amount needed to identify proteins by current proteomics approaches. Thus, our TurboID-ER approach in *C. elegans* requires a second step using deep-learning-based tools to determine whether a protein is classified as secreted vs. ER resident, Golgi, transmembrane, and so forth. and independent validation.

The sensitivity of our approach would still need to be further characterized. We did not expect to detect all *in silico* predicted secreted proteins because most of them are not expressed in a

given tissue, age, and condition. However, it is possible that we could identify additional intestine-secreted proteins by increasing the amount of starting material, the sensitivity of the mass spectrometry approach, or by assessing worms under different conditions that lead to the generation of additional secreted proteins (e.g., stress, nutrient starvation).

Finally, we acknowledge that the enzymatically dead mutant of ACP7 could affect other functions of the protein beyond its phosphatase activity. In addition, the stronger effect of *VAPA*/F53B6.4 knockdown compared to *VAPA*/F53B6.4 complete knockout on lifespan extension and immune regulation could reflect differences in residual *VAPA*/F53B6.4 levels across tissues or compensatory mechanisms that are triggered in the knockout (although we cannot exclude the possibility of off-target effects from *VAPA*/F53B6.4 RNAi). Finally, because of the rapid *C. elegans* defecation cycle,[131] it has been challenging to determine if some of the intestine-secreted proteins or secretory vesicles are released not just into the extracellular space but also into the intestinal lumen for intestinal digestion or barrier function.

RESOURCE AVAILABILITY

Lead contact

Requests for further information and resources should be directed to and will be fulfilled by the lead contact, Anne Brunet (abrunet1@stanford.edu).

Materials availability

- The following plasmids generated in this study have been deposited with Addgene: 260219, 260218, 260217, 260216, 260215, 260159, 260158, 260157, 260156, 260155, 260154.
- Select *C. elegans* strains generated in this study have been deposited to the Caenorhabditis Genetics Center: ABR269, ABR273, ABR275, ABR287, ABR291, ABR297, ABR327, ABR333, ABR337, ABR388, ABR417, ABR429, ABR429, ABR461, ABR489, and PHX9731.

Data and code availability

- The mass spectrometry proteomics data have been deposited at ProteomeXchange Consortium via the PRIDE[132] partner repository with the dataset identifier PRIDE: PXD057064 and are publicly available as of the date of publication.
- The RNA-sequencing data have been deposited at Gene Expression Omnibus (GEO) as NCBI GEO: GSE307266 and are publicly available as of the date of publication.
- All original code has been deposited at GitHub and is publicly available at Zenodo: https://doi.org/10.5281/zenodo.21210820 as of the date of publication and at GitHub: https://github.com/miklasja/Intestine-Secretome-Paper
- Any additional information required to reanalyze the data reported in this paper is available from the lead contact upon request.

ACKNOWLEDGMENTS

We thank A. Fire for helpful discussions and insight. We thank C. Froekjaer-Jensen for his help in generating a worm-optimized GreenLantern fluorescent protein. We thank all Brunet lab members for helpful discussion, particularly C. Bedbrook, L. Booth, A. Hosseini, B. Laham, R. Nath, and J. Yang for reading the manuscript and providing insightful comments. We thank N. Rappoport for helpful discussion and independent code-checking. We thank J. Long and his lab members and A. Ting's lab members for their help with TurboID questions and A. Ori for his help with the proteomics analysis. This work was supported by NIH R01AG054201 (A.B.), the Biohub Investigator Program (A.B.), the Knight Initiative for Brain Resilience at Stanford University (M.A.-R.), the Arc Institute (M.A.-R.), the Chan Zuckerberg Initiative Neurodegeneration Challenge Network (2024-338545) (M.A.-R.), the Biohub and its donors, Priscilla Chan and Mark Zuckerberg (J.E.E.), Stanford University's School of Medicine Dean's Postdoctoral Fellowship (J.W.M.), and a Fellowship Research Grant from the Larry Hillblom Foundation (J.W.M.). Elements of Figures 1, 2, 3, 4, 5, 6, and 7 were created with BioRender. We thank the Caenorhabditis Genetics Center (CGC) for some strains; the CGC is funded by NIH Office of Research Infrastructure Programs (P40 OD010440).

AUTHOR CONTRIBUTIONS

This study was designed by J.W.M. and A.B.; J.W.M. generated *C. elegans* strains and performed all experiments in the manuscript, except when indicated below. K.P. performed independent lifespan experiments (see source data) and determined conserved metal-binding sites for ACP7. E.D.S. helped with proteomics statistical analysis, PCA, volcano plots, and code checking. A.T. helped with VAPA localization experiments, ACP7 and VAPA longevity pathway experiments (crossing strains, fluorescent microscopy and quantification), and worm genotyping. N.R.H. helped with mass spectrometry experiments, worm genotyping, imaging (*in vivo* validation), and performed western blots. B.A. helped with transcriptomic statistical analysis, PCA, and volcano plots. U.N.M. provided guidance for ACP7 human and *C. elegans* protein isolation under the supervision of M.A.-R. D.R. helped with transcriptomic data. F.M. performed all proteomics and protein identification experiments under the supervision of J.E.E. at the BioHub. K.L.A. from Dr. Andy Fire's lab generated the PD1299 *pha-1* mutant strain. A.H. helped purify human ACP7 protein, with guidance from U.N.M., A.L., and M.A-R. O.Y.Z. wrote code for lifespan summary visualization. J.W.M. wrote the manuscript with the help of A.B. All the authors provided intellectual input and commented on the manuscript.

DECLARATION OF INTERESTS

A.B. is a scientific advisory board member of Calico.

STAR★METHODS

Detailed methods are provided in the online version of this paper and include the following:

- KEY RESOURCES TABLE
- EXPERIMENTAL MODEL AND STUDY PARTICIPANT DETAILS
  - C. elegans
  - Bacteria
  - Cell line
- METHOD DETAILS
  - Generation of transgenic strain constructs
  - Generation of transgenic strains
  - Generation of PD1299 *Pha-1(cc1299 [e2123ts])*
  - *VAPA*/F53B6.4 CRISPR knockout strain
  - Generation of an HA-tagged *VAPA*/F53B6.4 knockin strain
  - RNAi knockdown
  - Western blot
  - Immunohistochemistry
  - Confocal microscopy for TurboID localization
  - Confocal microscopy for secretome and secretory machinery protein compartment localization
  - Quantitative mass spectrometry
  - Analysis of mass spectrometry data
  - RNA isolation for RT-qPCR
  - RT-qPCR
  - RNA-sequencing
  - ACP7/F21A3.11 protein sequence alignment
  - VAPA/F53B6.4 3D protein structure alignment
  - Lifespan assays (overexpressing strains and RNAi)
  - Widefield microscopy for RNAi knockdown validation

- Widefield microscopy for translational and transcriptional reporter assays
- Phosphatase assay for ACP7
- Human ACP7 protein expression and purification for phosphatase assay
- Tyrosine phosphatase assays
- Serine/threonine phosphatase assays
- Prediction of ACP7/F21A3.11 substrates
- Verification of proteomic evidence for VAPA/F53B6.4 changes with age
- VAPA/F53B6.4 secretory pathway association
- Intestinal barrier function assay (smurf assay)

● QUANTIFICATION AND STATISTICAL ANALYSIS

SUPPLEMENTAL INFORMATION

Supplemental information can be found online at https://doi.org/10.1016/j.celrep.2026.117902.

Received: November 1, 2024
Revised: June 22, 2026
Accepted: August 7, 2026
Published: August 27, 2026

REFERENCES

1. López-Otín, C., Blasco, M.A., Partridge, L., Serrano, M., and Kroemer, G. (2023). Hallmarks of aging: An expanding universe. Cell *186*, 243–278. https://doi.org/10.1016/j.cell.2022.11.001.
2. Droujinine, I.A., Meyer, A.S., Wang, D., Udeshi, N.D., Hu, Y., Rocco, D., McMahon, J.A., Yang, R., Guo, J., Mu, L., et al. (2021). Proteomics of protein trafficking by in vivo tissue-specific labeling. Nat. Commun. *12*, 2382. https://doi.org/10.1038/s41467-021-22599-x.
3. Savini, M., and Wang, M.C. (2022). Lysosome Lipid Signaling from the Periphery to Neurons Regulates Longevity. Nat. Cell Biol. *24*, 906–916. https://doi.org/10.1038/s41556-022-00926-8.
4. Zhang, Q., Wu, X., Chen, P., Liu, L., Xin, N., Tian, Y., and Dillin, A. (2018). The Mitochondrial Unfolded Protein Response Is Mediated Cell-Non-autonomously by Retromer-Dependent Wnt Signaling. Cell *174*, 870–883.e17. https://doi.org/10.1016/j.cell.2018.06.029.
5. Berendzen, K.M., Durieux, J., Shao, L.W., Tian, Y., Kim, H.e., Wolff, S., Liu, Y., and Dillin, A. (2016). Neuroendocrine Coordination of Mitochondrial Stress Signaling and Proteostasis. Cell *166*, 1553–1563.e10. https://doi.org/10.1016/j.cell.2016.08.042.
6. Frakes, A.E., Metcalf, M.G., Tronnes, S.U., Bar-Ziv, R., Durieux, J., Gildea, H.K., Kandahari, N., Monshietehadi, S., and Dillin, A. (2020). Four glial cells regulate ER stress resistance and longevity via neuropeptide signaling in C. elegans. Science *367*, 436–440. https://doi.org/10.1126/science.aaz6896.
7. Madhivanan, K., Greiner, E.R., Alves-Ferreira, M., Soriano-Castell, D., Rouzbeh, N., Aguirre, C.A., Paulsson, J.F., Chapman, J., Jiang, X., Ooi, F.K., et al. (2018). Cellular clearance of circulating transthyretin decreases cell-nonautonomous proteotoxicity in Caenorhabditis elegans. Proc. Natl. Acad. Sci. USA *115*, E7710–E7719. https://doi.org/10.1073/pnas.1801117115.
8. Shen, K., Durieux, J., Mena, C.G., Webster, B.M., Tsui, C.K., Zhang, H., Joe, L., Berendzen, K.M., and Dillin, A. (2024). The germline coordinates mitokine signaling. Cell *187*, 4605–4620.e17. https://doi.org/10.1016/j.cell.2024.06.010.
9. Lee, K., and Mylonakis, E. (2017). An Intestine-Derived Neuropeptide Controls Avoidance Behavior in Caenorhabditis elegans. Cell Rep. *20*, 2501–2512. https://doi.org/10.1016/j.celrep.2017.08.053.
10. Savini, M., Folick, A., Lee, Y.T., Jin, F., Cuevas, A., Tillman, M.C., Duffy, J.D., Zhao, Q., Neve, I.A., Hu, P.W., et al. (2022). Lysosome lipid signalling from the periphery to neurons regulates longevity. Nat. Cell Biol. *24*, 906–916. https://doi.org/10.1038/s41556-022-00926-8.
11. Zhou, S., Novak, K.E., Kaletsky, R., Weng, Y., Ange, J.S., Stevenson, M.E., Toraason, E., Zhang, Y., Zhang, W., Dong, M.Q., and Murphy, C.T. (2025). Body-to-brain insulin and Notch signaling regulates memory through neuronal CREB activity. Nat. Aging *5*, 1232–1248. https://doi.org/10.1038/s43587-025-00873-7.
12. Kenyon, C. (2011). The first long-lived mutants: discovery of the insulin/IGF-1 pathway for ageing. Phil. Trans. R. Soc. B. *366*, 9–16. https://doi.org/10.1098/rstb.2010.0276.
13. Babey, M.E., Krause, W.C., Chen, K., Herber, C.B., Torok, Z., Nikkanen, J., Rodriguez, R., Zhang, X., Castro-Navarro, F., Wang, Y., et al. (2024). A maternal brain hormone that builds bone. Nature *632*, 357–365. https://doi.org/10.1038/s41586-024-07634-3.
14. Campbell, J.E., and Drucker, D.J. (2013). Pharmacology, physiology, and mechanisms of incretin hormone action. Cell Metab. *17*, 819–837. https://doi.org/10.1016/j.cmet.2013.04.008.
15. Rajan, A., and Perrimon, N. (2012). Drosophila cytokine unpaired 2 regulates physiological homeostasis by remotely controlling insulin secretion. Cell *151*, 123–137. https://doi.org/10.1016/j.cell.2012.08.019.
16. Ennequin, G., Sirvent, P., and Whitham, M. (2019). Role of exercise-induced hepatokines in metabolic disorders. American Journal of Physiology-Endocrinology and Metabolism *317*, E11–E24. https://doi.org/10.1152/ajpendo.00433.2018.
17. Wilding, J.P.H., Batterham, R.L., Calanna, S., Davies, M., Van Gaal, L.F., Lingvay, I., McGowan, B.M., Rosenstock, J., Tran, M.T.D., Wadden, T.A., et al. (2021). Once-Weekly Semaglutide in Adults with Overweight or Obesity. N. Engl. J. Med. *384*, 989–1002. https://doi.org/10.1056/NEJMoa2032183.
18. Sun, B.B., Chiou, J., Traylor, M., Benner, C., Hsu, Y.H., Richardson, T.G., Surendran, P., Mahajan, A., Robins, C., Vasquez-Grinnell, S.G., et al. (2023). Plasma proteomic associations with genetics and health in the UK Biobank. Nature *622*, 329–338. https://doi.org/10.1038/s41586-023-06592-6.
19. Shen, X., Kellogg, R., Panyard, D.J., Bararpour, N., Castillo, K.E., Lee-McMullen, B., Delfarah, A., Ubellacker, J., Ahadi, S., Rosenberg-Hasson, Y., et al. (2023). Multi-omics microsampling for the profiling of lifestyle-associated changes in health. Nat. Biomed. Eng. *8*, 11–29. https://doi.org/10.1038/s41551-022-00999-8.
20. Gallotta, I., Sandhu, A., Peters, M., Haslbeck, M., Jung, R., Agilkaya, S., Blersch, J.L., Rödelsperger, C., Röseler, W., Huang, C., et al. (2020). Extracellular proteostasis prevents aggregation during pathogenic attack. Nature *584*, 410–414. https://doi.org/10.1038/s41586-020-2461-z.
21. Katsumura, S., Siddiqui, N., Goldsmith, M.R., Cheah, J.H., Fujikawa, T., Minegishi, G., Yamagata, A., Yabuki, Y., Kobayashi, K., Shirouzu, M., et al. (2022). Deadenylase-dependent mRNA decay of GDF15 and FGF21 orchestrates food intake and energy expenditure. Cell Metab. *34*, 564–580.e8. https://doi.org/10.1016/j.cmet.2022.03.005.
22. Hill, C.M., Albarado, D.C., Coco, L.G., Spann, R.A., Khan, M.S., Qualls-Creekmore, E., Burk, D.H., Burke, S.J., Collier, J.J., Yu, S., et al. (2022). FGF21 is required for protein restriction to extend lifespan and improve metabolic health in male mice. Nat. Commun. *13*, 1897. https://doi.org/10.1038/s41467-022-29499-8.
23. Wan, X., Zinselmeyer, B.H., Zakharov, P.N., Vomund, A.N., Taniguchi, R., Santambrogio, L., Anderson, M.S., Lichti, C.F., and Unanue, E.R. (2018). Pancreatic islets communicate with lymphoid tissues via exocytosis of insulin peptides. Nature *560*, 107–111. https://doi.org/10.1038/s41586-018-0341-6.
24. Meier, J.J. (2012). GLP-1 receptor agonists for individualized treatment of type 2 diabetes mellitus. Nat. Rev. Endocrinol. *8*, 728–742. https://doi.org/10.1038/nrendo.2012.140.

25. Gault, V.A., and Hölscher, C. (2008). GLP-1 agonists facilitate hippocampal LTP and reverse the impairment of LTP induced by beta-amyloid. Eur. J. Pharmacol. *587*, 112–117. https://doi.org/10.1016/j.ejphar.2008.03.025.

26. Wei, W., Riley, N.M., Yang, A.C., Kim, J.T., Terrell, S.M., Li, V.L., Garcia-Contreras, M., Bertozzi, C.R., and Long, J.Z. (2021). Cell type-selective secretome profiling in vivo. Nat. Chem. Biol. *17*, 326–334. https://doi.org/10.1038/s41589-020-00698-y.

27. Wei, W., Riley, N.M., Lyu, X., Shen, X., Guo, J., Raun, S.H., Zhao, M., Moya-Garzon, M.D., Basu, H., Sheng-Hwa Tung, A., et al. (2023). Organism-wide, cell-type-specific secretome mapping of exercise training in mice. Cell Metab. *35*, 1261–1279.e11. https://doi.org/10.1016/j.cmet.2023.04.011.

28. Oh, H.S.H., Rutledge, J., Nachun, D., Pálovics, R., Abiose, O., Moran-Losada, P., Channappa, D., Urey, D.Y., Kim, K., Sung, Y.J., et al. (2023). Organ aging signatures in the plasma proteome track health and disease. Nature *624*, 164–172. https://doi.org/10.1038/s41586-023-06802-1.

29. Shuken, S.R., Rutledge, J., Iram, T., Losada, P.M., Wilson, E.N., Andreasson, K.I., Leib, R.D., and Wyss-Coray, T. (2022). Limited Proteolysis-Mass Spectrometry Reveals Aging-Associated Changes in Cerebrospinal Fluid Protein Abundances and Structures. Nat. Aging *2*, 379–388. https://doi.org/10.1038/s43587-022-00196-x.

30. Higginbotham, L., Ping, L., Dammer, E.B., Duong, D.M., Zhou, M., Gearing, M., Hurst, C., Glass, J.D., Factor, S.A., Johnson, E.C.B., et al. (2020). Integrated proteomics reveals brain-based cerebrospinal fluid biomarkers in asymptomatic and symptomatic Alzheimer's disease. Sci. Adv. *6*, eaaz9360. https://doi.org/10.1126/sciadv.aaz9360.

31. Lehallier, B., Gate, D., Schaum, N., Nanasi, T., Lee, S.E., Yousef, H., Moran Losada, P., Berdnik, D., Keller, A., Verghese, J., et al. (2019). Undulating changes in human plasma proteome profiles across the lifespan. Nat. Med. *25*, 1843–1850. https://doi.org/10.1038/s41591-019-0673-2.

32. Shen, X., Wang, C., Zhou, X., Zhou, W., Hornburg, D., Wu, S., and Snyder, M.P. (2024). Nonlinear dynamics of multi-omics profiles during human aging. Nat. Aging *4*, 1619–1634. https://doi.org/10.1038/s43587-024-00692-2.

33. Basisty, N., Kale, A., Jeon, O.H., Kuehnemann, C., Payne, T., Rao, C., Holtz, A., Shah, S., Sharma, V., Ferrucci, L., et al. (2020). A proteomic atlas of senescence-associated secretomes for aging biomarker development. PLoS Biol. *18*, e3000599. https://doi.org/10.1371/journal.pbio.3000599.

34. Farinas, A., Rutledge, J., Bot, V.A., Western, D., Ying, K., Lawrence, K.A., Oh, H.S.H., Yoon, S., Ding, D.Y., Tsai, A.P., et al. (2025). Disruption of the cerebrospinal fluid-plasma protein balance in cognitive impairment and aging. Nat. Med. *31*, 2578–2589. https://doi.org/10.1038/s41591-025-03831-3.

35. Narayan, V., Ly, T., Pourkarimi, E., Murillo, A.B., Gartner, A., Lamond, A.I., and Kenyon, C. (2016). Deep Proteome Analysis Identifies Age-Related Processes in C. elegans. Cell Syst. *3*, 144–159. https://doi.org/10.1016/j.cels.2016.06.011.

36. Walther, D.M., Kasturi, P., Zheng, M., Pinkert, S., Vecchi, G., Ciryam, P., Morimoto, R.I., Dobson, C.M., Vendruscolo, M., Mann, M., and Hartl, F.U. (2015). Widespread Proteome Remodeling and Aggregation in Aging C. elegans. Cell *161*, 919–932. https://doi.org/10.1016/j.cell.2015.03.032.

37. David, D.C., Ollikainen, N., Trinidad, J.C., Cary, M.P., Burlingame, A.L., and Kenyon, C. (2010). Widespread protein aggregation as an inherent part of aging in C. elegans. PLoS Biol. *8*, e1000450. https://doi.org/10.1371/journal.pbio.1000450.

38. Koyuncu, S., Loureiro, R., Lee, H.J., Wagle, P., Krueger, M., and Vilchez, D. (2021). Rewiring of the ubiquitinated proteome determines ageing in C. elegans. Nature *596*, 285–290. https://doi.org/10.1038/s41586-021-03781-z.

39. Chen, Y.R., Harel, I., Singh, P.P., Ziv, I., Moses, E., Goshtchevsky, U., Machado, B.E., Brunet, A., and Jarosz, D.F. (2024). Tissue-specific landscape of protein aggregation and quality control in an aging vertebrate. Dev. Cell *59*, 1892–1911.e13. https://doi.org/10.1016/j.devcel.2024.04.014.

40. Harel, I., Chen, Y.R., Ziv, I., Singh, P.P., Heinzer, D., Navarro Negredo, P., Goshtchevsky, U., Wang, W., Astre, G., Moses, E., et al. (2024). Identification of protein aggregates in the aging vertebrate brain with prion-like and phase-separation properties. Cell Rep. *43*, 112787. https://doi.org/10.1016/j.celrep.2023.112787.

41. Kelmer Sacramento, E., Kirkpatrick, J.M., Mazzetto, M., Baumgart, M., Bartolome, A., Di Sanzo, S., Caterino, C., Sanguanini, M., Papaevgeniou, N., Lefaki, M., et al. (2020). Reduced proteasome activity in the aging brain results in ribosome stoichiometry loss and aggregation. Mol. Syst. Biol. *16*, e9596. https://doi.org/10.15252/msb.20209596.

42. Tan, C.H., Wang, T.Y., Park, H., Lomenick, B., Chou, T.F., and Sternberg, P.W. (2024). Single-tissue proteomics in Caenorhabditis elegans reveals proteins resident in intestinal lysosome-related organelles. Proc. Natl. Acad. Sci. USA *121*, e2322588121. https://doi.org/10.1073/pnas.2322588121.

43. Xiao, H., Jedrychowski, M.P., Schweppe, D.K., Huttlin, E.L., Yu, Q., Heppner, D.E., Li, J., Long, J., Mills, E.L., Szpyt, J., et al. (2020). A Quantitative Tissue-Specific Landscape of Protein Redox Regulation during Aging. Cell *180*, 968–983.e24. https://doi.org/10.1016/j.cell.2020.02.012.

44. Yu, Y., Gao, S.M., Guan, Y., Hu, P.W., Zhang, Q., Liu, J., Jing, B., Zhao, Q., Sabatini, D.M., Abu-Remaileh, M., et al. (2024). Organelle proteomic profiling reveals lysosomal heterogeneity in association with longevity. eLife *13*, e85214. https://doi.org/10.7554/eLife.85214.

45. Laqtom, N.N., Dong, W., Medoh, U.N., Cangelosi, A.L., Dharamdasani, V., Chan, S.H., Kunchok, T., Lewis, C.A., Heinze, I., Tang, R., et al. (2022). CLN3 is required for the clearance of glycerophosphodiesters from lysosomes. Nature *609*, 1005–1011. https://doi.org/10.1038/s41586-022-05221-y.

46. Rajan, A., Housden, B.E., Wirtz-Peitz, F., Holderbaum, L., and Perrimon, N. (2017). A Mechanism Coupling Systemic Energy Sensing to Adipokine Secretion. Dev. Cell *43*, 83–98.e6. https://doi.org/10.1016/j.devcel.2017.09.007.

47. Ammeux, N., Housden, B.E., Georgiadis, A., Hu, Y., and Perrimon, N. (2016). Mapping signaling pathway cross-talk in Drosophila cells. Proc. Natl. Acad. Sci. USA *113*, 9940–9945. https://doi.org/10.1073/pnas.1610432113.

48. Branon, T.C., Bosch, J.A., Sanchez, A.D., Udeshi, N.D., Svinkina, T., Carr, S.A., Feldman, J.L., Perrimon, N., and Ting, A.Y. (2018). Efficient proximity labeling in living cells and organisms with TurboID. Nat. Biotechnol. *36*, 880–887. https://doi.org/10.1038/nbt.4201.

49. Tüshaus, J., Müller, S.A., Kataka, E.S., Zaucha, J., Sebastian Monasor, L., Su, M., Güner, G., Jocher, G., Tahirovic, S., Frishman, D., et al. (2020). An optimized quantitative proteomics method establishes the cell type-resolved mouse brain secretome. Embo J *39*, e105693. https://doi.org/10.15252/embj.2020105693.

50. Kim, K.E., Park, I., Kim, J., Kang, M.G., Choi, W.G., Shin, H., Kim, J.S., Rhee, H.W., and Suh, J.M. (2021). Dynamic tracking and identification of tissue-specific secretory proteins in the circulation of live mice. Nat. Commun. *12*, 5204. https://doi.org/10.1038/s41467-021-25546-y.

51. Enström, A., Carlsson, R., Buizza, C., Lewi, M., and Paul, G. (2024). Pericyte-Specific Secretome Profiling in Hypoxia Using TurboID in a Multicellular in Vitro Spheroid Model. Mol. Cell. Proteomics *23*, 100782. https://doi.org/10.1016/j.mcpro.2024.100782.

52. Bosch, J.A., Beltran, P.M.J., Cavers, C., LaGraff, J.T., Melanson, R., Singh, A., Chen, W., Hu, Y., Tattikota, S.G., Liu, Y., et al. (2026). Multi-omic mapping of Drosophila protein secretomes reveals tissue-specific origins and inter-organ trafficking. Nat. Commun. *17*, 5425. https://doi.org/10.1038/s41467-026-71763-8.

53. Plucińska, K., Wayne, C.R., Sanford, H., Mathew, B., Ropek, N., Adaniya, S.M., Model, C., Gómez-Banoy, N., Morozova, K., Cao, X., et al. (2026). Cell-type-specific proximity labeling of organ secretomes reveals energy balance-dependent proteomic remodeling. Cell Rep. *45*, 117507. https://doi.org/10.1016/j.celrep.2026.117507.

54. Crowley, K.S., Liao, S., Worrell, V.E., Reinhart, G.D., and Johnson, A.E. (1994). Secretory proteins move through the endoplasmic reticulum membrane via an aqueous, gated pore. Cell *78*, 461–471. https://doi.org/10.1016/0092-8674(94)90424-3.

55. Qin, W., Cho, K.F., Cavanagh, P.E., and Ting, A.Y. (2021). Deciphering molecular interactions by proximity labeling. Nat. Methods *18*, 133–143. https://doi.org/10.1038/s41592-020-01010-5.

56. Xu, N., Zhang, S.O., Cole, R.A., McKinney, S.A., Guo, F., Haas, J.T., Bobba, S., Farese, R.V., Jr., and Mak, H.Y. (2012). The FATP1-DGAT2 complex facilitates lipid droplet expansion at the ER-lipid droplet interface. J. Cell Biol. *198*, 895–911. https://doi.org/10.1083/jcb.201201139.

57. Cho, K.F., Branon, T.C., Udeshi, N.D., Myers, S.A., Carr, S.A., and Ting, A.Y. (2020). Proximity labeling in mammalian cells with TurboID and split-TurboID. Nat. Protoc. *15*, 3971–3999. https://doi.org/10.1038/s41596-020-0399-0.

58. Kaletsky, R., Yao, V., Williams, A., Runnels, A.M., Tadych, A., Zhou, S., Troyanskaya, O.G., and Murphy, C.T. (2018). Transcriptome analysis of adult Caenorhabditis elegans cells reveals tissue-specific gene and isoform expression. PLoS Genet. *14*, e1007559. https://doi.org/10.1371/journal.pgen.1007559.

59. Han, S., Schroeder, E.A., Silva-García, C.G., Hebestreit, K., Mair, W.B., and Brunet, A. (2017). Mono-unsaturated fatty acids link H3K4me3 modifiers to C. elegans lifespan. Nature *544*, 185–190. https://doi.org/10.1038/nature21686.

60. Castiglioni, V.G., Pires, H.R., Rosas Bertolini, R., Riga, A., Kerver, J., and Boxem, M. (2020). Epidermal PAR-6 and PKC-3 are essential for larval development of C. elegans and organize non-centrosomal microtubules. eLife *9*, e62067. https://doi.org/10.7554/eLife.62067.

61. Ericson, V.R., Spilker, K.A., Tugizova, M.S., and Shen, K. (2014). MTM-6, a phosphoinositide phosphatase, is required to promote synapse formation in Caenorhabditis elegans. PLoS One *9*, e114501. https://doi.org/10.1371/journal.pone.0114501.

62. Riga, A., Cravo, J., Schmidt, R., Pires, H.R., Castiglioni, V.G., van den Heuvel, S., and Boxem, M. (2021). Caenorhabditis elegans LET-413 Scribble is essential in the epidermis for growth, viability, and directional outgrowth of epithelial seam cells. PLoS Genet. *17*, e1009856. https://doi.org/10.1371/journal.pgen.1009856.

63. Josephson, M.P., Aliani, R., Norris, M.L., Ochs, M.E., Gujar, M., and Lundquist, E.A. (2017). The Caenorhabditis elegans NF2/Merlin Molecule NFM-1 Nonautonomously Regulates Neuroblast Migration and Interacts Genetically with the Guidance Cue SLT-1/Slit. Genetics *205*, 737–748. https://doi.org/10.1534/genetics.116.191957.

64. Huang, W., Kew, C., Fernandes, S.d.A., Löhrke, A., Han, L., Demetriades, C., and Antebi, A. (2022). Decreased spliceosome fidelity and egl-8 intron retention inhibit mTORC1 signaling to promote longevity. Nat. Aging *2*, 796–808. https://doi.org/10.1038/s43587-022-00275-z.

65. Grant, B., and Greenwald, I. (1997). Structure, function, and expression of SEL-1, a negative regulator of LIN-12 and GLP-1 in C. elegans. Development *124*, 637–644. https://doi.org/10.1242/dev.124.3.637.

66. Lee, K.E., Cho, J.H., and Song, H.O. (2023). a Ca(2+) Binding Protein, Is Required for Dauer Formation in Caenorhabditis elegans. Biology *12*, 464. https://doi.org/10.3390/biology12030464.

67. Ghenea, S., Chiritoiu, M., Tacutu, R., Miranda-Vizuete, A., and Petrescu, S.M. (2022). Targeting EDEM protects against ER stress and improves development and survival in C. elegans. PLoS Genet. *18*, e1010069. https://doi.org/10.1371/journal.pgen.1010069.

68. Shen, X., Ellis, R.E., Lee, K., Liu, C.Y., Yang, K., Solomon, A., Yoshida, H., Morimoto, R., Kurnit, D.M., Mori, K., and Kaufman, R.J. (2001). Complementary signaling pathways regulate the unfolded protein response and are required for C. elegans development. Cell *107*, 893–903. https://doi.org/10.1016/s0092-8674(01)00612-2.

69. Bai, M., Vozdek, R., Hnízda, A., Jiang, C., Wang, B., Kuchar, L., Li, T., Zhang, Y., Wood, C., Feng, L., et al. (2018). Conserved roles of C. elegans and human MANFs in sulfatide binding and cytoprotection. Nat. Commun. *9*, 897. https://doi.org/10.1038/s41467-018-03355-0.

70. McGhee, J. (2007). The C. elegans intestine. In WormBook (The C. elegans Research Community, Pasadena (CA)), pp. 1–36. https://doi.org/10.1895/wormbook.1.133.

71. Perez, M.F., and Lehner, B. (2019). Vitellogenins - Yolk Gene Function and Regulation in Caenorhabditis elegans. Front. Physiol. *10*, 1067. https://doi.org/10.3389/fphys.2019.01067.

72. Ødum, M.T., Teufel, F., Thumuluri, V., Almagro Armenteros, J.J., Johansen, A.R., Winther, O., and Nielsen, H. (2024). DeepLoc 2.1: multi-label membrane protein type prediction using protein language models. Nucleic Acids Res. *52*, W215–W220. https://doi.org/10.1093/nar/gkae237.

73. Campbell, B.C., Nabel, E.M., Murdock, M.H., Lao-Peregrin, C., Tsoulfas, P., Blackmore, M.G., Lee, F.S., Liston, C., Morishita, H., and Petsko, G.A. (2020). mGreenLantern: a bright monomeric fluorescent protein with rapid expression and cell filling properties for neuronal imaging. Proc. Natl. Acad. Sci. USA *117*, 30710–30721. https://doi.org/10.1073/pnas.2000942117.

74. Fares, H., and Greenwald, I. (2001). Genetic analysis of endocytosis in Caenorhabditis elegans: coelomocyte uptake defective mutants. Genetics *159*, 133–145. https://doi.org/10.1093/genetics/159.1.133.

75. Gribble, F.M., and Reimann, F. (2019). Function and mechanisms of enteroendocrine cells and gut hormones in metabolism. Nat. Rev. Endocrinol. *15*, 226–237. https://doi.org/10.1038/s41574-019-0168-8.

76. Hung, R.J., Hu, Y., Kirchner, R., Liu, Y., Xu, C., Comjean, A., Tattikota, S.G., Li, F., Song, W., Ho Sui, S., and Perrimon, N. (2020). A cell atlas of the adult Drosophila midgut. Proc. Natl. Acad. Sci. USA *117*, 1514–1523. https://doi.org/10.1073/pnas.1916820117.

77. Zhao, T.J., Sakata, I., Li, R.L., Liang, G., Richardson, J.A., Brown, M.S., Goldstein, J.L., and Zigman, J.M. (2010). Ghrelin secretion stimulated by beta1-adrenergic receptors in cultured ghrelinoma cells and in fasted mice. Proc. Natl. Acad. Sci. USA *107*, 15868–15873. https://doi.org/10.1073/pnas.1011116107.

78. Worthington, J.J., Reimann, F., and Gribble, F.M. (2018). Enteroendocrine cells-sensory sentinels of the intestinal environment and orchestrators of mucosal immunity. Mucosal Immunol. *11*, 3–20. https://doi.org/10.1038/mi.2017.73.

79. McGee, M.D., Weber, D., Day, N., Vitelli, C., Crippen, D., Herndon, L.A., Hall, D.H., and Melov, S. (2011). Loss of intestinal nuclei and intestinal integrity in aging C. elegans. Aging Cell *10*, 699–710. https://doi.org/10.1111/j.1474-9726.2011.00713.x.

80. Salazar, A.M., Aparicio, R., Clark, R.I., Rera, M., and Walker, D.W. (2023). Intestinal barrier dysfunction: an evolutionarily conserved hallmark of aging. Dis. Model. Mech. *16*, dmm049969. https://doi.org/10.1242/dmm.049969.

81. Rera, M., Clark, R.I., and Walker, D.W. (2012). Intestinal barrier dysfunction links metabolic and inflammatory markers of aging to death in Drosophila. Proc. Natl. Acad. Sci. USA *109*, 21528–21533. https://doi.org/10.1073/pnas.1215849110.

82. Sovran, B., Hugenholtz, F., Elderman, M., Van Beek, A.A., Graversen, K., Huijskes, M., Boekschoten, M.V., Savelkoul, H.F.J., De Vos, P., Dekker, J., and Wells, J.M. (2019). Age-associated Impairment of the Mucus Barrier Function is Associated with Profound Changes in Microbiota and Immunity. Sci. Rep. *9*, 1437. https://doi.org/10.1038/s41598-018-35228-3.

83. Egge, N., Arneaud, S.L., Wales, P., Mihelakis, M., McClendon, J., Fonseca, R.S., Savelle, C., Gonzalez, I., Ghorashi, A., Yadavalli, S., et al. (2019). Age-Onset Phosphorylation of a Minor Actin Variant Promotes

Intestinal Barrier Dysfunction. Dev. Cell *51*, 587–601.e7. https://doi.org/10.1016/j.devcel.2019.11.001.

84. Grant, B., and Hirsh, D. (1999). Receptor-mediated endocytosis in the Caenorhabditis elegans oocyte. Mol. Biol. Cell *10*, 4311–4326. https://doi.org/10.1091/mbc.10.12.4311.

85. Zhai, C., Zhang, N., Li, X., Chen, X., Sun, F., and Dong, M. (2022). Fusion and expansion of vitellogenin vesicles during Caenorhabditis elegans intestinal senescence. Aging Cell *21*, e13719. https://doi.org/10.1111/acel.13719.

86. Ljusberg, J., Ek-Rylander, B., and Andersson, G. (1999). Tartrate-resistant purple acid phosphatase is synthesized as a latent proenzyme and activated by cysteine proteinases. Biochem. J. *343 Pt 1*, 63–69.

87. Rathod, B., Desai, S., Samvelyan, H.J., Bock, L., Wu, J., Ohlsson, C., Palmquist, A., Alm, J.J., Newton, P.T., Andersson, G., and Windahl, S.H. (2024). Tartrate-resistant acid phosphatase (TRAP/ACP5) promotes bone length, regulates cortical and trabecular bone mass, and maintains growth plate architecture and width in a sex- and site-specific manner in mice. Bone *188*, 117223. https://doi.org/10.1016/j.bone.2024.117223.

88. Schenk, G., Mitić, N., Hanson, G.R., and Comba, P. (2013). Purple acid phosphatase: a journey into the function and mechanism of a colorful enzyme. Coord. Chem. Rev. *257*, 473–482. https://doi.org/10.1016/j.ccr.2012.03.020.

89. Tang, Q., Li, Y., and He, J. (2022). MANF: an emerging therapeutic target for metabolic diseases. Trends Endocrinol. Metab. *33*, 236–246. https://doi.org/10.1016/j.tem.2022.01.001.

90. Weir, M.L., Xie, H., Klip, A., and Trimble, W.S. (2001). VAP-A binds promiscuously to both v- and tSNAREs. Biochem. Biophys. Res. Commun. *286*, 616–621. https://doi.org/10.1006/bbrc.2001.5437.

91. Halleen, J.M., Kaija, H., Stepan, J.J., Vihko, P., and Väänänen, H.K. (1998). Studies on the protein tyrosine phosphatase activity of tartrate-resistant acid phosphatase. Arch. Biochem. Biophys. *352*, 97–102. https://doi.org/10.1006/abbi.1998.0600.

92. Medoh, U.N., Hims, A., Chen, J.Y., Ghoochani, A., Nyame, K., Dong, W., and Abu-Remaileh, M. (2023). The Batten disease gene product CLN5 is the lysosomal bis(monoacylglycero)phosphate synthase. Science *381*, 1182–1189. https://doi.org/10.1126/science.adg9288.

93. Schenk, G., Elliott, T.W., Leung, E., Carrington, L.E., Mitić, N., Gahan, L.R., and Guddat, L.W. (2008). Crystal structures of a purple acid phosphatase, representing different steps of this enzyme's catalytic cycle. BMC Struct. Biol. *8*, 6. https://doi.org/10.1186/1472-6807-8-6.

94. Kenyon, C., Chang, J., Gensch, E., Rudner, A., and Tabtiang, R. (1993). elegans mutant that lives twice as long as wild type. Nature *366*, 461–464. https://doi.org/10.1038/366461a0.

95. Murphy, C.T., McCarroll, S.A., Bargmann, C.I., Fraser, A., Kamath, R.S., Ahringer, J., Li, H., and Kenyon, C. (2003). Genes that act downstream of DAF-16 to influence the lifespan of Caenorhabditis elegans. Nature *424*, 277–283. https://doi.org/10.1038/nature01789.

96. Lapierre, L.R., De Magalhaes Filho, C.D., McQuary, P.R., Chu, C.C., Visvikis, O., Chang, J.T., Gelino, S., Ong, B., Davis, A.E., Irazoqui, J.E., et al. (2013). The TFEB orthologue HLH-30 regulates autophagy and modulates longevity in Caenorhabditis elegans. Nat. Commun. *4*, 2267. https://doi.org/10.1038/ncomms3267.

97. Troemel, E.R., Chu, S.W., Reinke, V., Lee, S.S., Ausubel, F.M., and Kim, D.H. (2006). p38 MAPK regulates expression of immune response genes and contributes to longevity in C. elegans. PLoS Genet. *2*, e183. https://doi.org/10.1371/journal.pgen.0020183.

98. Taylor, R.C., and Dillin, A. (2013). XBP-1 is a cell-nonautonomous regulator of stress resistance and longevity. Cell *153*, 1435–1447. https://doi.org/10.1016/j.cell.2013.05.042.

99. Durieux, J., Wolff, S., and Dillin, A. (2011). The cell-non-autonomous nature of electron transport chain-mediated longevity. Cell *144*, 79–91. https://doi.org/10.1016/j.cell.2010.12.016.

100. Henderson, S.T., and Johnson, T.E. (2001). daf-16 integrates developmental and environmental inputs to mediate aging in the nematode Caenorhabditis elegans. Curr. Biol. *11*, 1975–1980. https://doi.org/10.1016/s0960-9822(01)00594-2.

101. Shivers, R.P., Kooistra, T., Chu, S.W., Pagano, D.J., and Kim, D.H. (2009). Tissue-specific activities of an immune signaling module regulate physiological responses to pathogenic and nutritional bacteria in C. elegans. Cell Host Microbe *6*, 321–330. https://doi.org/10.1016/j.chom.2009.09.001.

102. Kapulkin, V., Hiester, B.G., and Link, C.D. (2005). Compensatory regulation among ER chaperones in C. elegans. FEBS Lett. *579*, 3063–3068. https://doi.org/10.1016/j.febslet.2005.04.062.

103. Benedetti, C., Haynes, C.M., Yang, Y., Harding, H.P., and Ron, D. (2006). Ubiquitin-like protein 5 positively regulates chaperone gene expression in the mitochondrial unfolded protein response. Genetics *174*, 229–239. https://doi.org/10.1534/genetics.106.061580.

104. Soumya, P.R., Vengavasi, K., and Pandey, R. (2022). Adaptive strategies of plants to conserve internal phosphorus under P deficient condition to improve P utilization efficiency. Physiol. Mol. Biol. Plants *28*, 1981–1993. https://doi.org/10.1007/s12298-022-01255-8.

105. Halleen, J.M., Alatalo, S.L., Suominen, H., Cheng, S., Janckila, A.J., and Väänänen, H.K. (2000). Tartrate-resistant acid phosphatase 5b: a novel serum marker of bone resorption. J. Bone Miner. Res. *15*, 1337–1345. https://doi.org/10.1359/jbmr.2000.15.7.1337.

106. Yuan, Y., Kadiyala, C.S., Ching, T.T., Hakimi, P., Saha, S., Xu, H., Yuan, C., Mullangi, V., Wang, L., Fivenson, E., et al. (2012). Enhanced energy metabolism contributes to the extended life span of calorie-restricted Caenorhabditis elegans. J. Biol. Chem. *287*, 31414–31426. https://doi.org/10.1074/jbc.M112.377275.

107. Lev, S., Halevy, D.B., Peretti, D., and Dahan, N. (2008). The VAP protein family: from cellular functions to motor neuron disease. Trends Cell Biol. *18*, 282–290. https://doi.org/10.1016/j.tcb.2008.03.006.

108. Espelt, M.V., Estevez, A.Y., Yin, X., and Strange, K. (2005). Oscillatory Ca2+ signaling in the isolated Caenorhabditis elegans intestine: role of the inositol-1,4,5-trisphosphate receptor and phospholipases C beta and gamma. J. Gen. Physiol. *126*, 379–392. https://doi.org/10.1085/jgp.200509355.

109. Zou, L., Wu, D., Zang, X., Wang, Z., Wu, Z., and Chen, D. (2019). Construction of a germline-specific RNAi tool in C. elegans. Sci. Rep. *9*, 2354. https://doi.org/10.1038/s41598-019-38950-8.

110. Qadota, H., Inoue, M., Hikita, T., Köppen, M., Hardin, J.D., Amano, M., Moerman, D.G., and Kaibuchi, K. (2007). Establishment of a tissue-specific RNAi system in C. elegans. Gene *400*, 166–173. https://doi.org/10.1016/j.gene.2007.06.020.

111. Gkikas, I., Daskalaki, I., Kounakis, K., Tavernarakis, N., and Lionaki, E. (2023). MitoSNARE Assembly and Disassembly Factors Regulate Basal Autophagy and Aging in C. elegans. Int. J. Mol. Sci. *24*, 4230. https://doi.org/10.3390/ijms24044230.

112. Zhang, Z., Luo, S., Barbosa, G.O., Bai, M., Kornberg, T.B., and Ma, D.K. (2021). The conserved transmembrane protein TMEM-39 coordinates with COPII to promote collagen secretion and regulate ER stress response. PLoS Genet. *17*, e1009317. https://doi.org/10.1371/journal.pgen.1009317.

113. An, J.H., and Blackwell, T.K. (2003). SKN-1 links C. elegans mesendodermal specification to a conserved oxidative stress response. Genes Dev. *17*, 1882–1893. https://doi.org/10.1101/gad.1107803.

114. Rea, S.L., Wu, D., Cypser, J.R., Vaupel, J.W., and Johnson, T.E. (2005). A stress-sensitive reporter predicts longevity in isogenic populations of Caenorhabditis elegans. Nat. Genet. *37*, 894–898. https://doi.org/10.1038/ng1608.

115. Gelino, S., Chang, J.T., Kumsta, C., She, X., Davis, A., Nguyen, C., Panowski, S., and Hansen, M. (2016). Intestinal Autophagy Improves

Healthspan and Longevity in C. elegans during Dietary Restriction. PLoS Genet. *12*, e1006135. https://doi.org/10.1371/journal.pgen.1006135.

116. Chelakkot, C., Ghim, J., and Ryu, S.H. (2018). Mechanisms regulating intestinal barrier integrity and its pathological implications. Exp. Mol. Med. *50*, 1–9. https://doi.org/10.1038/s12276-018-0126-x.

117. Dimov, I., Maduro, M.F., and The, C. (2019). elegans intestine: organogenesis, digestion, and physiology. Cell Tissue Res. *377*, 383–396. https://doi.org/10.1007/s00441-019-03036-4.

118. Liu, J., Jang, J.Y., Pirooznia, M., Liu, S., and Finkel, T. (2021). The secretome mouse provides a genetic platform to delineate tissue-specific in vivo secretion. Proc. Natl. Acad. Sci. USA *118*, e2005134118. https://doi.org/10.1073/pnas.2005134118.

119. Nikonorova, I.A., Wang, J., Cope, A.L., Tilton, P.E., Power, K.M., Walsh, J.D., Akella, J.S., Krauchunas, A.R., Shah, P., and Barr, M.M. (2022). Isolation, profiling, and tracking of extracellular vesicle cargo in Caenorhabditis elegans. Curr. Biol. *32*, 1924–1936.e6. https://doi.org/10.1016/j.cub.2022.03.005.

120. Oh, H.S.H., Le Guen, Y., Rappoport, N., Urey, D.Y., Farinas, A., Rutledge, J., Channappa, D., Wagner, A.D., Mormino, E., Brunet, A., et al. (2025). Plasma proteomics links brain and immune system aging with healthspan and longevity. Nat. Med. *31*, 2703–2711. https://doi.org/10.1038/s41591-025-03798-1.

121. Patel, S.K., Bons, J., Rose, J.P., Chappel, J.R., Beres, R.L., Watson, M.A., Webster, C., Burton, J.B., Bruderer, R., Desprez, P.Y., et al. (2025). Exosomes released from senescent cells and circulatory exosomes isolated from human plasma reveal aging-associated proteomic and lipid signatures. Aging (Albany NY) *17*, 1929–1965. https://doi.org/10.18632/aging.206292.

122. Evans, D.S., Young, D., Tanaka, T., Basisty, N., Bandinelli, S., Ferrucci, L., Campisi, J., and Schilling, B. (2024). Proteomic Analysis of the Senescence-Associated Secretory Phenotype: GDF-15, IGFBP-2, and Cystatin-C Are Associated With Multiple Aging Traits. J. Gerontol. A Biol. Sci. Med. Sci. *79*, glad265. https://doi.org/10.1093/gerona/glad265.

123. Sim, X., Ong, R.T.H., Suo, C., Tay, W.T., Liu, J., Ng, D.P.K., Boehnke, M., Chia, K.S., Wong, T.Y., Seielstad, M., et al. (2011). Transferability of type 2 diabetes implicated loci in multi-ethnic cohorts from Southeast Asia. PLoS Genet. *7*, e1001363. https://doi.org/10.1371/journal.pgen.1001363.

124. Willett, J.D.S., Waqas, M., Choi, Y., Ngai, T., Mullin, K., Tanzi, R.E., and Prokopenko, D. (2025). Identification of 16 novel Alzheimer's disease loci using multi-ancestry meta-analyses. Alzheimer's Dement. *21*, e14592. https://doi.org/10.1002/alz.14592.

125. Hayman, A.R., Bune, A.J., Bradley, J.R., Rashbass, J., and Cox, T.M. (2000). Osteoclastic tartrate-resistant acid phosphatase (Acp 5): its localization to dendritic cells and diverse murine tissues. J. Histochem. Cytochem. *48*, 219–228. https://doi.org/10.1177/002215540004800207.

126. Ek-Rylander, B., Flores, M., Wendel, M., Heinegård, D., and Andersson, G. (1994). Dephosphorylation of osteopontin and bone sialoprotein by osteoclastic tartrate-resistant acid phosphatase. Modulation of osteoclast adhesion in vitro. J. Biol. Chem. *269*, 14853–14856.

127. Ferrari, E., Tinti, M., Costa, S., Corallino, S., Nardozza, A.P., Chatrayamontri, A., Ceol, A., Cesareni, G., and Castagnoli, L. (2011). Identification of new substrates of the protein-tyrosine phosphatase PTP1B by Bayesian integration of proteome evidence. J. Biol. Chem. *286*, 4173–4185. https://doi.org/10.1074/jbc.M110.157420.

128. Huang, C.F., Gottardi, C.J., and Mrksich, M. (2022). Tyrosine phosphatase activity is restricted by basic charge substituting mutation of substrates. Sci. Rep. *12*, 15095. https://doi.org/10.1038/s41598-022-19133-4.

129. Horowitz, A.M., Fan, X., Bieri, G., Smith, L.K., Sanchez-Diaz, C.I., Schroer, A.B., Gontier, G., Casaletto, K.B., Kramer, J.H., Williams, K.E., and Villeda, S.A. (2020). Blood factors transfer beneficial effects of exercise on neurogenesis and cognition to the aged brain. Science *369*, 167–173. https://doi.org/10.1126/science.aaw2622.

130. Douglas, P.M., Baird, N., Simic, M., Uhlein, S., McCormick, M., Wolff, S., Kennedy, B., and Dillin, A. (2015). Heterotypic Signals from Neural HSF-1 Separate Thermotolerance from Longevity. Cell Rep. *12*, 1196–1204. https://doi.org/10.1016/j.celrep.2015.07.026.

131. Dal Santo, P., Logan, M.A., Chisholm, A.D., and Jorgensen, E.M. (1999). The inositol trisphosphate receptor regulates a 50-second behavioral rhythm in C. elegans. Cell *98*, 757–767. https://doi.org/10.1016/s0092-8674(00)81510-x.

132. Perez-Riverol, Y., Bai, J., Bandla, C., García-Seisdedos, D., Hewapathirana, S., Kamatchinathan, S., Kundu, D., Prakash, A., Frericks-Zipper, A., Eisenacher, M., et al. (2022). The PRIDE database resources in 2022: a hub for mass spectrometry-based proteomics evidences. Nucleic Acids Res. *50*, D543–D552. https://doi.org/10.1093/nar/gkab1038.

133. Silva-García, C.G., Lanjuin, A., Heintz, C., Dutta, S., Clark, N.M., and Mair, W.B. (2019). Single-Copy Knock-In Loci for Defined Gene Expression in Caenorhabditis elegans. G3 *9*, 2195–2198. https://doi.org/10.1534/g3.119.400314.

134. Granato, M., Schnabel, H., and Schnabel, R. (1994). pha-1, a selectable marker for gene transfer in C. elegans. Nucleic Acids Res. *22*, 1762–1763. https://doi.org/10.1093/nar/22.9.1762.

135. Szklarczyk, D., Gable, A.L., Lyon, D., Junge, A., Wyder, S., Huerta-Cepas, J., Simonovic, M., Doncheva, N.T., Morris, J.H., Bork, P., et al. (2019). STRING v11: protein-protein association networks with increased coverage, supporting functional discovery in genome-wide experimental datasets. Nucleic Acids Res. *47*, D607–D613. https://doi.org/10.1093/nar/gky1131.

136. Holm, L., Laiho, A., Törönen, P., and Salgado, M. (2023). DALI shines a light on remote homologs: One hundred discoveries. Protein Sci. *32*, e4519. https://doi.org/10.1002/pro.4519.

137. Bankhead, P., Loughrey, M.B., Fernández, J.A., Dombrowski, Y., McArt, D.G., Dunne, P.D., McQuaid, S., Gray, R.T., Murray, L.J., Coleman, H.G., et al. (2017). QuPath: Open source software for digital pathology image analysis. Sci. Rep. *7*, 16878. https://doi.org/10.1038/s41598-017-17204-5.

138. Sinitcyn, P., Tiwary, S., Rudolph, J., Gutenbrunner, P., Wichmann, C., Yılmaz, Ş., Hamzeiy, H., Salinas, F., and Cox, J. (2018). MaxQuant goes Linux. Nat. Methods *15*, 401. https://doi.org/10.1038/s41592-018-0018-y.

139. Teufel, F., Almagro Armenteros, J.J., Johansen, A.R., Gíslason, M.H., Pihl, S.I., Tsirigos, K.D., Winther, O., Brunak, S., von Heijne, G., and Nielsen, H. (2022). SignalP 6.0 predicts all five types of signal peptides using protein language models. Nat. Biotechnol. *40*, 1023–1025. https://doi.org/10.1038/s41587-021-01156-3.

140. Redemann, S., Schloissnig, S., Ernst, S., Pozniakowsky, A., Ayloo, S., Hyman, A.A., and Bringmann, H. (2011). Codon adaptation-based control of protein expression in C. elegans. Nat. Methods *8*, 250–252. https://doi.org/10.1038/nmeth.1565.

141. Fire, A., Harrison, S.W., and Dixon, D. (1990). A modular set of lacZ fusion vectors for studying gene expression in Caenorhabditis elegans. Gene *93*, 189–198. https://doi.org/10.1016/0378-1119(90)90224-f.

142. Arribere, J.A., Bell, R.T., Fu, B.X.H., Artiles, K.L., Hartman, P.S., and Fire, A.Z. (2014). Efficient marker-free recovery of custom genetic modifications with CRISPR/Cas9 in Caenorhabditis elegans. Genetics *198*, 837–846. https://doi.org/10.1534/genetics.114.169730.

143. Kim, H., Ishidate, T., Ghanta, K.S., Seth, M., Conte, D., Jr., Shirayama, M., and Mello, C.C. (2014). A co-CRISPR strategy for efficient genome editing in Caenorhabditis elegans. Genetics *197*, 1069–1080. https://doi.org/10.1534/genetics.114.166389.

144. Zhang, H., Artiles, K.L., and Fire, A.Z. (2015). Functional relevance of "seed" and "non-seed" sequences in microRNA-mediated promotion of C. elegans developmental progression. RNA *21*, 1980–1992. https://doi.org/10.1261/rna.053793.115.

145. Ward, J.D. (2015). Rapid and precise engineering of the Caenorhabditis elegans genome with lethal mutation co-conversion and inactivation of NHEJ repair. Genetics *199*, 363–377. https://doi.org/10.1534/genetics.114.172361.

146. Dickinson, D.J., Ward, J.D., Reiner, D.J., and Goldstein, B. (2013). Engineering the Caenorhabditis elegans genome using Cas9-triggered homologous recombination. Nat. Methods *10*, 1028–1034. https://doi.org/10.1038/nmeth.2641.

147. Paix, A., Folkmann, A., Rasoloson, D., and Seydoux, G. (2015). High Efficiency, Homology-Directed Genome Editing in Caenorhabditis elegans Using CRISPR-Cas9 Ribonucleoprotein Complexes. Genetics *201*, 47–54. https://doi.org/10.1534/genetics.115.179382.

148. Papsdorf, K., Miklas, J.W., Hosseini, A., Cabruja, M., Morrow, C.S., Savini, M., Yu, Y., Silva-García, C.G., Haseley, N.R., Murphy, L.M., et al. (2023). Lipid droplets and peroxisomes are co-regulated to drive lifespan extension in response to mono-unsaturated fatty acids. Nat. Cell Biol. *25*, 672–684. https://doi.org/10.1038/s41556-023-01136-6.

149. Rappsilber, J., Mann, M., and Ishihama, Y. (2007). Protocol for micro-purification, enrichment, pre-fractionation and storage of peptides for proteomics using StageTips. Nat. Protoc. *2*, 1896–1906. https://doi.org/10.1038/nprot.2007.261.

150. Li, J., Han, S., Li, H., Udeshi, N.D., Svinkina, T., Mani, D., Xu, C., Guajardo, R., Xie, Q., Li, T., et al. (2020). Cell-Surface Proteomic Profiling in the Fly Brain Uncovers Wiring Regulators. Cell *180*, 373–386.e15. https://doi.org/10.1016/j.cell.2019.12.029.

151. Cho, K.F., Branon, T.C., Rajeev, S., Svinkina, T., Udeshi, N.D., Thoudam, T., Kwak, C., Rhee, H.W., Lee, I.K., Carr, S.A., and Ting, A.Y. (2020). Split-TurboID enables contact-dependent proximity labeling in cells. Proc. Natl. Acad. Sci. USA *117*, 12143–12154. https://doi.org/10.1073/pnas.1919528117.

152. Dobin, A., Davis, C.A., Schlesinger, F., Drenkow, J., Zaleski, C., Jha, S., Batut, P., Chaisson, M., and Gingeras, T.R. (2013). STAR: ultrafast universal RNA-seq aligner. Bioinformatics *29*, 15–21. https://doi.org/10.1093/bioinformatics/bts635.

153. Liao, Y., Smyth, G.K., and Shi, W. (2014). featureCounts: an efficient general purpose program for assigning sequence reads to genomic features. Bioinformatics *30*, 923–930. https://doi.org/10.1093/bioinformatics/btt656.

154. Muzellec, B., Teleńczuk, M., Cabeli, V., and Andreux, M. (2023). PyDESeq2: a python package for bulk RNA-seq differential expression analysis. Bioinformatics *39*, btad547. https://doi.org/10.1093/bioinformatics/btad547.

155. Wolf, F.A., Angerer, P., and Theis, F.J. (2018). SCANPY: large-scale single-cell gene expression data analysis. Genome Biol. *19*, 15. https://doi.org/10.1186/s13059-017-1382-0.

156. Waskom, M. (2021). Seaborn: statistical data visualization. J. Open Source Softw. *6*, 3021. https://doi.org/10.21105/joss.03021.

157. Blom, N., Sicheritz-Pontén, T., Gupta, R., Gammeltoft, S., and Brunak, S. (2004). Prediction of post-translational glycosylation and phosphorylation of proteins from the amino acid sequence. Proteomics *4*, 1633–1649. https://doi.org/10.1002/pmic.200300771.

STAR★METHODS

KEY RESOURCES TABLE

REAGENT or RESOURCE	SOURCE	IDENTIFIER
Antibodies		
Streptavidin, Alexa Fluor 680 Conjugate	Invitrogen	S32358
Anti-HA tag	Roche	11867423001; RRID: AB_390918
Anti-Alpha Tubulin	Sigma-Aldrich	T6074; RRID: AB_477582
Anti-GFP	Santa Cruz Biotechnology	sc-9996; RRID: AB_627695
Goat anti-rat 594 (IHC)	Invitrogen	A-21209
Donkey anti-mouse 488 (IHC)	Invitrogen	A-21202
Goat anti-rat 680 (Western blot)	LI-COR	926–68076
Goat anti-mouse 800 (Western blot)	LI-COR	926–32210
Bacterial and virus strains		
OP50-1	M.-W. Tan	
HT115	Ahringer library	
10-beta Competent *E. coli*	NEB	C3019H
Chemicals, peptides, and recombinant proteins		
RIPA buffer	Alfa Aesar	J62524
Nitrocellulose membrane	Bio-Rad	1620094
Zirconia/Silica Beads 0.1 mm dia	BioSpec Products	11079101Z
Sodium deoxycholate	EMD Millipore	264103
Protein LoBind conical tubes 15 mL	Eppendorf	30122216
Transfer buffer - Tris	Fisher BioReagents	BP152-5
Glycerol	Fisher BioReagents	BP229-1
Triton X-100	Fisher Scientific	BP151
0.5M Tris pH 6.8	Fisher Scientific	AAJ63735AP
1M Tris-HCl pH 8.0	Fisher Scientific	15-568-025
PBS (10X), pH 7.4	Gibco	70011069
Alt-R S.p. Cas9 Nuclease V3	IDT	1081058
MOPS buffer	Invitrogen	NP001
Transfer buffer - Glycine	Invitrogen	15527013
NuPage gel	Invitrogen	NP0321BOX
UHPLC column	Ionopticks	AUR3-25075C18A
Licor buffer	LI-COR	927–60001
HEPES, 1M, pH 7.3	Millipore Sigma	7365-45-9
Adenosine 5′-triphosphate disodium salt hydrate (ATP)	Millipore Sigma	A2383
Urea	Millipore Sigma	U5378
Sodium Carbonate	Millipore Sigma	S7795
EPPS	Millipore Sigma	E1894
Loading dye	NEB	B7703S
Protein Ladder	NEB	P7719S
QIAzol lysis reagent	Qiagen	79306
Inhibitor (cOmplete mini)	Roche	11836153001
NaCl	Sigma	71376
$MgCl_2$	Sigma	M3634
Valproic acid sodium salt	Sigma	P4543
D-(+)-Glucose	Sigma	G8270

(*Continued on next page*)

Continued

REAGENT or RESOURCE	SOURCE	IDENTIFIER
Collagenase IV	Sigma-Aldrich	C-5138
$CaCl_2$ · 2H2O	Sigma-Aldrich	C7902
Bovin serum albumin	Sigma-Aldrich	A7979
2-Mercaptoethanol	Sigma-Aldrich	M6250
Tween 20	Sigma-Aldrich	P1379
Ponceau solution	Sigma-Aldrich	P7170
Sodium dodecyl sulfate (SDS)	Sigma-Aldrich	L3771
Leupeptin	Sigma-Aldrich	L8511
Pepstatin A	Sigma-Aldrich	P5318
1M Tris pH 7.6	ThermoFisher Scientific	J61036.K2
16% Formaldehyde	ThermoFisher Scientific	28906
PMSF	ThermoFisher Scientific	36978B
HALT Protease Inhibitor Cocktail	ThermoFisher Scientific	78429
LC-MS Grade Water	ThermoFisher Scientific	51140
Dithiothreitol (DTT)	ThermoFisher Scientific	20290
TURBO DNase	ThermoFisher Scientific	AM2238
Acid Phenol:Chloroform	ThermoFisher Scientific	AM9720
SYBR Green PCR Master Mix	ThermoFisher Scientific	4309155
Pierce anti-HA magnetic beads	ThermoFisher Scientific	88837
Halt Protease Inhibitor Cocktail, EDTA free	ThermoFisher Scientific	87785
Streptavidin magnetic beads	ThermoFisher Scientific	88817
HisPur Ni-NTA	ThermoFisher Scientific	88221
Expi293F expression media	ThermoFisher Scientific	A1435101
Freestyle 293 expression media	ThermoFisher Scientific	12338018
TMTpro 16plex	ThermoFisher Scientific	A44521
Acetonitrile, 99.9%, extra dry, AcroSeal	ThermoFisher Scientific	448391000
Low protein binding microcentrifuge tubes 2.0 mL	ThermoFisher Scientific	88379
PEI STAR	Tocris	7854
Probe Sonicator	Virtis Versonic	
Achromobacter lyticus Lysyl Endopeptidase	VWR	100369–826
Sep-Pak tC18	Waters	WAT054960
RIPA buffer	Alfa Aesar	J62524
Nitrocellulose membrane	Bio-Rad	1620094
Zirconia/Silica Beads 0.1 mm dia	BioSpec Products	11079101Z
Sodium deoxycholate	EMD Millipore	264103
Protein LoBind conical tubes 15 mL	Eppendorf	30122216
Transfer buffer - Tris	Fisher BioReagents	BP152-5
Glycerol	Fisher BioReagents	BP229-1
Triton X-100	Fisher Scientific	BP151
0.5M Tris pH 6.8	Fisher Scientific	AAJ63735AP
Imidazole	Boston Bioproducts	BB-1117
Critical commercial assays		
High Capacity cDNA Reverse Transcription Kit	Fisher Scientific	43-688-13
BCA kit	ThermoFisher Scientific	23225
EnzChek phosphatase assay kit	ThermoFisher Scientific	E12020
Protein Tyrosine Phosphatase Assay Kit	abcam	ab241032
Serine/Threonine Phosphatase Assay System	Promega	V2460

(*Continued on next page*)

Continued

REAGENT or RESOURCE	SOURCE	IDENTIFIER
Pierce High pH Reversed-Phase Peptide Fractionation Kit	ThermoFisher Scientific	84868
Deposited data		
Code for mass spec analysis and transcriptomics	Github	https://github.com/miklasja/Intestine-Secretome-Paper
Code for mass spec analysis and transcriptomics	Zenodo	https://doi.org/10.5281/zenodo.21210820
Mass spectrometry data	Proteome Xchange	http://www.proteomexchange.org/
RNA-sequencing data	Gene Expression Omnibus (GEO)	https://www.ncbi.nlm.nih.gov/geo/
Experimental models: Cell lines		
Expi293F	ThermoFisher Scientific	A14527
Experimental models: Organisms/strains		
C. elegans: Bristol (N2) strain as wild-type (WT)	CGC	N2
C. elegans: CGC1	Fire lab	WormBase: CGC1
C. elegans: Strain PD1299: *pha-1(cc1299 [e2123ts])* in CGC1 background	This study(Fire lab)	PD1299
C. elegans: ABR273: [*pha-1*(cc1299 [e2123ts]); sybIs6766[*ges-1p::TurboID-ER::unc-54 3'UTR; myo-2p::mCherry::unc-54 3′UTR; pha-1*(+)]	This study(integrated at Sunybiotech)	ABR273
C. elegans: ABR388: [*pha-1*(cc1299 [e2123ts]); sybIs7982[*ges-1p::TurboID::unc-54 3′UTR; myo-2p::mCherry::unc-54 3′UTR; pha-1*(+)]	This study(integrated at Sunybiotech)	ABR388
C. elegans: VS25: hjIs14*[vha-6p::GFP::C34B2.10(SP12) + unc-119*(+)]	CGC	WormBase: VS25
C. elegans: ABR302: [*pha-1*(cc1299 [e2123ts]); sybIs6766[*ges-1p::TurboID-ER::unc-54 3′UTR; myo-2p::mCherry::unc-54 3′UTR; pha-1*(+)]; hjIs14[*vha-6p::GFP::C34B2.10(SP12) + unc-119*(+)]	This study	ABR302
C. elegans: ABR303: [*pha-1*(cc1299 [e2123ts]); sybIs7982[*ges-1p::TurboID::unc-54 3′UTR; myo-2p::mCherry::unc-54 3′UTR; pha-1*(+)]; hjIs14[*vha-6p::GFP::C34B2.10(SP12) + unc-119*(+)]	This study	ABR303
C. elegans: ABR287: [*pha-1*(cc1299 [e2123ts]); staEx11[*ges-1p::F21A3.11-2xLinker-WormScarlet::SL2WormGreenLantern::unc-54 3′UTR*; *pha-1*(+)]	This study	ABR287
C. elegans: ABR305: [*pha-1*(cc1299 [e2123ts]); staEx12[*ges-1p::F21A3.11-2xLinker-WormScarlet::unc-54 3′UTR + pha-1*(+)]; hjIs8[*ges-1p::GFP-PTS1*]	This study	ABR305
C. elegans: ABR306: [*pha-1*(cc1299 [e2123ts]); staEx12[*ges-1p::F21A3.11-2xLinker-WormScarlet::unc-54 3′UTR + pha-1*(+)]; hjIs9[*ges-1p::glo-1::GFP + unc-119*(+)]	This study	ABR306
C. elegans: ABR307: [*pha-1*(cc1299 [e2123ts]); staEx12[*ges-1p::F21A3.11-2xLinker-WormScarlet::unc-54 3′UTR + pha-1*(+)]; hjIs14[*vha-6p::GFP::C34B2.10(SP12) + unc-119*(+)]	This study	ABR307

(*Continued on next page*)

Continued

REAGENT or RESOURCE	SOURCE	IDENTIFIER
C. elegans: ABR327: [*pha-1*(cc1299 [e2123ts]); staEx13[*ges-1p::T05E12.3-2xLinker-WormScarlet::SL2WormGreenLantern::unc-54 3′UTR; pha-1*(+)]	This study	ABR327
C. elegans: ABR349: [*pha-1*(cc1299 [e2123ts]); staEx14[*ges-1p::T05E12.3-2xLinker-WormScarlet::unc-54 3′UTR + pha-1*(+)]; hjIs8[*ges-1p::GFP-PTS1*]	This study	ABR349
C. elegans: ABR350: [*pha-1*(cc1299 [e2123ts]); staEx14[*ges-1p::T05E12.3-2xLinker-WormScarlet::unc-54 3′UTR + pha-1*(+)]; hjIs9[*ges-1p::glo-1::GFP + unc-119*(+)]	This study	ABR350
C. elegans: ABR351: [*pha-1*(cc1299 [e2123ts]); staEx14[*ges-1p::T05E12.3-2xLinker-WormScarlet::unc-54 3′UTR + pha-1*(+)]; hjIs14[*vha-6p::GFP::C34B2.10(SP12) + unc-119*(+)]	This study	ABR351
C. elegans: ABR337: [*pha-1*(cc1299 [e2123ts]); staEx15[*ges-1p::C02A12.4-2xLinker-WormScarlet::SL2WormGreenLantern::unc-54 3′UTR; pha-1*(+)]	This study	ABR337
C. elegans: ABR346: [*pha-1*(cc1299 [e2123ts]); staEx16[*ges-1p::C02A12.4-2xLinker-WormScarlet::unc-54 3′UTR + pha-1*(+)]; hjIs8[*ges-1p::GFP-PTS1*]	This study	ABR346
C. elegans: ABR347: [*pha-1*(cc1299 [e2123ts]); staEx16[*ges-1p::C02A12.4-2xLinker-WormScarlet::unc-54 3′UTR + pha-1*(+)]; hjIs9[*ges-1p::glo-1::GFP + unc-119*(+)]	This study	ABR347
C. elegans: ABR348: [*pha-1*(cc1299 [e2123ts]); staEx16[*ges-1p::C02A12.4-2xLinker-WormScarlet::unc-54 3′UTR + pha-1*(+)]; hjIs14[*vha-6p::GFP::C34B2.10(SP12) + unc-119*(+)]	This study	ABR348
C. elegans: ABR333: [*pha-1*(cc1299 [e2123ts]); staEx17[*ges-1p::F56F10.1-2xLinker-WormScarlet::SL2WormGreenLantern::unc-54 3′UTR; pha-1*(+)]	This study	ABR333
C. elegans: ABR369: [*pha-1*(cc1299 [e2123ts]); staEx18[*ges-1p::F56F10.1-2xLinker-WormScarlet::unc-54 3′UTR + pha-1*(+)];hjIs8 [*ges-1p::GFP-PTS1*]	This study	ABR369
C. elegans: ABR370: [*pha-1*(cc1299 [e2123ts]); staEx18[*ges-1p::F56F10.1-2xLinker-WormScarlet::unc-54 3′UTR + pha-1*(+)]; hjIs9[*ges-1p::glo-1::GFP + unc-119*(+)]	This study	ABR370
C. elegans: ABR371: [*pha-1*(cc1299 [e2123ts]); staEx18[*ges-1p::F56F10.1-2xLinker-WormScarlet::unc-54 3′UTR + pha-1*(+)]; hjIs14[*vha-6p::GFP::C34B2.10(SP12) + unc-119*(+)]	This study	ABR371
C. elegans: ABR291: [*pha-1*(cc1299 [e2123ts]); staEx19[*ges-1p::F53B6.4-2xLinker-WormScarlet::SL2WormGreenLantern::unc-54 3′UTR; pha-1*(+)]	This study	ABR291

(*Continued on next page*)

Continued

REAGENT or RESOURCE	SOURCE	IDENTIFIER
C. elegans: ABR319: [*pha-1*(cc1299 [e2123ts]); staEx20[*ges-1p::F53B6.4-2xLinker-WormScarlet::unc-54 3′UTR + pha-1*(+)]; hjIs8[*ges-1p::GFP-PTS1*]	This study	ABR319
C. elegans: ABR320: [*pha-1*(cc1299 [e2123ts]); staEx20[*ges-1p::F53B6.4-2xLinker-WormScarlet::unc-54 3′UTR + pha-1*(+)]; hjIs9[*ges-1p::glo-1::GFP + unc-119*(+)]	This study	ABR320
C. elegans: ABR321: [*pha-1*(cc1299 [e2123ts]); staEx20[*ges-1p::F53B6.4-2xLinker-WormScarlet::unc-54 3′UTR + pha-1*(+)]; hjIs14[*vha-6p::GFP::C34B2.10(SP12) + unc-119*(+)]	This study	ABR321
C. elegans: ABR405: [*pha-1*(cc1299 [e2123ts]); staEx21[*ges-1p::GFP::unc-54 3′UTR; ges-1:SP-WormScarlet::unc-54 3′UTR; pha-1*(+)]	This study	ABR405
C. elegans: ABR279: staEx22[*ges-1p::WormScarlet::SL2WormGreen Lantern::unc-54 3′UTR; pha-1*(+)]	This study	ABR279
C. elegans: ABR355: [*pha-1*(cc1299 [e2123ts]); staEx20[*ges-1p::F53B6.4-2xLinker-WormScarlet::unc-54 3′UTR + pha-1*(+)]; [*unc-119*(ed3); pwIs170[*vha-6p::GFP::rab-7; Cbr-unc-119*(+)]	This study	ABR355
C. elegans: ABR486: [*pha-1*(cc1299 [e2123ts]); staEx20[*ges-1p::F53B6.4-2xLinker-WormScarlet::unc-54 3′UTR + pha-1*(+)]; ldrIs1[*dhs-3p::dhs-3::GFP; unc-76*(+)]]	This study	ABR486
C. elegans: ABR297: [*pha-1*(cc1299 [e2123ts]); staEx23[*ges-1p::(ΔSP)F21A3.11-2xLinker-WormScarlet::SL2WormGreenLantern::unc-54 3′UTR; pha-1*(+)]	This study	ABR297
C. elegans: ABR269: staEx24[*ges-1p::(ΔSP)F21A3.11::SL2WormScarlet::unc-54 3′UTR*]	This study	ABR269
C. elegans: ABR275: staEx25[*ges-1p::F21A3.11::SL2WormScarlet::unc-54 3′UTR*]	This study	ABR275
C. elegans: ABR417: [*pha-1*(cc1299 [e2123ts]); staEx27[*ges-1p::F21A3.11-3xHA-tag::SL2WormScarlet::unc-54 3′UTR*]	This study	ABR417
C. elegans: ABR429: [*pha-1*(cc1299 [e2123ts]); staEx28[*ges-1p::F21A3.11-7A-3xHA-tag::SL2WormScarlet::unc-54 3′UTR*]	This study	ABR429
C. elegans: ABR295: staEx30[*F21A3.11p::F21A3.11::2xLinker::WormScarlet::F21A3.11 3′UTR+ pha-1* (+)]; *pha*-1(cc1299 [e2123ts])	This study	ABR295
C. elegans: ABR433: [*pha-1*(cc1299 [e2123ts]); staEx29[*ges-1p::F21A3.11-7A-2xlinker-WormScarlet::unc-54 3′UTR; pha-1*(+)]	This study	ABR433
C. elegans: ABR317: [*pha-1*(cc1299 [e2123ts]); staEx20[*ges-1p::F53B6.4-2xLinker-WormScarlet::unc-54 3′UTR + pha-1*(+)]	This study	ABR317
C. elegans: VP303*: rde-1(ne219) V;* kbIs7 *[nhx-2p::rde-1 + rol-6*(su1006)*].*	CGC	VP303
C. elegans: DCL569*: rde-1(mkc36)* V; mkcSi13 *[sun-1p::rde-1::sun-1 3′UTR + unc-119*(+)] II.	CGC	DCL569

(*Continued on next page*)

Continued

REAGENT or RESOURCE	SOURCE	IDENTIFIER
C. elegans: ABR489: F53B6.4(sta15) I	This study	ABR489
C. elegans: NR350: rde-1(ne219) V; kzIs20 [hlh-1p::rde-1 + sur-5p::NLS::GFP]	CGC	NR350
C. elegans: TJ356: zIs356[daf-16p::daf-16a/b::GFP + rol-6(su1006)] IV	CGC	TJ356
C. elegans: MAH235: sqIs19[hlh-30p::hlh-30::GFP + rol-6(su1006)]	CGC	MAH235
C. elegans: LD1: ldIs7[skn-1b/c::GFP + rol-6(su1006)]	CGC	LD1
C. elegans: AU78: agIs219[T24B8.5p::GFP::unc-54 3′ UTR + ttx-3p::GFP::unc-54 3′ UTR] III	CGC	AU78
C. elegans: SJ4005: zcIs4[hsp-4::GFP] V	CGC	SJ4005
C. elegans: SJ4100: zcIs13[hsp-6p::GFP + lin-15(+)] V	CGC	SJ4100
C. elegans: TJ375: gpIs1[hsp-16.2p::GFP]	CGC	TJ375
C. elegans: ABR461: sybIs8667[ges-1p::F21A3.11::SL2::WormScarlet::unc-54 3′UTR]	This study(integrated at Sunybiotech)	ABR461
C. elegans: ABR504: zIs356[daf-16p::daf-16a/b::GFP + rol-6(su1006)] IV; sybIs8667[ges-1p::F21A3.11::SL2::WormScarlet::unc-54 3′UTR]	This study	ABR504
C. elegans: ABR512: agIs219[T24B8.5p::GFP::unc-54 3′ UTR + ttx-3p::GFP::unc-54 3′ UTR] III; F53B6.4(sta15) I	This study	ABR512
C. elegans: ABR522: zcIs4[hsp-4::GFP] V; sybIs8667[ges-1p::F21A3.11::SL2::WormScarlet::unc-54 3′UTR]	This study	ABR522
C. elegans: ABR523: zcIs13[hsp-6p::GFP + lin-15(+)] V; sybIs8667[ges-1p::F21A3.11::SL2::WormScarlet::unc-54 3′UTR]	This study	ABR523
C. elegans: ABR526: sqIs19[hlh-30p::hlh-30::GFP + rol-6(su1006)]; sybIs8667[ges-1p::F21A3.11::SL2::WormScarlet::unc-54 3′UTR]	This study	ABR526
C. elegans: ABR435: staEx26[*ges-1p::ER SP-WormScarlet-KDEL::unc-54 3′UTR*]	This study	ABR435
C. elegans: PHX9731: F53B6.4-3xHA(syb9731)	This study(Sunybiotech)	PHX9731
Oligonucleotides		
act-1 forward RT-qPCR CTCTTGCCCCATCAACCATG	Han et al.[59]	N/A
act-1 reverse RT-qPCR CTTGCTTGGAGATCCACATC	Han et al.[59]	N/A
F21A3.11 forward RT-qPCR GGAGATCTGGGGGTCGAGAA	This study	N/A
F21A3.11 reverse RT-qPCR GTACGCGAAATCTCCAACGTG	This study	N/A
F53B6.4 forward RT-qPCR TCTTGACTGCCAATGCCAAC	This study	N/A
F53B6.4 reverse RT-qPCR TCGAATCGATTGTTTAGGCAGC	This study	N/A

(*Continued on next page*)

Continued

REAGENT or RESOURCE	SOURCE	IDENTIFIER
F53B6.4 forward genomic sequencing GAGCGTCGAAGAGTGGGAAA	This study	N/A
F53B6.4 reverse genomic sequencing ACTTTGTTGGACATGAGAGAGAC	This study	N/A
F53B6.4 off-target (F26F12.19) forward TCGCTTTTCATTTATGCTCCTCAC	This study	N/A
F53B6.4 off-target (F26F12.19) reverse TTCGAAATTTTTGCAATTTTCAATACC	This study	N/A
dpy-10 off target (R12E2.15) forward GTTGGGTATGCTCCTCCTTGTG	Silva-Garcia et al.[133]	
dpy-10 off target (R12E2.15) reverse AGAAGACTACATACGACGGCTGG	Silva-Garcia et al.[133]	
dpy-10 crRNA GCTACCATAGGCACCACGAG	IDT	Ce.Cas9.DPY-10.1.AQ
F53B6.4 crRNA GUCAAGACUGCUACCACCUC	IDT	Ce.Cas9.F53B6.4.1.AC
tracrRNA	IDT	1072532
Recombinant DNA		
pC1 (*pha-1* rescue)	Granato et al.[134]	pC1
Myo-2p::mCherry::unc-54 3′UTR	Addgene: 19327	pCFJ90
ges-1p::ER-SP-3xHA-TurboID-ER-KDEL::unc-54 3′UTR	This study	N/A
ges-1p::F21A3.11-2xLinker-WormScarlet::SL2WormGreenLantern::unc-54 3′UTR	This study	N/A
ges-1::F21A3.11-2xLinker-WormScarlet::unc-54 3′UTR	This study	N/A
ges-1p::T05E12.3-2xLinker-WormScarlet::SL2WormGreenLantern::unc-54 3′UTR	This study	N/A
ges-1::T05E12.3-2xLinker-WormScarlet::unc-54 3′UTR	This study	N/A
ges-1p::C02A12.4-2xLinker-WormScarlet::SL2WormGreenLantern::unc-54 3′UTR	This study	N/A
ges-1::C02A12.4-2xLinker-WormScarlet::unc-54 3′UTR	This study	N/A
ges-1p::F56F10.1-2xLinker-WormScarlet::SL2WormGreenLantern::unc-54 3′UTR	This study	N/A
ges-1::F56F10.1-2xLinker-WormScarlet::unc-54 3′UTR	This study	N/A
ges-1p::F53B6.4-2xLinker-WormScarlet::SL2WormGreenLantern::unc-54 3′UTR	This study	N/A
ges-1::F53B6.4-2xLinker-WormScarlet::unc-54 3′UTR	This study	N/A
ges-1:SP-WormScarlet::unc-54 3′UTR	This study	N/A
ges-1p::GFP::unc-54 3′UTR	This study	N/A
ges-1p::WormScarlet::SL2WormGreen Lantern::unc-54 3′UTR	This study	N/A
ges-1p::(ΔSP)F21A3.11-2xLinker-WormScarlet::SL2WormGreenLantern::unc-54 3′UTR	This study	N/A

(*Continued on next page*)

Continued

REAGENT or RESOURCE	SOURCE	IDENTIFIER
ges-1p::(ΔSP)F21A3.11::SL2WormScarlet::unc-54 3′UTR	This study	N/A
ges-1p::F21A3.11::SL2WormScarlet::unc-54 3′UTR	This study	N/A
ges-1p::F21A3.11-7A::SL2WormScarlet::unc-54 3′UTR	This study	N/A
ges-1p::F21A3.11-3xHA-tag::SL2WormScarlet::unc-54 3′UTR	This study	N/A
ges-1p::F21A3.11-7A-3xHA-tag::SL2WormScarlet::unc-54 3′UTR	This study	N/A
F21A3.11p::F21A3.11::2x Linker::WormScarlet::F21A3.11 3′UTR	This study	N/A
ges-1p::F21A3.11-7A-2xlinker-WormScarlet::unc-54 3′UTR	This study	N/A
CMVp::ACP7-6xHIS::SV40 PolyA	This study	N/A
Software and algorithms		
Prism 10	GraphPad (commercially available)	https://www.graphpad.com/
Image Studio v5.2	LI-COR (commercially available)	https://www.licor.com/
FIJI	FIJI (commercially available)	https://fiji.sc/
SigmaPlot 14.0	Grafiti (commercially available)	https://grafiti.com/
Jupyter Notebook	Jupyter (commercially available)	https://jupyter.org/
String	Szklarczyk et al.[135]	https://string-db.org/
Dali	Holm et al.[136]	http://ekhidna2.biocenter.helsinki.fi/dali/index.html#
QuPath v0.4.4	Bankhead et al.[137]	https://qupath.github.io/
TrimGalore		https://github.com/FelixKrueger/TrimGalore
RStudio v4.4.4		https://posit.co/download/rstudio-desktop/
MaxQuant v2.4.2.0	Sinitcyn et al.[138]	https://maxquant.org/
Bioconductor v3.21		org.Ce.e.g.,.db

EXPERIMENTAL MODEL AND STUDY PARTICIPANT DETAILS

C. elegans

All *C. elegans* wild-type and mutant strains used in this study are listed in the table of reagents above. All strains were maintained on Nematode Growth Media (NGM) plates with 50 μg/mL streptomycin (Gibco) and a lawn of OP50-1 bacteria (a gift from M.-W. Tan) from stationary phase cultures. Nematodes were grown at 20°C, except the PD1299 (*pha-1* mutant) strain which was maintained at 15°C (permissive temperature). The genotype of strains was verified by genotyping PCR and Sanger sequencing. Integrated extrachromosomal array strains were backcrossed 6 times into our laboratory's N2 strain and *VAPA*/F53B6.4 CRISPR knockout mutant strain were backcrossed 4 times into our laboratory's N2 strain. *VAPA*/F53B6.4 CRISPR knockin strain (PHX9731) was not backcrossed.

Bacteria

OP-50 *E. coli* bacteria and RNAi bacterial strains (HT115) were grown in LB media at 37°C overnight.

Cell line

Human Expi293F cells were purchased from ThermoFisher Scientific (#A14527) and were maintained in suspension in a mixture of one-third Expi293 growth media (ThermoFisher Scientific, #A1435101) and two-third Freestyle293 growth media (ThermoFisher Scientific, #12338018) cultured in a shaking humidified incubator at 37°C and 8% CO_2. Mycoplasma testing was performed every 3 months.

METHOD DETAILS

Generation of transgenic strain constructs

To generate *C. elegans* expression vectors, NEBridge Golden Gate Assembly (NEB) cloning was used. A multi-site Golden Gate Assembly compatible plasmid was generated by modifying plasmid L3691 (Addgene #1587) to contain paired restriction sites for the type IIS restriction endonucleases PaqCI, BsmBI, and BsaI.

To generate a *C. elegans* strain expressing TurboID in the cytoplasm (TurboID-Cytoplasm), a worm codon-optimized TurboID sequence with a 3xHA-tag at the N-terminal was obtained from pAS31 (Addgene #118220).[48] To generate a *C. elegans* strain expressing TurboID in the ER (TurboID-ER), the same 3xHA-TurboID was modified to include an endoplasmic reticulum (ER) signal and ER retention peptide. An ER signal peptide (KTLFLLGLIALSAVSVYC) was added to the N-terminal of TurboID. An ER retention signal (KDEL) was added to the C-terminal of TurboID (GenScript). Intestine TurboID-ER and intestine TurboID-Cytoplasm were expressed from the intestinal *ges-1* promoter and used the *unc-54* 3′UTR. For the intestine TurboID-ER construct, the same *ges-1p* (3.0 kb region upstream of the transcriptional start site) and *unc-54* 3′UTR (631 bp) were amplified from pAS31.

To generate a *C. elegans* strain expressing WormScarlet in the ER (TurboID-ER), an endoplasmic reticulum (ER) signal and ER retention peptide were added. An ER signal peptide (KTLFLLGLIALSAVSVYC) was added to the N-terminal of WormScarlet. An ER retention signal (KDEL) was added to the C-terminal of WormScarlet. Intestine WormScarlet-ER and intestine WormScarlet (Cytoplasm) were expressed from the intestinal *ges-1* promoter and used the *unc-54* 3′UTR.

To generate ACP7/F21A3.11 translational reporter driven by its endogenous promoter, GoldenGate assembly was used. A plasmid containing the 616 bp promoter of *ACP7*/F21A3.11, and the full gene 2347 bp without a stop codon was followed by a 2xlinker sequence (GGGGSGGGGS) and worm scarlet protein followed by a stop codon and 107 bp of the *ACP7*/F21A3.11 3′UTR.

To generate intestine-specific overexpression of *ACP7*/F21A3.11, the full F21A3.11 gene (introns and exons) was used. A plasmid construct was generated using the *ges-1p*, followed by *ACP7*/F21A3.11 with an unc-*54* 3′UTR. To generate an overexpression construct of a non-secreted form of ACP7 (ACP7-ΔSP), the *ges-1p* was used to drive intestine expression followed by the *ACP7*/F21A3.11 gene that was lacking the first 69 base pairs after the start codon (encoding for the first 21 amino acids) as this was determined to be the secretion signal for the ACP7 protein by SignalP6.0.[139] The *unc-54* 3′UTR was used for this construct. Finally, to generate a secreted but catalytically dead form of ACP7 (ACP7-7A), 7 point mutations were made in the *ACP7*/F21A3.11 gene to convert 7 predicted metal binding ion amino acids to alanines (D156A, D185A, Y188A, N220A, H301A, H349A, and H351A). Conserved amino acids were identified by alignment of ACP7 in different species. The *unc-54* 3′UTR was used for this construct. To visualize each of these proteins, a new construct for each overexpression strain was generated with an inserted 2xlinker and WormScarlet before the stop codon of the protein. To generate HA-tagged ACP7 constructs for protein isolation and phosphatase assay, a 2xlinker with a 3xHA-tag (Addgene #118220) was inserted before the stop codon of ACP7 or ACP7-7A constructs.

To generate a construct to visualize VAPA/F53B6.4 expression in the intestine, a plasmid was generated using the intestine specific *ges-1* promoter (*ges-1p)*, the full F53B6.4 gene (introns and exons), skipping the stop codon, followed by a 2xlinker, WormScarlet and a stop codon. The *unc-54* 3′UTR was used.

To generate the dual reporter strain to validate via microscopy whether a protein could be secreted from the intestine, a construct design was used as follows: the secreted protein was tagged with a red fluorophore (WormScarlet) and the intestine cytoplasm was tagged with a green fluorophore (WormGreenLantern). A plasmid was generated to encompass the intestine-specific *ges-1* promoter (*ges-1p)*, followed by the full gene (exons and introns) encoding a secretome or secretory machinery protein of interest with the stop codon removed. After the gene, we inserted a 2xlinker and WormScarlet followed by a stop codon. Next, an SL2 transcript splice sequence was inserted, followed by the worm-optimized sequence of GreenLantern,[73] termed WormGreenLantern. The online webtool, WormBuilder (https://wormbuilder.org/) was used to codon optimize the mammalian GreenLantern DNA sequence for high expression in *C. elegans* using the Henrik Bringmann optimization method.[140] Three synthetic introns were added at consensus splice sites to ensure efficient processing of the transcript.[141] Following the WormGreenLantern sequence, the *unc-54* 3′UTR was inserted.

To generate a secreted WormScarlet, the signal peptide from F21A3.11 was used. The signal peptide consisted of the first 21 amino acids after the methionine in F21A3.11, which were added after the start codon for WormScarlet to generate a secreted WormScarlet (SP-WormScarlet). This was followed by the *unc-54 3′UTR*. This plasmid was co-injected with an intestine GFP reporter (*ges-1p::GFP::unc-54 3′UTR*) to generate a strain that has a secreted red fluorescent protein (SP-WormScarlet) and a green intestine.

Generation of transgenic strains

Transgenic strains were generated in either the N2 (for lifespan transgenics, except for the ACP7-7A strain which was generated in the PD1299 background) or PD1299 background. Using standard microinjection technique, an injection mixture of 30 ng/μL of expression vector and 70 ng/μL of filler DNA (pBluescript II SK(+), Agilent Technologies: 212205) was used for transgenesis in N2 worms. For PD1299 worms, a rescue construct containing wild-type *pha-1* (pC1) was used. The injection mixture for PD1299 strain generation consisted of 30 ng/μL of expression vector, 20 ng/μL of filler DNA (pBluescript II SK(+)) and 50 ng/μL of pC1. For the TurboID-Cytoplasm and TurboID-ER strains, 30 ng/μL of expression vector, 17.5 ng/μL of filler DNA (pBluescript II SK(+), 50 ng/μL of pC1, and 2.5 ng/μL of pCFJ90 (Addgene #44472, pharynx fluorescent marker) was used. Integration of extrachromosomal arrays was performed by SunyBiotech.

Generation of PD1299 *Pha-1(cc1299 [e2123ts])*

To recreate the *Pha-1*(e2123) allele in the VC2010 (wild type N2 subculture) strain background, we engineered a single point mutation in the endogenous *Pha-1* locus using a CRISPR-based co-conversion strategy previously described.[142–144] This new strain was generated as the original mutation was obtained from a mutagenesis (EMS) screen.[134] We chose a CRISPR target sequence (ATGAATAACTTGATGAACAT) and repair template (oligo AF-KLA-358 with sequence ''CAAAATACGAATCGAAGACTCAAAAAGAG TATaCTGTATGATTACCGATGTTCATCAAGTTATTCATAAATCATTGATAG'') previously shown[145] to successfully recreate the conversion of G>A at the *Pha-1(e2123)* locus. An injection mix comprised of the following was injected into CGC1 (VC2010) worms: 50 ng/μL pDD162 (*Cas9* expression vector[146]), 25 ng/μL pJA58 (*dpy-10* gRNA vector[142]), 0.5 μM AF-ZF-827 (*dpy-10* repair oligonucleotide[142]), 50 ng/μL pPD207.862 (L8260) (*Pha-1* gRNA expression vector constructed in this paper using the pRB1017 backbone, and 0.5 μM of a *Pha-1(e2123)* mutation-containing repair template oligonucleotide AF-KLA-358). F1 progeny of injected parents were screened by PCR for G>A conversion. Homozygous lines were established from single F2 progeny lacking the co-conversion phenotype. Genotypes at the *Pha-1* and d*py-10* loci were assessed by PCR, and embryonic lethal temperature sensitivity was validated by comparing worm development at 16°C, 20°C, and 23°C.

VAPA/F53B6.4 CRISPR knockout strain

A *VAPA*/F53B6.4 knockout strain was generated in the N2 background using CRISPR/Cas9.[147] We chose a CRISPR target sequence (GTCAAGACTGCTACCACCTC), targeting exon 2, using the IDT CRISPR-Cas9 online design tool. To generate the gRNA, 200 μM F53B6.4 crRNA, 200 μM of tracrRNA (IDT, 1072532), and a 1:12 ratio of *dpy-10* crRNA (IDT) were mixed together, heated at 95°C for 5 min and then left on the bench top to cool to room temperature. To generate the RNP (ribonucleotide protein) complex, 50 μM of gRNA was mixed with 61 μM Alt-R Cas9 Protein (IDT, 1081058) and incubated for 10–20 min at room temperature. The final injection mix consisted of 1 μL RNP complex, 15.2 ng/μL of single-stranded DNA template to generate *dpy-10* mutation (CACTTGAACTTCAATACGGCAAGATGAGAATGACTGGAAACCGTACCGCATGCGGTGCCTATGGTAGCGGAGCTTCACA TGGCTTCAGACCAACAGCCTAT), and PBS for a final volume of 6 μL. F1 progeny of injected parents were screened by PCR for mutations in the F53B6.4 gene. Homozygous lines were established from singled F2 progeny. PCR and sanger-sequencing was performed to confirm the homozygous mutation in the strain. The *VAPA*/F53B6.4 CRISPR knockout strain has a 31 bp deletion, resulting in mis-sense protein (in the region encoded by exon 2) and an early stop codon (in the region encoded by exon 3). This strain was outcrossed to N2 animals to remove the *dpy-10* mutation and then backcrossed 4 more times to N2 animals. To ensure there were no off-target mutations generated when using the *dpy-10* crRNA and F53B6.4 crRNA, the top predicted off-target gene for each crRNA was tested. R12E2.15 was the top predicted off-target gene for the *dyp-10* crRNA[133] while F26F12.19 was the top predicted off-target gene for the F53B6.4 crRNA. The genomic region surrounding the predicted binding sites of these off-targets genes was amplified using PCR and the products were Sanger-sequenced to ensure no mutations were present.

Generation of an HA-tagged *VAPA*/F53B6.4 knockin strain

To generate an endogenously tagged *VAPA*/F53B6.4 knockin strain, CRISPR/Cas9 was used. This knockin strain was generated by SunyBiotech. A 3xHA-tag was knocked into the endogenous F53B6.4 locus, just before the stop codon of *VAPA*/F53B6.4. The 3xHA-tag sequence inserted is: TACCCATACGACGTCCCAGACTACGCCTACCCATATGATGTCCCGGATTACGCTTACCCA TACGATGTTCCAGATTACGCT.

RNAi knockdown

To knock down expression of specific genes, we fed worms HT115 (*Escherichia coli*) bacteria expressing double-stranded RNA targeting a specific gene. The HT115 strains expressing RNAi targeting the genes of interest were obtained from the Ahringer library (gift from A. Fire). For whole-worm RNAi knockdown, wild-type (N2) hermaphrodites were used. For tissue-specific RNAi knockdown, VP303[108] (intestine-specific), DCL569[109] (germline-specific), and NR350[110] (muscle-specific) hermaphrodites were used. All RNAi constructs from the Ahringer library were Sanger-sequenced to ensure they were targeting the correct gene of interest. RNAi targeting F21A3.11 and F53B6.4 were further validated by protein knockdown (see below).

To generate RNAi-expressing bacteria, a single bacterial colony was used to inoculate LB medium containing 100 μg/mL ampicillin (Sigma Aldrich). The bacteria were cultured overnight at 37°C to stationary phase and the expression of the double-stranded RNA was induced with 0.4 mM isopropyl thiogalactoside (IPTG; Thermo Fisher) for 4 h at 37°C. The cultures were centrifuged and the bacterial pellet resuspended in LB supplemented with 100 μg/mL ampicillin and 0.4 mM IPTG at 1:30 of the initial volume. This bacterial resuspension was stored at 4°C for no longer than 2 weeks. Concentrated bacteria (1:30) were seeded onto 6-cm NGM plates containing 100 μg/mL ampicillin and 0.4 mM IPTG (''RNAi plates''). Worms were fed RNAi from hatch.

Western blot

Protein samples for western blot were generated by age-synchronizing hermaphrodites by bleaching adult gravid non-starved hermaphrodites, allowing L1 arrest to occur overnight in M9 buffer (22 mM KH_2PO_4, 34 mM K_2HPO_4, 86 mM NaCl, 1 mM $MgSO_4$) buffer followed by plating out animals (~500–1000) onto 3–4 10-cm NGM plates. To generate synchronized adult animals, the adult worms were washed each day during their reproductive period to separate adult worms from larvae and eggs.[148] Worms were

collected in EN50 (1 mM EDTA, 50 mM NaCl) buffer in a 15 mL tube and allowed to settle to the bottom of the tube. The supernatant was removed, and adult worms were resuspended in 15 mL of fresh EN50. This washing procedure was repeated five times and the adult worms were transferred to 10 cm NGM plates containing a bacterial lawn (OP50). *C. elegans* were harvested at adulthood day 1, 5, and 10 using M9, transferred into an Eppendorf tube, and centrifuged at 400 g for 1 min. The excess M9 buffer was removed, and samples were flash frozen in a bath of ethanol and dry ice. RIPA buffer (Alfa Aesar, J62524) with cOmplete Mini Protease Inhibitor (Roche, 11836153001) was added to the frozen *C. elegans* pellet and thawed on ice. Bead beating was performed to break apart the *C. elegans*. Zirconia/silica 0.1 mm diameter beads (BioSpec, 11079101Z) were added and samples were beaten at 25 Hz for 30 s and left on ice for 5 min (TissueLyser II, Qiagen). This step was repeated twice. Samples were then centrifuged at 4°C, 20,000 g for 5 min. The supernatant was transferred to a new tube and sonicated on ice for 5 s followed by 5 s off for a total of 50 s (Virsonic 600 Ultrasonic Homogenizer, Virtis Versonic, power level 5). Samples were centrifuged at 4°C, 20,000 g for 5 min and protein concentration was determined using the Pierce BCA Protein Assay Kit (ThermoFisher, 23225).

Protein lysates were normalized to 10 μg of protein each and mixed with 6*x* Reducing Blue Protein Loading Dye (NEB, B7703S) in a 50 μL volume and boiled at 95°C for 5 min. Equal volume of lysate was loaded onto a 4–12% NuPAGE gel (Invitrogen, NP0321), transferred to a nitrocellulose membrane (Bio-Rad, 1620094), and stained with Ponceau S solution (Sigma-Aldrich, P7170). Blots were blocked using Intercept (TBS) Blocking Buffer (LI-COR, 927–60001), probed with anti-alpha-tubulin (1:10,000, mouse monoclonal, Sigma #T5168) and anti-HA (1:5,000, rat monoclonal, Roche #11867423001, lot #70720400) primary antibodies, and detected with secondary antibody (1:10,000 goat anti-mouse IRDye 800CW, Licor #926–32210) and 1:10,000 goat anti-rat IRDye 680RD, Licor #926–68076). For biotinylation detection, we used streptavidin (1:3000, Alexa Fluor 680 Conjugate S32358, Invitrogen #S32358) in combination with anti-alpha-tubulin primary and anti-mouse secondary antibodies described above. Blots were imaged on an LI-COR Odyssey Fc using Image Studio version 5.2.

Immunohistochemistry

C. elegans were harvested at their respective ages (∼300 worms) using M9 buffer (22 mM KH_2PO_4, 34 mM K_2HPO_4, 86 mM NaCl, 1 mM $MgSO_4$) and fixed in 500 μL of 4 % formaldehyde (Thermo Scientific, 28906) for 30 min. Fixed worms were washed 3 times in 1 mL of PBS-Tween 20 (0.05 % Tween 20 in 1*x* PBS) and then treated with 1 mL of beta-mercaptoethanol (bME) solution (133 mM Tris (pH 6.8), 1 % Triton X-100, 5% bME in water) rotating overnight at 37°C. Worms were washed 3 times in 1 mL of PBS-Tween 20, for 1 h per wash, rotating on a nutator. Next, worm samples were treated with 150 μL of collagenase solution (2 mg/mL collagenase IV, Sigma C-5138), 1 mM $CaCl_2$, 0.1 M pH 7.4 Tris in water) at 37°C shaking at ∼2000 rpm. Once 20 % of worms were broken (visual inspection under a dissecting microscope), samples were placed on ice for 5 min followed by 2 washes with 1*x* PBS-Tween, followed by one wash in anti-body A (AbA) solution (1 % BSA and 0.5 % Triton X-100 in 1*x* PBS).

Antibody staining was performed overnight in AbA solution with anti-HA (1:100, rat monoclonal, Roche #11867423001) and anti-GFP for subcellular localization images in the intestine (1:100, mouse monoclonal, Santa Cruz sc-9996) followed by three 1 h washes with 1 mL AbA solution at room temperature. Secondary antibodies were diluted in AbA solution (1:100, goat anti-rat Alexa Fluor 594, Invitrogen #A-21209, and for intestine subcellular localization anti-mouse Alexa Fluor 488, Invitrogen #A-21202) for 2 h at room temperature followed by 3 washes of 1 mL AbA solution, 1 h each wash.

Confocal microscopy for TurboID localization

Confocal microscopy was performed on a Zeiss LSM900 Axio Observer. Animals were hatched onto RNAi plates with HT115 empty vector bacteria and imaged at adult day 1 or 2 (3 or 4 days post hatch).

To determine whether intestine TurboID-Cytoplasm and intestine TurboID-ER were expressed in the correct tissue, a 20*x* air objective (Plan-Apochromat 20×/0.8 M27) with a z stack interval of 1 μm with processed using Zen software (3.0, blue) was performed. The head region and first 3 intestine cells were imaged. Animals were imaged in the green channel to visualize the endoplasmic reticulum GFP reporter (VS25 strain), and in the near-red channel to visualize TurboID. To determine whether intestine TurboID-ER co-localized with the ER reporter, a 63*x* oil objective (Plan-Apochromat 63×/1.40 oil DIC M27) with a z stack interval of 0.25 μm with the same processing and filters as above. Images were taken of the first 4 intestine cells.

Confocal microscopy for secretome and secretory machinery protein compartment localization

To determine whether a candidate secretome or secretory machinery protein co-localized with a specific compartment within the *C. elegans* intestine confocal microscopy was performed to determine co-localization of a secretome or secretory machinery protein and a compartment reporter GFP tagged protein. *C. elegans* strains expressing a candidate protein of interested tagged with WormScarlet in the intestine were crossed to strains expressing GFP in the cytoplasm, ER (VS25 strain), peroxisome (VS15 strain), lysosome (VS17 strain), endosome (RT476 strain), or lipid droplet protein (LIU1 strain). Confocal microscopy was performed on a Zeiss LSM900 Axio Observer. A 63*x* oil objective (Plan-Apochromat 63×/1.40 oil DIC M27) with a z stack interval of 1 μm with the same processing and filters as above. Animals were hatched onto RNAi plates with HT115 empty vector bacteria and imaged at adult day 1 or 2 (3 or 4 days post hatch). Worms were mounted on a 2 % agar pad, anesthetized with 50 mM sodium azide and covered with a glass cover slide. Images were taken of the first 4 or final 2 intestine cells.

Quantitative mass spectrometry

Sample lysis and biotinylated protein pull-down

For quantitative mass spectrometry, we generated 4 independent biological replicates of pooled worms (3 mL of wet worms) for the intestine TurboID-ER and intestine TurboID-Cytoplasm strains (and 1 independent biological replicate for wild type N2 (negative control) per tissue and per compartment). These strains are generated by integrating extrachromosomal arrays, which leads to stable overexpression of TurboID-Cytoplasm or TurboID-ER in intestinal cells (at levels likely saturating for biotinylation). We note that our western blot experiments indicate a slight decrease in TurboID-Cytoplasm expression with age in the intestine. These changes in expression with age are slight, and smaller than those observed in Branon et al.[48] (which used non-integrated *C. elegans* strains TurboID strains in response to temperature changes and observed strong changes in transgene expression), making it unlikely that the changes in TurboID expression would be solely responsible for changes in labeling with age.

To grow *C. elegans* at a high density, OP50 was concentrated 5*x* and seeded onto 15 cm NGM plates. To generate a synchronized population of *C. elegans*, worm bleach synchronization (as performed for western blot samples) was done with overnight L1 arrest and adult day 1 (3 days post-hatch) was collected (for intestine TurboID-Cytoplasm and TurboID-ER strains). To generate synchronized aging worm populations for middle-age (adult day 5, 8 days post-hatch) and old (adult day 10, 13 days post-hatch) samples (for intestine TurboID-Cytoplasm and TurboID-ER strains), *C. elegans* were washed off plates with 3 mL of EN50 (1 mM EDTA, 50 mM NaCl), transferred to 15 mL conical tubes, and filled with EN50 buffer. The tubes were inverted and then left for 3-5 min to allow adults to settle to the bottom of the tube, while larval worms were distributed throughout the rest of the tube. The buffer and larval worms were aspirated and fresh EN50 was used to fill the tube. This process was repeated until no larval worms were found in the supernatant.

To harvest adult day 1 (3 days post-hatch), 5 (8 days post-hatch), and 10 (13 days post-hatch) samples, after the final wash, worms were transferred to 1.5 mL Eppendorf tubes. Worms were spun at 1000 g for 1 min, excess buffer was aspirated, and the worm pellets were flash frozen in an ethanol bath of dry ice. Samples were then thawed and resuspended in high SDS RIPA buffer (50 mM Tris-HCl pH 8.0; 150 mM NaCl; 1 % SDS; 0.5 % sodium deoxycholate; 1 % Triton X-100; 1 mM PMSF; 1*x* HALT; 2.5 mg/mL Leupeptin (Sigma Aldrich #L8511); 5 mg/mL Pepstatin A (Sigma Aldrich #P5318)). Samples were then mechanically disrupted via bead beating using 0.1 mm silica beads (BioSpec Products #11079101Z) at 25 Hz, 30 s pulse (3*x*) with 5 min breaks on ice. Next, samples were sonicated on ice with 5 s on, followed by 5 s off, repeated for 50 s total. Sonication was performed on the protein lysate (not including *C. elegans* cuticles or not fully broken apart *C. elegans*) for intestine TurboID-Cytoplasm and TurboID-ER samples. Sonication was performed on total (protein lysate, including *C. elegans* cuticles and partially disrupted *C. elegans*). Samples were then spun at 4°C for 10 min to pellet debris and the supernatant was transferred to a fresh low protein bind tube (ThermoScientific #88379). Samples were diluted using SDS-free RIPA buffer to achieve a final SDS concentration of 0.2 %. Samples were then left to rotate for 1 h at 4°C. Total protein was then quantified and an overnight pull-down of biotinylated proteins using streptavidin magnetic beads at 4°C was performed (8 μg protein/1 μL beads). After overnight biotinylated protein pull-down onto streptavidin beads, samples were washed for 2 min each with 1 mL of the following wash buffers and indicated number of repeats: RIPA buffer (2*x*), 1M KCl (1*x*), 0.1M Na_2CO_3 (1*x*), 2M urea (1*x*), 4M urea (1*x*), RIPA (2*x*), PBS (5*x*).

Peptide preparation and mass spectrometry

Proteins bound to beads followed a modified protocol from Cho et al.,[57] but an additional digestion step was performed by adding 2 mAU of LysC (VWR, #100369-826), an endopeptidase, to each sample and incubating at room temperature for 24 h, before trypsin digestion. After digestion, peptides were desalted on in-house prepared Styrenedivinylbenzene Reversed Phase Sulfonate packed Stagetips.[149] Briefly, Stagetips were activated with 100 % methanol, conditioned with 80 % acetonitrile/0.1 % Trifluoroacetic acid (TFA), and equilibrated with 0.2 % TFA. This was followed by sample loading, washing with 99.9 % isopropanol/0.1 % TFA, washed twice with 0.2 % TFA and once with 0.1 % formic acid. Peptides were eluted with 60 % acetonitrile/0.5 % ammonium hydroxide. Desalted peptides were flash frozen, dried by centrifugal evaporation, and resuspended in 100 μL of 100 mM 4-(2-hydroxyethyl)piperazine-1-propanesulfonic acid (EPPS) pH 8.5 buffer. Peptides were not re-quantified as to not introduce potential technical artifacts. Next, 0.5 mg per tag of TMTPro 16 plex reagents (tandem mass tags, Thermofisher Scientific, # A44521) were resuspended in 20 μL of 99.9 % extra dry acetonitrile and incubated at room temperature while shaking for 5 min. For the TMT-Plexing strategy for intestine dataset, see Section "TMT-Plexing strategy" below and Table S1A. Next, 100 μL of peptides were added to each TMTPro label and incubated at room temperature while shaking for 1 h. Labeling reaction was quenched by adding 5 μL of 5 % hydroxylamine and incubating at room temperature while shaking for 15 min. TMTPro labeled samples were combined, acidified and acetonitrile reduced to 4 % by adding 4*x* volume of 1 % TFA. Labeled and combined peptides were then desalted on 50 mg C18 Sep-Pak cartridges. Briefly, cartridges were activated with 100 % methanol, conditioned with 80 % acetonitrile/0.1 % TFA, and equilibrated with 0.2 % TFA. This step was followed by sample loading and washing with 2 % acetonitrile/0.1 % TFA. Peptides were eluted with 80 % acetonitrile/0.1 % TFA. Desalted peptides were flash frozen then dried by centrifugal evaporation and resuspended in 2 % acetonitrile/0.1 % TFA. Next, 25 μg of each sample set was fractionated using the Pierce High pH Reverse-Phase Peptide Fractionation Kit (Thermo Fisher Scientific, #84868) according to the manufacturer's instructions. All fractions were flash frozen then dried by centrifugal evaporation and resuspended in 2 % acetonitrile/0.1 % TFA.

Peptides were analyzed on a Fusion Lumos mass spectrometer (Thermo Fisher Scientific, San Jose, CA) equipped with a Thermo EASY-nLC 1200 LC system (Thermo Fisher Scientific, San Jose, CA) and nanoFlex ESI source. Peptides were separated by capillary reverse phase chromatography on a 25 cm column (75 μm inner diameter, packed with 1.7 μm C18 resin, AUR3-25075C18A,

Ionopticks, Victoria Australia). Electrospray ionization voltage was set to 2000 V. Peptides were introduced into the Fusion Lumos mass spectrometer using a two-step linear gradient, 6–35 % buffer B (0.1 % (v/v) formic acid in 80 % (v/v) acetonitrile) for 145 min followed by 35–47 % buffer B for 15 min, with a flow rate of 300 nL/min. Column temperature was maintained at 50°C throughout the procedure. Data was acquired in top speed data-dependent MS3 mode. Full MS scans were acquired in the Orbitrap mass analyzer (FTMS) with a resolution of 120,000 (FWHM) and a m/z scan range of 400-1,500 m/z. For tandem mass spectrometry (MS/MS), MS2, the top 10 most intense precursor ions were subjected to fragmentation using collision-induced dissociation (CID) with a quadrupole isolation window of 0.5 m/z, a fixed normalized collision energy of 34 %, activation time of 10 ms and Activation Q set to 0.25. CID fragments were analyzed in the Ion Trap mass analyzer (ITMS) with the scan rate set to Turbo and scan range set to Auto. Fragmented ions were dynamically excluded from further selection for a period of 120 s. For MS3, a defined precursor selection range was set between 400 and 1200 m/z. Quadrupole isolation of precursors with a charge state of 2, 3, 4 or 5–6 were isolated with a window of 1.3 m/z, 1 m/z, 0.8 m/z and 0.7 m/z respectively. The top 10 most intense CID fragments were selected by Synchronous Precursor Selection within the Ion Trap (ITMS) using an isolation window of 2 m/z and subjected to HCD fragmentation with a normalized collision energy of 45 %. The released reporter ions were then analyzed in the Orbitrap mass analyzer (FTMS) at a resolution of 50,000 (FWHM) and a m/z scan range of 110–500 m/z. The AGC target was set to 1,000,000 for full MS1, standard for MS2 and 150,000 for MS3 scans, while the maximum injection time was set to 100 ms for full MS1, 35 ms for MS2 and 150 ms for MS3 scans.

TMT-Plexing strategy

For the intestine secretome TurboID-Cytoplasm and TurboID-ER (Young, Middle-age, Old), we used the following TMT-Plexing strategy (across ages).

Intestine experiment - TurboID-Cytoplasm TMT-Plex 1 of 2

Sample number	Strain	Age	TMTPlex set	TMTPro label	TMTPro mass
1	ABR388 Cyto	Young	cytoplasm	1	126.12772
2	ABR388 Cyto	Young	cytoplasm	2	127.12476
3	ABR388 Cyto	Young	cytoplasm	3	127.13108
4	ABR388 Cyto	Young	cytoplasm	4	128.12811
5	ABR388 Cyto	Middle-Aged	cytoplasm	5	128.13443
6	ABR388 Cyto	Middle-Aged	cytoplasm	6	129.13147
7	ABR388 Cyto	Middle-Aged	cytoplasm	7	129.13779
8	ABR388 Cyto	Middle-Aged	cytoplasm	8	130.13482
9	ABR388 Cyto	Old	cytoplasm	9	130.14114
10	ABR388 Cyto	Old	cytoplasm	10	131.13818
11	ABR388 Cyto	Old	cytoplasm	11	131.1445
12	ABR388 Cyto	Old	cytoplasm	12	132.14153
13	N2	Young	cytoplasm	13	132.14785
14	N2	Middle-Aged	cytoplasm	14	133.14489
15	N2	Old	cytoplasm	15	133.15121
Blank	Blank	Blank	cytoplasm	16	134.14824

Intestine experiment -TurboID-ER TMT-Plex 2 of 2

Sample number	Strain	Age	TMTPlex set	TMTPro label	TMTPro mass
16	ABR273 ER	Young	ER	1	126.12772
17	ABR273 ER	Young	ER	2	127.12476
18	ABR273 ER	Young	ER	3	127.13108
19	ABR273 ER	Young	ER	4	128.12811
20	ABR273 ER	Middle-Aged	ER	5	128.13443
21	ABR273 ER	Middle-Aged	ER	6	129.13147
22	ABR273 ER	Middle-Aged	ER	7	129.13779
23	ABR273 ER	Middle-Aged	ER	8	130.13482
24	ABR273 ER	Old	ER	9	130.14114
25	ABR273 ER	Old	ER	10	131.13818

(*Continued on next page*)

Continued

Intestine experiment -TurboID-ER TMT-Plex 2 of 2					
Sample number	Strain	Age	TMTPlex set	TMTPro label	TMTPro mass
26	ABR273 ER	Old	ER	11	131.1445
27	ABR273 ER	Old	ER	12	132.14153
28	N2	Young	ER	13	132.14785
29	N2	Middle-Aged	ER	14	133.14489
30	N2	Old	ER	15	133.15121
Blank	Blank	Blank	ER	16	134.14824

LC-MS raw data processing

Resulting mass spectrometry raw data files were searched against a *Caenorhabditis elegans* Uniprot database (downloaded on April 12, 2024) using a reverse-decoy method and quantified using MaxQuant software (version 2.4.2.0) set to 16plex MS3 reporter type and default settings. Briefly, a 1 % false discovery rate was set at the peptide spectrum and protein matching with a minimum peptide length of 7, 2 missed cleavages were allowed, and enzyme was set to trypsin. A minimum of one razor and unique peptide per protein group was required for an observation. Reverse sequences, peptide identified by site and potential contaminants were filtered from protein groups. The dataset was filtered for a minimum of 1 valid abundance value across the entire dataset. Oxidation of methionine and protein N-terminal acetylation were set as variable modifications and carbamidomethylation of cysteines was set as a fixed modification. Match between runs was activated. The mass spectrometry proteomics data have been deposited to the ProteomeXchange Consortium via the PRIDE[132] partner repository with the dataset identifier PXD057064.

Analysis of mass spectrometry data

Processing and normalization

For processing and normalization, we removed any protein with only a single razor and unique peptide, keeping peptides with 2 or more razor and unique peptides as per the TurboID protocol paper.[57] Next, each sample was protein-normalized by summing each samples protein abundances, then dividing each protein's abundance by the sample's total protein abundance sum and then re-scaling each protein by multiplying by 10^{10} ("normalized protein abundance").[39] Raw protein abundance from MaxQuant can be found in Table S1B for intestine. Peptides removed and sample normalized data can be found in Table S1C for intestine.

Correlation analysis

For correlation analysis, we computed the pairwise Pearson correlation between the Log_2-normalized protein abundances between the quadruplicates within an age, compartment, and strain group. We noted that there was a large difference between the Young condition and either the Middle-age or the Old condition for TurboID-ER replicates, whereas this difference was not as marked for the TurboID-Cytoplasm replicates. With age, there could be a larger number of proteins accumulating in the endoplasmic reticulum (due to misfolding, stress responses, etc). This could explain why the abundance of proteins found in the Middle-age and Old TurboID-ER condition is higher on average.

Principal component analysis

For principal component analysis (PCA), we used sample normalized protein values and Log_2-transformed the protein abundance with an added pseudocount in order to facilitate no zero values for the log transformation ("log-transformed protein abundance"). We standardized (*Z* score) the Log_2-transformed protein abundances, dropped any proteins with zero abundances in all conditions, and projected the data onto the first two principal components.

Identification of compartment-enriched proteins

To identify compartment-enriched proteins (TurboID-Cytoplasm-enriched vs. TurboID-ER-enriched), we compared protein abundance for each compartment (TurboID-Cytoplasm, TurboID-ER) for each strain (intestine) at each age (Young, Middle-age, Old). To calculate the fold change between compartments, we calculated the average protein abundance value across the 4 independent replicates for each compartment. Then, we calculated the Log_2(Fold Change) value of TurboID-ER/TurboID-Cytoplasm. For visualization of the proteins that are unique to each compartment ('0' values in TurboID-Cytoplasm or '0' values in TurboID-ER for intestine dataset), we gave a very large value for the Log_2(Fold Change) in the volcano plot: +15 for unique TurboID-ER and −15 for unique TurboID-Cytoplasm.

To determine the *p*-value for the compartment-enriched proteins, we used a two-sided Welch's *t* test. To calculate *p*-values, each protein abundance value for each replicate was log_2-transformed, with the addition of a +1 (to handle the '0' values). We did not perform FDR correction and instead used a *p*-value <0.1 as being significant, which has been used by other proximity labeling studies[150] and allows subsequent analysis to be more permissive. Compartment Log_2(Fold Change) and *p*-values for each age in the intestine can be found in Table S2A. Positive values indicate the protein is more abundant in TurboID-ER (TurboID-ER enriched) while negative values indicate the protein is more abundant in the TurboID-Cytoplasm (TurboID-Cytoplasm enriched).

Identifying and visualizing positive control proteins

To determine if our intestine TurboID-Cytoplasm and TurboID-ER pull-downs were compartment-specific, we identified 20 intestine cytoplasm proteins (cytoplasmic and nuclear)[60–64] and 20 intestine secretome proteins (endoplasmic reticulum, Golgi, or secreted)[65–69] from the *C. elegans* literature and WormBook[70] to use as positive control proteins. We visualized these proteins in the volcano plot of intestine TurboID-Cytoplasm enriched and TurboID-ER enriched in young animals and verified they were in the correct compartment (Figure S1K; Table S2A).

Generation of high-confidence compartment-enriched protein lists

To identify high-confidence TurboID-ER-enriched and high-confidence TurboID-Cytoplasm-enriched proteins, we first determined if a protein corresponding transcript is predicted to be expressed in the intestine. Using a combination of published transcriptomic datasets[58,59] and Wormbase, we identified in which tissue the transcript encoding an identified protein was expressed. We identified a high percentage of proteins expressed in the correct tissue, ranging from 98 to 100% (Figures 1L and S1H). If a protein's corresponding transcript was determined to not be expressed in the intestine (rare events), these proteins were not carried forward for the high-confidence compartment-enriched protein lists.

We then identified a high-confidence set of proteins by optimizing for the largest number and for the highest purity (percentage) of compartment-specific proteins for a given set of cutoff values (Log_2(Fold Change) and *p*-value). Predicted protein subcellular annotations were determined using the tool DeepLoc2.1.[72] This tool predicts whether a protein is localized to the cytoplasm, nucleus, ER, cell membrane, secreted, mitochondria, Golgi, etc. We considered compartment-specific proteins for TurboID-ER to be all proteins that transit through the ER: endoplasmic reticulum (ER), cell membrane, and secreted. We considered compartment-specific proteins for TurboID-Cytoplasm to be all proteins predicted to be cytoplasmic and nuclear (as most nuclear proteins are generated in and transit through the cytoplasm). There were also a number of proteins localized to more than one compartment, but to simplify the analysis we used the main compartment definition.

The list of TurboID-ER enriched and TurboID-Cytoplasm enriched proteins, their tissue annotation, compartment annotation, and list of optimization calculations can be found in Tables S2C–S2F. Note that we used relaxed *p*-values to determine cut-offs as this permissive *p*-value allows for more proteins to be screened[39] and it has been used before in other proximity labeling papers.[150,151] For example, for young intestine high-confidence TurboID-ER enriched proteins, we found that a Log_2(Fold Change) > 2 and a *p*-value <0.50 cutoff resulted in the ER, cell membrane, and extracellular proteins representing 67.98% (while the cytoplasm and nuclear proteins were 18.71%). This cutoff identified a total 177 secreted/extracellular proteins (36.80% of the compartment, Table S2C, row highlighted in green). For young intestine high-confidence TurboID-Cytoplasm enriched proteins, we found that a Log_2(Fold Change) < −1 and a *p*-value <0.10 cutoff resulted in the cytoplasm and nuclear proteins representing 79.87% (while the ER, cell membrane, and extracellular/secreted proteins were 10.44% of the compartment, Table S2C, row highlighted in green). There were other cutoffs that gave more compartment specific proteins, but resulted in less selective percentage for the specific compartment. There were yet other cutoffs that gave a more selective percentage for the specific compartment but yielded less compartment proteins overall. These analyses yielded lists of high-confidence TurboID-ER enriched and high-confidence TurboID-Cytoplasm enriched proteins at a specific age for the intestine datasets. We verified that 20 positive control proteins for each compartment were indeed found in the correct compartment (Figure S1K; Table S2A). Finally, we also generated a list of intestine high-confidence TurboID-ER enriched and high-confidence TurboID-Cytoplasm enriched proteins across ages (union) (Table S2F).

Changes with age

To determine how the intestine secretome changes across ages, we used our high-confidence TurboID-ER enriched and high-confidence TurboID-Cytoplasm enriched protein lists (Table S2F). To determine age-dependent changes, we calculated the Log_2(Fold Change) and *p*-value of proteins in a pairwise manner between the 3 ages (Young vs. Old, Young vs. Middle-age, and Middle-age vs. Old). The Log_2(Fold Change) and *p*-value calculations (two-sided Welch's *t* test) were performed in the same manner as described above for the compartment analysis. A protein was considered significantly changing with age if the *p*-value was less than 0.1. This is a permissive *p*-value, which allows for more proteins to be screened[39] and has been used before in other proximity labeling papers.[150,151]

Finally, we generated a list of age-changed high-confidence TurboID-ER enriched proteins and age-changed high-confidence TurboID-Cytoplasm enriched proteins. For this, we took the union of proteins that exhibited significant age changes in pairwise comparisons from the high-confidence TurboID-ER enriched proteins and the high-confidence TurboID-Cytoplasm enriched proteins (Tables S3B and S3G).

Heatmaps for proteomics data

For heatmaps, we used sample normalized protein values and Log_2-transformed the protein abundance with an added pseudocount ("log-transformed protein abundance"). We then determined the *Z* score for a protein across samples and plotted these values.

GO term analysis for proteomics data

Gene ontology terms for proteomics data were determined using STRING version 12.0 (https://string-db.org) analysis. For background, we used the list of identified proteins from the intestine for analyses.

Protein sequence conservation

Protein sequence conservation was determined by blasting the *C. elegans* protein sequence against all human protein sequences using NCBI Blastp (https://blast.ncbi.nlm.nih.gov/Blast.cgi?PAGE=Proteins).

RNA isolation for RT-qPCR

RNA samples were generated from animals ~1000 animals at adult day 1 (3 days post-hatch), 5 (8 days post-hatch), and 10 (13 days post-hatch) for RT-qPCR experiments and just adult day 1 (3 days post-hatch) for RNA-Seq experiment. *C. elegans* were harvested and washed three times at day 1 (3 days post-hatch), 5 (8 days post-hatch), and 10 (13 days post-hatch) using M9 buffer (22 mM KH_2PO_4, 34 mM K_2HPO_4, 86 mM NaCl, 1mM $MgSO_4$), transferring into an Eppendorf tube, removing M9 buffer, and then flash freezing the samples in a bath of ethanol and dry ice. To isolate total RNA, the frozen worm pellets were resuspended in 500 μL of QIAzol Lysis Reagent (Qiagen) and bead beating was performed to break apart the *C. elegans*. Zirconia/silica 0.1 mm diameter beads (BioSpec, 11079101Z) were added and samples were beaten at 25 Hz for 30 s and left to rest on ice for 5 min (TissueLyser II, Qiagen). This step was repeated twice. RNA was extracted according to the standard QIAzol procedure, resuspended in 50 μL of RNase- and DNase-free water and quantified. The RNA was treated with TURBO DNase (ThermoFisher scientific), purified and reprecipitated using acid-phenol:chloroform (ThermoFisher scientific).

RT-qPCR

RNA samples were generated from animals ~1000 animals at adult day 1 (3 days post-hatch), 5 (8 days post-hatch), and 10 (13 days post-hatch). *C. elegans* were harvested and washed three times at day 1 (3 days post-hatch), 5 (8 days post-hatch), and 10 (13 days post-hatch) using M9 buffer (22 mM KH_2PO_4, 34 mM K_2HPO_4, 86 mM NaCl, 1mM $MgSO_4$), transferring into an Eppendorf tube, removing M9 buffer, and then flash freezing the samples in a bath of ethanol and dry ice. To isolate total RNA, the frozen worm pellets were resuspended in 500 μL of QIAzol Lysis Reagent (Qiagen) and bead beating was performed to break apart the *C. elegans*. Zirconia/silica 0.1 mm diameter beads (BioSpec, 11079101Z) were added and samples were beaten at 25 Hz for 30 s and left to rest on ice for 5 min (TissueLyser II, Qiagen). This step was repeated twice. RNA was extracted according to the standard QIAzol procedure, resuspended in 50 μL of RNase- and DNase-free water and quantified. The RNA was treated with TURBO DNase (ThermoFisher scientific), purified and reprecipitated using acid-phenol:chloroform (ThermoFisher scientific). cDNA was generated via reverse transcription (Fisher scientific) and SYBR Green PCR Master Mix (ThermoFisher Scientific) was used in a 25 μL reaction volume for the RT-qPCR reaction. Primers were designed to span exon-exon junction and used at a final concentration of 500 nM. RT-qPCR was performed using a LightCycler 480 II (Roche). Melt curves were examined to ensure the specificity of the primers. Results were analyzed using the $\Delta\Delta C_t$ method. For each biological replicate, the mean Ct value of three technical replicates was analyzed. *act-1* served as the housekeeping gene for normalization. Experiments were performed two-three independent times with three technical replicates, which were averaged to obtain a single value per biological replicate. To test for statistical significance, a one-way ANOVA was performed.

RNA-sequencing

RNA isolation for RNA-sequencing

For the transcriptomic experiments, RNA samples were generated from animals ~1000 animals at adult day 1 (3 days post-hatch). *C. elegans* were harvested at day 1 (3 days post-hatch) and washed three times with EN-50 buffer. RNA extraction was performed exactly as described as above in ''RNA isolation for RT-qPCR''. RNA was resuspended in 50 μL of H_2O. Next, 10 μg of RNA was incubated with 1 μL of TURBO DNase (ThermoFisher scientific) for 30 min (in 50 μL of H_2O and 5 μL of 10*x* TURBO DNase buffer) and the reaction was then stopped with 5 μL of DNase inactivation reagent (according to the manufacturer's protocol). An RNA purification and precipitation was performed using 100 μL of acid-phenol:chloroform (ThermoFisher scientific) followed by ethanol precipitation according to the manufacturer's protocol. Purified RNA was resuspended in 20 μL of H_2O. Purified RNA was sent to Novogene for library generation and sequencing according to Novogene's protocol. Briefly, messenger RNA was purified from total RNA using poly-T oligo-attached magnetic beads. After fragmentation, the first strand cDNA was synthesized using random hexamer primers followed by second strand cDNA synthesis. End repair, A-tailing, adapter ligation, size selection, amplification, and purification were performed. The RNA-seq library was checked with Qubit and real-time PCR for quantification and bio-analyzer for size distribution detection. Quantified RNA-seq libraries were pooled and sequenced on the Illumina platform, according to effective library concentration and data amount following Novagene's protocol.

Transcriptomics analysis

Raw FASTQ files were processed with TrimGalore and then aligned to the *C. elegans* reference genome (WBcel235) with STAR.[152] Gene counts were generated from uniquely mapped reads with featureCounts.[153] Genes with fewer than 10 total counts across all replicates were removed, and differential expression analysis was performed with PyDESeq2.[154] A Wald test was used to determine the *p*-values, and the Benjamini-Hochberg method was used to adjust them for multiple testing (P_{adj}-values). Read counts were normalized using the variance stabilizing transformation (VST) implemented in PyDESeq2. The VST-transformed read counts were used for both PCA and heatmaps. Genes shown in the heatmap are significantly differentially expressed genes (Log_2(Fold Change) ≥ 1 and $P_{adj} \leq 0.05$). PCA was performed using the PCA function from Scanpy[155] and heatmaps were created with clustermap from seaborn.[156] GO term enrichment analysis was performed with STRING analysis, on significantly differentially expressed genes (Log_2(Fold Change) ≥ 1 and $P_{adj} \leq 0.05$), using the *C. elegans* transcriptome as background. For visualization, genes with $P_{adj} = 0$ were set to $1*e^{-300}$.

ACP7/F21A3.11 protein sequence alignment

Protein sequences for human ACP7 and *C. elegans* ACP7/F21A3.11 were obtained from Uniprot and NCBI, respectively. Protein sequence alignment was performed using Clustal Omega multiple sequence alignment (https://www.ebi.ac.uk/jdispatcher/msa/clustalo). Protein structures based on AlphaFold predictions for human ACP7 and *C. elegans* ACP7 were obtained from Uniprot (https://www.uniprot.org/). Highly conserved metal-ion binding amino acids in the calcineurin phosphoesterase domain were retrieved from the *C. elegans* protein (F21A3.11) and mapped on the protein sequence. Pymol was used for visualization of the protein structure.

VAPA/F53B6.4 3D protein structure alignment

Protein structures based on AlphaFold predictions for human VAPA and *C. elegans* VAPA/F53B6.4 were obtained from Uniprot (https://www.uniprot.org/). The Dali protein structure comparison server was used to generate the alignment between the human VAPA and *C. elegans* VAPA/F53B6.4 protein structures.

Lifespan assays (overexpressing strains and RNAi)

C. elegans lifespan assays were performed at 20°C on RNAi plates. Hermaphrodites were age-synchronized with a short 4 h egg lay using synchronized young adults (adult day 1, 3 days post-hatch) parents. Lifespan assays were performed on HT115 empty vector or specific RNAi bacteria. All the plasmids containing the RNAi constructs were verified by Sanger sequencing. As ACP7/F21A3.11 RNAi construct is not present in the RNAi library, we used the RNAi construct for F21A3.2 and we confirmed by sequencing that it targets F21A3.11 and not F21A3.2. For lifespan assays, the hermaphrodites were transferred and scored every day to new plates until adult day 8, at which point the hermaphrodites were transferred and scored every other day. Each lifespan assay was performed with five plates of 20 worms per 6-cm RNAi plate (100 worms in total), except for the lifespan screen where on average 30 worms were used (see **Source Data**). Worms were scored as censored if they crawled off the media or died following vulva rupture/internal hatching. Worms were scored as dead when they failed to move following gentle prodding with a platinum wire pick (90% Pt, 10% Ir). For lifespan curves, censored worms were included until the day of censorship. All lifespan experiments were performed in a blinded and randomized manner. Kaplan-Meier survival curves were plotted in Prism. For pairwise comparison, the log rank Mantel-Cox statistical test in Prism was used.

Widefield microscopy for RNAi knockdown validation

RNAi against ACP7/F21A3.11 and VAPA/F53B6.4 were further validated against reporter strains overexpression ACP7/F21A3.11 or VAPA/F53B6.4 tagged with WormScarlet. Fluorescence microscopy was performed on a Zeiss AxioSkop 2 Plus with a 10*x* objective. Fluorescent reporter strains were hatched onto RNAi plates with HT115 empty vector bacteria or RNAi targeting *ACP7*/F21A3.11 or *VAPA*/F53B6.4 and imaged at adult day 1 (3 days post hatch). Worms were mounted on a 2% agar pad, anesthetized with 50 mM sodium azide and covered with a glass cover slide. Both brightfield and fluorescent images were taken of 10 worms).

Widefield microscopy for translational and transcriptional reporter assays

To determine if ACP7/F21A3.11 overexpression or *VAPA*/F53B6.4 knockdown regulate well-known longevity pathways, we used translation and transcriptional reporters for these pathways. For translational reporters, quantification was done at adult day 1 (3-day after hatch). Specifically, we assessed nuclear localization of transcription factors FOXO/DAF-16 (strain TJ356, *daf-16p::daf-16a/b::GFP* + *rol-6(su1006)*)[100] or TFEB/HLH-30 (strain MAH235, *hlh-30p::hlh-30::GFP* + *rol-6(su1006)*)[96] in the context of ACP7/F21A3.11 overexpression and *VAPA*/F53B6.4 knockdown via RNAi. Nuclear localization of NRF-2/SKN-1 (strain LD1, *skn-1b/c::GFP* + *rol-6(su1006)*)[113] was assessed at adult day 1 (3-day after hatch) in the context of *VAPA*/F53B6.4 knockdown via RNAi. Animals were considered positive for nuclear localization of these transcription factors if green fluorescent nuclei were observed. As a positive control for FOXO/DAF-16 nuclear localization, *daf-2* RNAi was used. As a positive control for TFEB/HLH-30 nuclear localization, 6h of complete starvation was used.

For transcriptional reporters, quantification was performed at adult day 1 (3 days post hatch). We assessed transcriptional activity by measuring green fluorescence intensity in the reporter strains for the p38 MAPK/PMK-1 innate immune pathway (Strain AU78, *T24B8.5p::GFP*[101]), the unfolded protein response in the endoplasmic reticulum (UPR-ER, strain SJ4005,[102] *hsp-4p::GFP*), the unfolded protein response in the mitochondria (UPR-mitochondria, strain SJ4100,[4,103] *hsp-6p::GFP*), and the unfolded protein response in the cytoplasm (UPR-cytoplasm, strain TJ375,[114] *hsp-16.2p::GFP*). Fluorescence microscopy was performed on a Zeiss AxioSkop 2 Plus with a 10*x* objective. *C. elegans* were hatched onto RNAi plates with HT115 empty vector bacteria or RNAi targeting *VAPA*/F53B6.4. The positive control RNAi used were: *vhp-1* RNAi for p38 MAPK/PMK-1, *sec-13* RNAi for UPR-ER, and *cco-1* RNAi for UPR-mitochondria. The positive control for UPR-cytoplasm was a heat shock at 35°C for 2 h in a water bath.

For both translational and transcriptional reporters, individual worms (n = 9–38) were mounted on a 2 % agar pad, anesthetized with 50 mM sodium azide and covered with a glass cover slide. Worms were imaged at 10*x* on a Zeiss Axioskop 2 plus microscope using an Axiocam 503 color. For translational reporters (transcription factor localization), percentage of animals that had positive green fluorescent nuclei were quantified. For transcriptional reporters, GFP fluorescence intensity was quantified in the intestine by manually circling the intestine and quantifying using ImageJ. Both nuclear scoring and GFP fluorescence intensity quantifications were performed in a blinded manner.

Phosphatase assay for ACP7

To generate *C. elegans* ACP7 and ACP7-7A (catalytically dead) protein to be used in the phosphatase assay, whole worm protein lysate of adult day 1 worms was generated the same way as for western blots using a pull-down specific lysis buffer consisting of (50 mM HEPES pH 7.3, 100 mM NaCl, 5 % glycerol, 1 mM DTT, 1 % triton X-100, and 1*x* Halt Protease Inhibitor Cocktail). Total protein was quantified and an overnight pull-down using HA-magnetic beads (ThermoFisher scientific, 25 μL beads per 1 μg of total protein) was performed at 4°C overnight with end-over-end rotation. After overnight incubation, beads were washed for 1 min with 1 mL of 3 different wash solutions (Wash Solution 1: 50 mM HEPES pH 7.3, 300 mM NaCl, 5 % Glycerol, 1 mM DTT; Wash Solution 2: 50 mM HEPES pH 7.3, 400 mM NaCl, 5 % Glycerol, 1 mM DTT, 5 mM MgCl2, 10 mM ATP; Wash Solution 3: 50 mM HEPES pH 7.3, 500 mM NaCl, 5 % Glycerol, 1 mM DTT). Finally, a desired volume of beads (20 μL) were aliquoted into Eppendorf tubes and flash frozen in liquid nitrogen.

To determine phosphatase activity of *C. elegans* ACP7 and ACP7-7A, the EnzChek phosphatase assay kit (ThermoFisher Scientific, #E12020) was used. The assay was performed according to the manufacturer's instructions. As ACP7 and ACP7-7A are bound to HA-beads in this assay, a background control of wild-type N2 *C. elegans* total protein lysate and subsequent HA-bead pull-down was also assessed. The assay was performed for 1 h at room temperature and fluorescence was measured using a Varioscan instrument (excitation at 360 nm and emission detection at 460 nm). Two different protein aliquots, tested in duplicates, were tested. Statistical significance calculated by Mann-Whitney test.

Human ACP7 protein expression and purification for phosphatase assay

Human ACP7 was cloned into the pRK5-HA-metap2 plasmid (Addgene, 100512) with a C-terminal 6xHis tag preceded by a short linker sequence (GGGGS). Human Expi293F cells were grown in a 1/3 Expi293 growth media (ThermoFisher Scientific, #A1435101) and 2/3 Freestyle293 growth media (ThermoFisher Scientific, #12338018) combination were transfected with plasmids at a density of $3x10^6$ cells/mL and cultured in a shaking incubator at 37°C and 8 % CO_2. Transfection was performed using the Polyethylenimine (PEI) STAR transfection reagent (Tocris, #7854) at ratios of 5 μg PEI STAR and 1 μg plasmid DNA per mL of cells. Immediately after transfection, cells were supplemented with glucose and valproic acid to final concentrations of 0.4 % glucose (w/v) and 0.05 % valproic acid (w/v). Two days post-transfection, cells were again supplemented with an equivalent amount of glucose. Cells were harvested three days post-transfection.

The cell media (supernatant) was collected, diluted 1:1 in 1*x* PBS (Phosphate buffered saline), and incubated with HisPur Ni-NTA resin (ThermoFisher Scientific, #88221) for 16 h at 4°C. The resin was then washed with four iterative washes of 2 volumes of bead-resin used (wash 1 composition: 50 mM HEPES pH 7.25, 500 mM NaCl, 0.1 mM EDTA, 5 mM beta-mercaptoethanol, 5 % glycerol [v/v], 20 mM imidazole pH 7.25, 1 mM DTT, 1 mM PMSF, cOmplete EDTA-free protease inhibitor cocktail (Roche), and 1 % Triton X-100 [v/v]; wash 2 composition: same as wash 1 composition without Triton X-100 and protease inhibitor and with 10 mM imidazole pH 7.25; wash 3 composition: same as wash 2 without imidazole and with 250 mM NaCl; wash 4 composition: same as wash 3 with 125 mM NaCl). The resin was packed onto a column and protein was eluted in a buffer containing 300 mM Imidazole pH 7.25, 50 mM HEPES pH 7.25, 125 mM NaCl, 5 mM BME, 5 % glycerol [v/v], 1 mM DTT, 1 mM PMSF, 0.1 mM EDTA, and protease inhibitors. Eluted fractions containing protein were pooled, concentrated using an Amicon 10 kDa MWCO concentrator, and flash-frozen in liquid nitrogen. The phosphatase activity of human ACP7 was assessed using the same protocol as described above in "Phosphatase assay for ACP7".

Tyrosine phosphatase assays

To determine if ACP7 could act as a tyrosine phosphatase, we used a commercially available kit with a chemically synthesized fluorogenic protein phosphatase substrate that is converted into a highly fluorescent product (Ex/Em = 368/460 nm) (Abcam, ab241032). We followed the manufacturer's protocol using purified human ACP7 protein (20 μL per sample), alkaline phosphatase as a positive control, and no human ACP7 (just reaction buffer) as the blank control. The reaction occurred for 1 h at 25°C. Immediately after 1 h, fluorescence was measured using a Varioscan instrument (excitation at 368 nm and emission detection at 460 nm). Two different protein aliquots of purified ACP7 protein, tested in duplicates, were assessed. Statistical significance calculated by Mann-Whitney test.

Serine/threonine phosphatase assays

To determine if ACP7 could act as a serine/threonine phosphatase, we used a commercially available kit with a chemically synthesized phosphopeptide RRA(pT)VA (Promega, V2460). We followed the manufacturer's protocol using human ACP7 protein (20 μL per sample), alkaline phosphatase as a positive control, and human ACP7 with no substrate as the negative control. The reaction was in PPase-2A reaction buffer (PPase-2A 5*x* buffer 250 mM imidazole (pH 7.2, 1 mM EGTA, 0.1 % β-mercaptoethanol, and 0.5 mg/mL BSA). The reaction occurred over 1 h at room temperature and then was stopped by adding 50 μL Molybdate Dye. After 15 min at room temperature, optical density for each well was measured using a Varioscan instrument (filter 630 nm). Two different protein aliquots, tested in duplicates, were assessed. Negative control was a single aliquot performed in duplicate. Statistical significance calculated by Mann-Whitney test.

Prediction of ACP7/F21A3.11 substrates

To identify potential protein substrates that could be dephosphorylated by ACP7 at tyrosine residues, we first generated a list of potential substrates of ACP7 that are present in the extracellular space. This list of extracellular proteins that could be potential

substrates of ACP7 was based on our high-confidence list of intestine secreted proteins that change with age and are conserved in humans (Table S4A). We then determined which of these conserved secreted proteins had 6 or more tyrosine residues that had a score >0.8 of being phosphorylated using the online tool NetPhos3.1,[157] in order to focus on high-confidence potential substrates.

Verification of proteomic evidence for VAPA/F53B6.4 changes with age

We identified and quantified 3 unique VAPA/F53B6.4 peptides across fractions 2 and 5 in the TurboID-Cytoplasm dataset. All of these are high scoring PSMs (Andromeda PEP score >40), supporting these peptides' validity and the identification of the underlying VAPA/F53B6.4 protein. All three peptides had intensities within the middle 50 percentile of abundance considering all measured peptides in the dataset, supporting that they are substantially above the limits of detection and unlikely to be influenced by low signal/noise errors. We have also examined the raw MS3 scan intensities for one representative example of the three peptides. The TMT signals at masses 126.12772, 127.12476, 127.13108, and 128.12811 were many fold greater than background signals. We also examined the summation of all the signal intensities for all TMT channels for the VAPA/F53B6.4 protein, indicating that the young signal is at least 3*x* greater than the middle-age or old signal in the TurboID-Cytoplasm dataset, and nearly three orders of magnitude more intense than signal measured from the blank TMT channel.

VAPA/F53B6.4 secretory pathway association

To test if VAPA/F53B6.4 is part of the secretory pathway, genes encoding secretory pathway proteins (USO-1 and TRPP-3) were knocked-down via RNAi, and VAPA/F53B6.4 protein localization in vesicle-like structures was assessed in a blinded manner. To visualize VAPA/F53B6.4, a transgenic strain expressing VAPA/F53B6.4 tagged with WormScarlet driven by the pan-intestine promoter, *ges-1p*, was generated. Animals were grown from hatch on RNAi plates seeded with either control, *uso-1,* or *trpp-3* RNAi. For these experiments, 8–10 animals were imaged at adult day 1 (3 days post hatch) of life. To image worms, they were mounted on a 2 % agar pad, anesthetized with 50 mM sodium azide and covered with a glass cover slide. Confocal microscopy was performed on a Zeiss LSM900 Axio Observer. A 20*x* air objective (Plan-Apochromat 20×/0.8 M27) was used. A 2*x* crop region was generated to image the first few intestine cells with a z stack interval of 1 μm with processed using Zen software (3.0, blue). Animals were imaged in the near-red channel to visualize F53B6.4-WormScarlet.

To quantify the number and size of VAPA/F53B6.4 vesicle-like structures, maximum intensity projections were generated in ImageJ–Fiji (2.14.0/1.54f), and then vesicle number and area were assessed in a blinded and automated manner using QuPath 0.4.4. To identify vesicles, an annotation was created for the entire image and each vesicle was segmented and counted based on a threshold of mean fluorescent intensity. Statistical significance calculated by Mann-Whitney test.

Intestinal barrier function assay (smurf assay)

To measure intestine barrier function, we used a Smurf assay[115] and assessed in a blinded manner. For this assay, hermaphrodites were age-synchronized with a 4 h egg lay. *C. elegans* hatched onto NGM plates seeded with OP50-1 bacteria and assessed at adult day 10 (13 days post hatch) for the 'Smurf phenotype'. The Smurf phenotype occurs when animals are fed a blue dye that leaks out of the intestine lumen into the animal's body cavity, suggesting intestine barrier function is lost.[115] To assess the 'Smurf phenotype', 6–39 worms per condition were transferred from RNAi plates to 250 μL of OP50 mixed with 5 % wt/vol FD and C Blue No. 1, Spectrum in a 1.5 mL Eppendorf tube and placed in a 20°C incubator. After 3 h, worms were transferred gently using a glass pipette to room temperature NGM plates. Plates were allowed to dry for 20 min. All worms were then transferred to clean NGM plates seeded with OP50-1 and scored. Images were taken by mounting worms on 2 % agar pads, and imaged at 10*x* on a Zeiss Axioskip 2 plus microscope using an Axiocam 503 color.

Quantification was performed in the following manner: worms with blue dye absent or blue dye restricted to the intestinal lumen were scored as non-Smurf. Worms with blue dye in the body cavity were scored as Smurf. Worms with blue dye in the germline but not the body cavity were excluded from analysis (censored), as it is unclear whether the blue dye entered the germline through the body cavity or the vulva. Statistical analysis was performed using Graphpad Prism 10. An average percentage of Smurfed worms was calculated for each replicate. Statistical significance calculated by Mann-Whitney test.

QUANTIFICATION AND STATISTICAL ANALYSIS

The *n* values, mean ± s.d. and significant *p* values are reported in the figures, figure legends and source data. For all experiments, except mass spectrometry data and RNA-sequencing (please refer to those sections), significance was defined as $p < 0.05$. Pairwise comparisons were made using the Mann–Whitney test or one-way ANOVA. When testing for correlation, Pearson's correlation test was used. For pairwise comparison of lifespan data, the log rank Mantel–Cox statistical test was used. * denotes $p < 0.05$, ** denotes $p < 0.01$ and *** denotes $p < 0.001$. All statistics are reported in the source data. Statistical analyses were performed using SigmaPlot 14.0 or Prism 10.